ABG-0324

# Passive Spectral Bathymetry Using Satellite Remote Sensing in Cockburn Sound W. A.

by

Robert J. Corner

presented as part of the requirements

for the award of the

Degree of Master of Science

(Surveying and Mapping)

of the

Curtin University of Technology

School of Surveying and Land Information

Perth, Western Australia

December 1992

School of Surveying and Land Information
Faculty of Engineering

curtin
University of Technolog
Perth Western Australi

GPO Box U 1987
Perth 6001
Western Australia
Fax (09) 351 2703
Telex AA92983
Telex AA92983

Telephone
(09) 351 7565/6

I ROBERT J CORNER, **hereby consent that my thesis** PASSIVE SPECTRAL BATHYMETRY USING SATELLITE REMOTE SENSING IN COCKBURN SOUND WA **may be loaned to any library at the discretion of the Head of School of Surveying and Land Information and that the Head of School shall be authorised to allow a copy of all or part of the thesis for the purpose of study or research.**

**DATE:** 19/3/92

Frontispiece : Colour composite image of Gage Roads and Cockburn Sound

# ABSTRACT

Conventional bathymetric surveying is a costly and time consuming business. Even today many areas of shallow inshore ocean, some which encompass potential oil and gas fields, are only minimally charted. There is a need for reconnaissance systems which can effectively direct more expensive detailed surveys to best effect. Remote spectral bathymetry is one such system.

A review of candidate sensor systems and processing algorithms highlighted problems due to changing bottom cover types and water quality parameters. A method, proposed and theoretically validated by other workers, was chosen for further investigation. This method develops an approximate relationship between the spectral content of the satellite data and water depths and then, by an iterative phase in the spatial domain, seeks to minimise the effect of spatially dependant variations.

A study site in Cockburn Sound, Western Australia was chosen for a demonstration of this method. Spectral data are from the Landsat Thematic Mapper instrument and depth data are taken from Admiralty Charts. A variation on the originally proposed algorithm introduces spatial preprocessing phase, in which the image is segmented into zones where spectral relationships are expected to be more uniform. Two different method of spatial mapping are used.

The results demonstrate the capability of spatial modelling to improve remotely sensed depth estimates in the depth range of 5 to 12 m. The need for further research to better understand the shallow water spectral relationships is identified.

## ACKNOWLEDGMENTS

The conduct of this research and preparation of this thesis would not have been possible without the support advice and assistance of a number of people. At Curtin University, Bill Larson first interested me in the use of remotely sensed data and presided over the launch of this work. Following his return to the United States, Dr. Doug Myers and Dr. Chris Worth provided encouragement and assisted with the navigation of the project until Professor Graham Lodwick provided the necessary pilotage to bring it to harbour.

The support and advice of colleagues in the CSIRO Western Australian Remote Sensing group has been invaluable, particularly that provided by Peter Hick. I am much indebted to my employer, CSIRO Division of Soils, and especially their senior regional officer Dr. Simon Cook, for their generous provision of facilities and a pragmatic approach to the allocation of my time.

Thanks are due to the Remote Sensing Applications Centre of the Western Australian Department of Land Administration and to CSIRO Division of Exploration Geoscience for providing access to data.

Lastly, but by no means least, thanks are due to my wife and family for enduring good-naturedly the regime demanded by concurrent full time employment and part time study.

# TABLE OF CONTENTS

ABSTRACT . . . . . iii

ACKNOWLEDGEMENTS . . . . . iv

TABLE OF CONTENTS . . . . . v

LIST OF FIGURES . . . . . x

LIST OF TABLES . . . . . xi

CHAPTER

1 INTRODUCTION . . . . . 1
- 1.1 Bathymetric Surveying . . . . . 1
- 1.2 Remote Sensing . . . . . 2
- 1.3 Remote Sensing Interpretation . . . . . 3
- 1.4 The Role of Passive Spectral Bathymetry . . . . . 4
  - 1.4.1 The Reconnaissance Role . . . . . 5
  - 1.4.2 The Survey Role . . . . . 5
- 1.5 Laser Airborne Depth Sounder (LADS) . . . . . 6
- 1.6 Aims of this Research . . . . . 7

2 DEVELOPMENT OF THE TECHNOLOGY . . . . . 8
- 2.1 Postulation of the Method . . . . . 8
- 2.2 Investigations Using Early Landsat MSS . . . . . 9
  - 2.2.1 The Ocean Bathymetry Experiment . . . . . 9
  - 2.2.2 Operational Charting . . . . . 9
- 2.3 Initial Work in Australia . . . . . 10
  - 2.3.1 Research Work on Great Barrier Reef . . . . . 10
  - 2.3.2 Operational Work on Great Barrier Reef . . . . . 12
  - 2.3.3 BRIAN processing . . . . . 12
- 2.4 Other Australian Studies . . . . . 14
  - 2.4.1 Monte Bello Study . . . . . 14
  - 2.4.2 Work in Torres Strait . . . . . 14
  - 2.4.3 Experimental Work in Cockburn Sound, W.A. . . . . 14

2.5 Work Using Landsat Thematic Mapper Data . . . . . 15
2.5.1 Work on Great Bahama Bank . . . . . 15
2.5.2 Australian Work Using Landsat TM Data . . . . . 16
2.6 Airborne Work . . . . . 17
2.6.1 M8 AMSS Active/Passive Instrument . . . . . 17
2.6.2 The Daedelus 1260 AMSS . . . . . 18
2.6.3 The Fluorescent Line Imager . . . . . 19
2.7 Studies Using SPOT . . . . . 19
2.8 Theoretical studies . . . . . 20
2.9 Summary . . . . . 21

3 SENSORS AND SENSOR PLATFORMS . . . . . 22
3.1 Accuracy and Resolution . . . . . 22
3.1.1 Scale . . . . . 22
3.1.2 Positional and Depth Accuracy . . . . . 23
3.2 Ability of Remote Sensing to Meet Requirements . . . . . 23
3.2.1 Spatial Considerations . . . . . 23
3.2.2 Effect of Data Quantisation . . . . . 24
3.2.3 Spectral Considerations . . . . . 25
3.3 Potential Satellite Sensors . . . . . 26
3.3.1 Landsat Thematic Mapper . . . . . 27
3.3.2 Landsat MultiSpectral Scanner . . . . . 28
3.3.3 SPOT . . . . . 29
3.4 Airborne Systems . . . . . 30
3.4.1 Geoscan Mk II Scanner . . . . . 31
3.4.2 Compact Airborne Imaging Spectrometer (CASI) . . . . 31
3.4.3 CSIRO Ocean Colour Scanner . . . . . 32
3.5 Summary . . . . . 32

4 PHYSICAL PRINCIPLES . . . . . 34
4.1 Radiative Transfer Model . . . . . 34
4.2 Atmospheric Transmission Effects . . . . . 36
4.3 Transmission Effects in the Water Column . . . . . 37
4.3.1 Absorption and Scattering - the Two Flow Model . . . . 38
4.3.2 The Diffuse Attenuation Coefficient . . . . . 39
4.3.3 Internal Reflection . . . . . 40
4.4 Summary . . . . . 41

5 DATA PROCESSING ALGORITHMS . . . . . 42
5.1 Depth of Penetration Methods . . . . . 42
5.2 Regression Methods . . . . . 44
5.2.1 Single Band Method . . . . . 44
5.2.2 Ratio Methods . . . . . 45
5.2.3 Multi-band Methods . . . . . 47
5.2.4 Multi-band Method with Spatial Iteration . . . . . 48
5.2.5 Multi-band Ratio Model . . . . . 49
5.2.6 Hybrid Methods . . . . . 49
5.3 Classification Methods . . . . . 50
5.4 Multi-temporal Methods . . . . . 50
5.5 Summary . . . . . 51

6 DATA ACQUISITION AND REGISTRATION . . . . . 52
6.1 Choice of Study Area . . . . . 52
6.2 TM Data Acquisition . . . . . 53
6.2.1 Image Characteristics . . . . . 54
6.2.2 Data Transfer . . . . . 54
6.3 Area Selection and Description . . . . . 55
6.4 Bathymetric Data . . . . . 56
6.4.1 Digitising . . . . . 58
6.4.2 Tidal Correction . . . . . 59
6.5 Co-registration of Data . . . . . 59
6.5.1 Australian Map Grid . . . . . 59
6.5.2 Warping and Resampling . . . . . 60
6.5.3 Transformation Software . . . . . 61
6.6 Registration of Soundings to AMG . . . . . 62
6.7 Registration of Image Data to AMG . . . . . 66
6.8 Summary . . . . . 67

7 SIGNAL PREPROCESSING AND NOISE REMOVAL . . . . . 69
7.1 Noise Characteristics . . . . . 69
7.1.1 Periodic Striping . . . . . 69
7.1.2 Sunglint . . . . . 70
7.2 Image Inspection . . . . . 72
7.2.1 Band 1 . . . . . 72
7.2.2 Band 2 . . . . . 72
7.2.3 Band 3 . . . . . 74
7.2.4 Band 4 . . . . . 74

7.3 Potential Methods of Noise Correction . . . . . 74
7.3.1 Periodic Striping . . . . . 74
7.3.2 Sunglint . . . . . 76
7.4 Application of Offset Destriping Method . . . . . 77
7.4.1 Determination of Offsets . . . . . 77
7.4.2 Application of Corrections . . . . . 78
7.5 Determination of Sunglint Correction Factors . . . . . 80
7.6 Summary . . . . . 81

8 IMAGE SEGMENTATION . . . . . 82
8.1 Depth of Penetration (DOP) Zones . . . . . 82
8.1.1 Derivation of Zones . . . . . 83
8.1.2 DOP Image Smoothing . . . . . 84
8.2 Bottom Cover Classes . . . . . 86
8.2.1 Training Site Selection . . . . . 86
8.2.2 Classification . . . . . 88
8.3 Summary . . . . . 90

9 DATA FITTING BY REGRESSION . . . . . 92
9.1 Extraction of Image Data . . . . . 92
9.1.1 Data Extraction Software . . . . . 93
9.1.2 Data Extraction and Sorting . . . . . 93
9.2 Regression Models . . . . . 93
9.2.1 Choice of Regression Variables . . . . . 94
9.2.2 Depth of Penetration Dataset . . . . . 95
9.2.3 Bottom Cover Dataset . . . . . 96
9.3 Regression Results . . . . . 96
9.3.1 DOP Zone 2 . . . . . 96
9.3.2 DOP Zone 3 . . . . . 98
9.3.3 Bottom Cover Classes . . . . . 101
9.4 Summary . . . . . 102

10 SPATIAL ITERATION AND MODEL TESTING . . . . . 104
10.1 Spatial Modelling . . . . . 104
10.2 Selection of Surface Generation Method . . . . . 104
10.2.1 Thiessen Polygons . . . . . 105
10.2.2 Distance Weighted Interpolation . . . . . 105
10.3 Data Masking . . . . . 106

10.4 Residual Surface Generation . . . . . 106
10.4.1 Distance Weighted Interpolation . . . . . 107
10.4.2 Generation of Thiessen polygons . . . . . 107
10.5 Testing the Models . . . . . 110
10.5.1 Data Extraction . . . . . 111
10.5.2 Comparison of Results . . . . . 111
10.6 Discussion of Results . . . . . 113
10.6.1 Distance Weighted Surface . . . . . 113
10.6.2 Thiessen Polygon Surface . . . . . 114
10.7 Summary . . . . . 114

11 CONCLUSIONS AND RECOMMENDATIONS . . . . . 120
11.1 Conclusions . . . . . 120
11.3 Recommendations . . . . . 124

REFERENCES . . . . . 127

APPENDIX

A PROPRIETARY SOFTWARE USED . . . . . 134
DISIMP . . . . . 135
IDRISI . . . . . 140
GRASS . . . . . 144
INTERACTIVE DATA LANGUAGE (IDL) . . . . . 146

B LISTING OF CUSTOM WRITTEN SOFTWARE . . . . . 148
DSOFFSET . . . . . 149
SOUNDER . . . . . 154
SIT2IMG . . . . . 160

C FILES USED IN THE DESTRIPING PROCESS . . . . . 163

# LIST OF FIGURES

FIGURE

Frontispiece Colour composite image of Gage Roads and Cockburn Sound . . ii
3.1 Depth versus digital number (DN) . . . . . 24
3.2 Depth versus resolution per DN . . . . . 25
3.3 Relationship between wavelength and transmittance for clear water at a range of depths . . . . . 26
4.1 Ray paths to a sensor . . . . . 34
4.2 Light paths in a water column . . . . . 38
5.1 Theoretical depth of penetration against wavelength . . . . . 43
6.1 The coastline of metropolitan Perth . . . . . 53
6.2 Parmelia Bank study area . . . . . 55
6.3 View westwards from Woodman Point . . . . . 57
6.4 Frequency distribution of control sounding set . . . . . 63
6.5 Frequency distribution of check sounding set . . . . . 63
6.6 Flowchart - Data input and coregistration . . . . . 67
7.1 Striping in a TM Band 1 image of Warnbro sound . . . . . 71
7.2 Striping patterns . . . . . 73
7.3 Plot of detector offsets for Band 1 . . . . . 78
7.4 Flowchart of de-striping process . . . . . 81
8.1 Smoothed DOP image . . . . . 86
8.2 Part of vertical air-photo. North of Woodman Point . . . . . 87
8.3 Smoothed bottom class image . . . . . 89
8.4 Flowchart for generation of DOP image . . . . . 91
8.5 Flowchart for generation of bottom cover image . . . . . 91
9.1 Flowchart illustrating data extraction and analysis . . . . . 103
10.1 Test Residual Surfaces for DOP zone 2 . . . . . 108
10.2 Spatial distribution of points in DOP zone 2 . . . . . 109
10.3 Spatial distribution of points in DOP zone 3 . . . . . 109
10.4 Combined residual surface using inverse distance weighting . . . . . 110
10.5 Combined residual surface using Theissen polygons . . . . . 110
10.6 Comparison of results - distance weighted residuals - DOP zone 2 . . . 115
10.7 Comparison of results - distance weighted residuals - DOP zone 3 . . . 116
10.8 Comparison of results - polygonal residuals - DOP zone 2 . . . . . 117
10.9 Comparison of results - polygonal residuals - DOP zone 3 . . . . . 118
10.10 Flowchart for generation and testing of residual surfaces . . . . . 119

# LIST OF TABLES

TABLE


4.1 Diffuse attenuation coefficient for five water types . . . . . 40
6.1 Residuals from digitiser to AMG transformation (first setup) . . . . . 64
6.2 Residuals from digitiser to AMG transformation (second setup) . . . . . 65
6.3 Residuals from image to AMG transformation . . . . . 66
7.1 Offsets for Band 1 destriping . . . . . 79
7.2 Covariance matrix for deep water area . . . . . 80
7.3 Correlation matrix for deep water area . . . . . 80
8.1 Band means and standard deviations for deep water area . . . . . 83
8.2 Values resulting from generation of DOP zones . . . . . 85
8.3 Training site statistics . . . . . 88
8.4 Pixel count for smoothed bottom class image . . . . . 90
9.1 Theoretical depths of penetration for coastal water types . . . . . 94
9.2 Data points in each bottom class . . . . . 96
9.3 Regression results for zone 2 using Bands 1 and 2 . . . . . 97
9.4 Regression results for zone 2 using Band 2 . . . . . 98
9.5 Regression results for zone 3 using Bands 1, 2, and 3 . . . . . 99
9.6 Regression results for zone 3 using Bands 2 and 3 . . . . . 100
9.7 Regression results for zone 3 using Bands 1 and 2 . . . . . 100
9.8 Regression results for zone 3 using Band 2 . . . . . 101
9.9 Summary of regression results for bottom cover classes . . . . . 101
10.1 Comparison of check values using distance weighted residual mapping . . . . . 112
10.2 Comparison of check values using polygonal residual mapping . . . . . 112
10.3 Correlation between uncorrected and corrected depth estimates . . . . . 113

# CHAPTER 1

# INTRODUCTION

## 1.1 Bathymetric Surveying

Since mankind first ventured onto the oceans, it has been of interest to know the depth of the waters in which navigation takes place. Descriptions of the Mediterranean coasts dating back before the time of Christ are still in existence (Hydrographer of the Navy, 1965).

The first charts, whilst not giving depths as soundings, indicate areas of shallow water where vessels were at risk. It was not until the mid 17th century that charts as we know them were first produced. In those early times, depths were determined by the use of a sounding line, and the indicated position of those soundings was often inaccurate.

Improvements in position fixing, through first the sextant and more recently the use of radio and satellite navigation systems, have greatly increased the accuracy of positioning. Similarly, the development and refinement of echo sounders has enabled the measurement of depths to a considerable degree of accuracy.

In order to determine the depths that are incorporated on a chart, it is necessary for a suitably equipped vessel to pass over the location whose depth is to be determined. If the chart is to comprehensively show the sea bed, then the vessel must pass on a large number of parallel tracks, often at a close spacing.

For a typical inshore survey, such as the approaches to a major port, the operation of this vessel requires a marine crew of at least two and a survey team comprising, typically, a surveyor and an electronics technician. Under some circumstances, it will also be necessary for shore personnel to be employed in the maintenance of positioning equipment.

A recent estimate by a commercial survey company put the operational cost of a fully equipped vessel at $6000 per day with an estimated data collection rate of 50 line km per 12 hour shift. This would increase to around $10,000 for an offshore survey, with no increase in line km. Whilst the use of recently developed swath echo sounders, such as the Atlas Fansweep, may reduce required line spacings somewhat, conventional hydrographic data collection still remains a costly exercise.

### 1.2 Remote Sensing

Remote Sensing has been defined as the acquisition of information about an object without physical contact (Simonett, 1983).

The term was first applied in the 1960's by US Naval researchers to information from photographic and non-photographic instruments. The method of depth determination by echo sounding referred to above is, in fact, a specialised form of remote sensing. The term, nowadays, is generally taken to mean the collection and processing of data from the electro-optical and electronic scanners mounted on various satellite and airborne platforms.

The first such multispectral scanners were not constructed until the 1960's and it was not until the launch of the first of the Landsat series of satellites, in

1972, that multispectral remote sensing moved from the area of research into that of applications.

Considerable advances have been made in those 20 years since the launch of Landsat 1. These have included improvements in the spectral and spatial resolution of sensors as well as the introduction, on systems such as the French SPOT satellite and the CASI airborne scanner, of better scanner mechanics. Possibly the most significant advances have been in the development of computer hardware and software to process the ever greater data flows emanating from remote sensing platforms.

### 1.3 Remote Sensing Interpretation

Initial remote sensing applications frequently depended on human interpretation of a colour composite image, enhanced to highlight the features or themes of interest. The reasons for this are two-fold. Firstly, this was a logical extension and use of the photo-interpretive skills of many of those who were working with the technology. Secondly, the computing systems available were extremely expensive and had, in today's terms, limited capabilities.

Modern computer systems have many times more power then those of 20 years ago. During those 20 years research has led to the development of algorithms and techniques, for the machine processing of remotely sensed data, that were unavailable to earlier workers. It is of interest to note that IBIS, an Image Based Information System developed by NASA's Jet Propulsion Laboratory in the 1970's, ran on a mainframe system with one megabyte of main memory. A typical desktop system of today has four megabytes of memory.

## 1.4 The Role of Passive Spectral Bathymetry

Passive spectral bathymetry may be defined as the use of multispectral data for the determination of water depth. In this context the spectral data are assumed to be collected by a digital multispectral imaging system rather than by the use of photographic techniques. The use of such data for bathymetric mapping has been described as being a comprehensive exercise in scene classification and parametric inversion (O'Neill et al. 1987).

A report in 1985 stated that some of the worlds largest vessels pass through waters that were last charted more than 100 years ago (Kilbride, 1985). As indicated above, the charting of waters by conventional means using echo sounding is a costly and time consuming process. A British Hydrographic Study Group, quoted in an early report on the use of multispectral data for chart updating, concluded that in excess of 500 ship years were required to bring charts of British territorial waters and other United Kingdom areas of responsibility up to modern standards (Hammack, 1977).

Water depth mapping from spectral data is constrained by the physical properties governing the attenuation of light, to shallow water of depth less than 40 m. It is, however, in this zone that shipping is most at risk, and where spectral bathymetry finds two possible roles. It may be used either as a reconnaissance tool to direct the deployment of other survey systems, or in optimal water conditions, as a bottom mapping tool. These two roles have different requirements in terms of the spatial resolution of the sensor employed and in terms of the supporting information required.

### 1.4.1 The Reconnaissance Role

Spectral data with broad coverage and moderate spatial resolution, such as that available from the Landsat series of satellites, are ideally suited to a reconnaissance role. Such data have been used successfully in the past. One notable example from Australian waters is the discovery, by analysis of Landsat Multispectral Scanner (MSS) data, of the Hydrographer's Passage. This channel, through the Great Barrier Reef, saves 600 km off the route of vessels carrying coal between Mackay and Japan (Richardson, 1989). Another well documented, early, example is the revision of charts in the Chagos Archipelago by a NASA team in the late 1970's (Hammack, 1977).

Potential operational scenarios for such reconnaissance work can be placed on three levels.

(a) The data can be used without any supporting ground truth information to provide a general survey planning tool.

(b) Water quality information, or pre-existing depth data, may be used to increase the degree of precision of the planning tool.

(c) A comprehensive plan of ground truthing may be developed to enable the production, from coarse spatial resolution data, of a small scale chart.

### 1.4.2 The Survey Role

There are a number of accuracy considerations, to be discussed later, which govern the selection of a suitable system for direct survey work. One may, however, postulate a system for detailed surveys.

In order to provide good spatial resolution, such a system should be

airborne and have some means of using its navigation system to position the sensor field of view. In order that ground truth be collected simultaneously, it is desirable to couple the passive multispectral device with an active laser device. This combines the superior accuracy of the laser system with the broader area coverage of the multispectral system. Such a system is under trial with some of the world's navies (Estep, 1990).

An alternative, and more commercially achievable method, is to arrange for the collection of data from a high resolution airborne sensor, whilst simultaneously acquiring conventional echo sounder data for part of the survey area. The survey vessel could be used to deploy floating, tethered, targets to assist in the registration of imagery. Such a system could be of use in the developing oil and gas fields of Northern Australia and in the Archipelagos of South East Asia.

### 1.5 Laser Airborne Depth Sounder (LADS)

The Royal Australian Navy Hydrographic Office have developed, in conjunction with major Australian engineering companies, a world leading active remote sensing instrument. LADS is capable of surveying 50 sq km per operational day, with a sounding spacing of 10 m. Depth penetration is water quality dependant, but is estimated to be generally 30 m. At first glance it may seem that this instrument renders the use of passive remote sensing unnecessary. However it should be noted that, with development cost of $40 million for the single operational system and an estimated cost of $10 million to build another unit, this technology currently remains out of the range of any commercial surveying enterprise.

## 1.6 Aims of this Research

A number of processing methods for the extraction of bathymetric data from spectral imagery have evolved over the 23 years since work began in this field. Some have represented improvements on previous work, whereas others represent significant new departures.

This research aims to evaluate existing algorithms and compare their suitability as a means of generating bathymetric charts. The most promising of these algorithms will be applied to Landsat Thematic Mapper data for a test site off the Perth metropolitan coastline. This should illustrate the feasibility of using such data in a reconnaissance role and indicate the potential that data of greater spatial and spectral resolution may provide.

# CHAPTER 2

# DEVELOPMENT OF THE TECHNOLOGY

Techniques for the extraction of water depth from multispectral data have their basic origins in the physical theory of the transmission of light through water. They were first suggested before multispectral satellite data became readily available in the early 1970's and have been refined considerably since then.

## 2.1 Postulation of the Method

Prior to the launch of ERTS-1, the first spacecraft in the Landsat series, the potential for such systems to map hydrographic features had been recognised. This was demonstrated by work carried out under the U.S. Naval Oceanographic Office Spacecraft Oceanography Project at The University of Michigan in the late 1960's (Polcyn and Satinger, 1969). That work investigated, not only the use of multispectral imagery, but also gave consideration to the analysis of wave refraction patterns and to the use of pulsed lasers.

By analysis of imagery acquired at a flying height of 10,000 ft, the multispectral part of their study concluded that the optimum waveband for water penetration is in the 0.55 to 0.58 $\mu$m region. This contrasts with the optimum wavelength suggested from the observations of physical oceanographers, who indicate a wavelength of 0.475 $\mu$m as having the greatest attenuation distance in clear water (Jerlov, 1976).

The processing algorithm suggested by the 1969 study is based on the radiative transfer theory for a light ray passing through an atmosphere and water column and has remained at the core of all further algorithm development.

## 2.2 Investigations Using Early Landsat MSS

### 2.2.1 The Ocean Bathymetry Experiment

A joint project undertaken by NASA and the Cousteau Society in 1975 made the first real demonstration of the feasibility of satellite spectral bathymetry. The work was carried out during late summer in the Bahamas, off the Florida coast. In the clear waters around Berry Island depths of up to 22 m were measured, with a 10 percent RMS accuracy as verified by conventional survey, and bottom features at a depth of 40 m were perceivable on the imagery (Polcyn, 1976). Depth penetration to 10 m was achieved in coastal waters.

The sensor used for the NASA/Cousteau experiment was the Multispectral Scanner (MSS) on board Landsat 2. The MSS was operated in high gain mode for the acquisition of these data. The study revealed that depths could be deduced from satellite measurements without a knowledge of the optical parameters of the local waters.

### 2.2.2 Operational Charting

Encouraged by the success of this experiment, the United States Defence Mapping Agency embarked, in 1976, upon a program of chart revision. At that stage it was felt that the use of digital data for depth extraction was still a matter requiring further research. Their efforts made use of photographic products

generated from Landsat 2 high-gain MSS data.

The team's first reported success in this field occurred when working with a photographic image of the Chaigos Archipelago (6° 30' S, 72° 30' E). These waters had last been surveyed by the Indian Navy in 1837, with relatively poor positional accuracy in areas that were out of sight of land. The positions of several reefs were revised and a previously unknown reef added to the chart (Hammack, 1977).

Other work using Landsat MSS data includes the use of density contoured digital imagery for charting in the Red Sea (Benny and Dawson, 1983).

## 2.3 Initial Work in Australia

A number of studies and some operational work using the MSS sensor also took place in Australia. The Great Barrier Reef off the Queensland coast represented an area of relatively shallow water of high optical clarity, that was not charted in great detail. It therefore presented, not only an ideal area for the development of techniques, but also an opportunity for the first large scale demonstration, in Australia, of the use of satellite data for offshore mapping. Other areas of the Australian coastline which were the subject of studies were the Torres Strait area and, in Western Australia, Cockburn Sound and the waters around the Monte Bello Islands.

### 2.3.1 Research Work on Great Barrier Reef

Initial work on the Great Barrier Reef was carried out by investigators in the United States using Landsat 1 data. This concentrated on the mapping of reef

zonation rather than depth (Smith et al., 1975).

The study area was in the vicinity of Cape Melville (14° 15' S, 144° 45' E) and covered both clear offshore and turbid onshore waters. Whilst the effect of turbid waters in confounding the signal was noted, the fact that coral reef requires non-turbid conditions for growth meant that those effects could be ignored in this study. Similarly the effects of atmospheric haze, although noted within the image, were discounted by careful selection of study site.

This work made use of digital processing techniques, which included simple single-band density slicing, colour compositing and multispectral classification. Comparisons of the depth from which bottom returns were received were made between panchromatic aerial photography and Landsat MSS Band 4 data (0.5 - 0.6 $\mu$m). There was found to be little difference in the maximum depths recorded, although this figure was never quantified.

The investigators were unable to obtain direct ground truth data for the reefs in the study. The classification work used aerial photography for the identification of training sites with only one training area for each of the zonal categories. These training areas were reported as being not necessarily fully representative. Nevertheless, the report concluded that the zonation by classification techniques was reasonable, particularly with regard to biological categories.

The study, as reported, made no attempt to extract bathymetric information nor apparently to take into account the effect of attenuation on the bottom signal. This approach is valid in coral reef areas, since the biological zonation of the

reef, and hence bottom cover type, is depth controlled.

### 2.3.2 Operational Work on Great Barrier Reef

With the formation of the Great Barrier Reef Marine Park and its associated Management Authority in 1976, the need to rapidly collect information for management purposes became acute. At that stage there was no satisfactory mapping base for the Marine Park (Jupp et al., 1984).

Recognising the potential demonstrated by the earlier research work, the Marine Park Authority sought the assistance of the Commonwealth Scientific and Industrial Research Organisation (CSIRO) in carrying out further research and development work. This led to the development by CSIRO, working with the Australian Survey Office and James Cook University, of the Barrier Reef Image Analysis system. This system has since further evolved to become the Micro-BRIAN desktop image processing system.

### 2.3.3 BRIAN processing

Landsat MSS imagery for use in the creation of the Great Barrier Reef base map was rectified to the Australian Map Grid (AMG). The accuracy criterion used for this rectification was essentially that for 1:250,000 scale mapping, i.e. that 90 percent of independently chosen ground control points should fall within 0.5 mm of their known position on the rectified image. To achieve this, an RMS error of 64 m or better is required. The imagery for the Great Barrier Reef is reported to have been rectified such that RMS errors of 50 m were routinely achieved. A three stage rectification procedure, together with the generation of predictive error images, ensured the best use of relatively sparse

ground control information.

The primary products from this work took the form of enhanced imagery in photographic form. Raw images, depth of penetration (DOP) images, exposure images and images classified into spectral classes were generated.

The generation of depth of penetration images depends on the fact that the attenuation of light in water is wavelength dependant. The MSS bands used in that study do not encompass the theoretical optimum wavelength for clear water penetration. DOP images were produced covering zones representing 0.5 - 5 m, 5 - 20 m, and greater than 20 m.

Exposure images were created by first generating depths using an un-calibrated model based on the theoretical attenuation relationship. These depths were then used to generate, via slope and aspect calculations, the degree of exposure to the prevailing wind.

Classified images were generated to describe the various bottom cover and exposed reef types found within each image. For some areas, image texture computed as a local RMS value was used to provide extra discrimination of bottom type in areas too deep for penetration by more than one MSS waveband. The classification procedure used was essentially a maximum likelihood classifier with an iterative phase to permit retraining (Jupp et al., 1985). Use was made of canonical variate analysis in the determination of classes and class labels.

## 2.4 Other Australian Studies

A number of other studies were conducted in Australia using MSS data but no other operational charting was carried out.

### 2.4.1 Monte Bello Study

Surveys carried out in the late 1970's off the Monte Bello islands (20° 30' S, 115° 30' E) afforded an opportunity for a comparison between multispectral bathymetry using Landsat MSS data and photogrammetric methods. Depth penetration of up to 20 m was achieved (Honey and Byrne, 1978).

### 2.4.2 Work in Torres Strait

Experiments carried out in Torres Strait reported water penetration of up to 20 m using Landsat MSS data with accuracy of 10 percent of measured value. Calculated but unverified depths of penetration of up to 40 m were reported for MSS Band 4 (Warne, 1978a). This study also investigated some of the noise components of Landsat MSS data, their implication for the use of digital data as a hydrographic mapping tool, and methods of overcoming some of them. The use of multi-temporal imagery to overcome optical anomalies in the water column was suggested. The radiometric and spatial resolution limitations of the MSS were noted as being impediments to the use of such data, other than for reconnaissance work in support of other depth determination methods (Warne, 1978b).

### 2.4.3 Experimental Work in Cockburn Sound, W.A.

In an experiment designed to compare the use of summer and winter data for bathymetric work, MSS data for the area of Cockburn Sound was analysed by

workers at the University of New South Wales in 1984. A single band model using Band 4 (0.5 - 0.6$\mu$m) was tested with apparently disappointing results. Depth resolution was reported as being only 25 percent of depth at 10 m for a June image. Penetration depth of up to 20 m was reported for the January image but the dynamic range of six digital counts from waterline to 10 m depth, and a further two to 20 m, highlighted the problems associated with using the MSS instrument. An interesting approach to removal of periodic striping adopted by this study was to apply offsets, derived from the supposedly uniform deep water response, to the relevant detectors (Gee and Forster, 1984). A destriping algorithm of this nature is only suitable for use with imagery containing large homogenous areas such as deep water.

## 2.5 Work Using Landsat Thematic Mapper Data

In 1982 data from the Landsat Thematic Mapper (TM) with its enhanced spatial, spectral and radiometric resolution became available to researchers. Such data were not available for Australia until 1986 when the CSIRO/AMIRA signal processing experiment began reception.

### 2.5.1 Work on Great Bahama Bank

One of the earliest and most extensive investigations of the use of Landsat TM data for bathymetry was carried out in the area of the Great Bahama Bank. This site had previously been used for a Photo-Bathymetry experiment, which had provided a quantity of support data. These support data were of a high degree of accuracy comprising soundings with a positional accuracy of better than 3.1 m and whose depths were recorded with an instrument resolving to 0.01 m (Tanis

and Hallada, 1984).

The researchers noted the improved radiometric resolution offered by the Thematic Mapper, as well as the presence on the instrument of detectors with a bandpass closer to the theoretical optimum for water penetration. Their work highlighted the problems associated with random noise and made some attempt at investigating the composition of that noise. It was reported that the accuracy of the work was affected by the effects of preprocessing of the data tapes prior to delivery (Hallada, 1989).

One and two band regression models were analysed and a bottom cover index map generated, in addition to bathymetric charts. The RMS error of predicted water depth was found to be of the order of 1 m for an un-vegetated bottom but up to 3.95 m for a vegetated bottom. This highlights the need to account for bottom cover variations. Depth penetration to 21 m for TM Band 1 was reported and 14 m for Band 2.

### 2.5.2 Australian Work Using Landsat TM Data

Work sponsored by the fishing industry in Western Australia and carried out by CSIRO was designed to use Thematic Mapper data to assess the suitability of shallow ocean areas north of Broome (17° 37' S, 122° 13' E) for both pearling and prawn trawling. This study, although not specifically aimed at the recovery of bathymetric information, did establish useful relationships between the TM data and bathymetry, especially for areas of uniform sandy bottom (Hick and Scoones, 1988).

A study of the optimum time of year for imagery was also undertaken with

the conclusion that midsummer was preferable. It is, however, important in tropical waters to avoid phyto-plankton blooms which can severely restrict depth penetration at all wavelengths (Hick, 1992).

## 2.6 Airborne Work

A number of workers have made use of airborne multispectral scanners (AMSS) for the collection of over-water data with the potential to yield bathymetric information.

These instruments typically have greater spatial resolution than satellite sensors and may have a considerable number of water penetrating bands. They also have, at altitudes appropriate for high spatial resolution, a narrow swath width and relatively poor geometric capabilities. This renders accurate georegistration of the data somewhat more difficult than for satellite data.

### 2.6.1 M8 AMSS Active/Passive Instrument

The Environmental Research Institute of Michigan, pioneers in the use of multispectral data for bathymetry, developed an active/passive scanner in the late 1970's.

This instrument combined a multispectral scanner with a tuned laser (LIDAR), with the intention of providing one LIDAR depth for every 7800 scanner pixels. The initial published work, relating to experiments in the Bahamas with this instrument, used data with a spatial resolution of 8 m (Lysenga, 1981). The data were processed using a variation on the algorithm for the determination of depth-independent bottom reflectance from satellite MSS data

(Lysenga, 1978), and a comparison was made between the results. The increased number of water penetrating bands in the data set from the M8 AMSS were cited as the reason for the superior performance of that instrument.

In a further experiment, the M8 multispectral data were calibrated using the tuned laser depths. Calibration was effected by regression between the LIDAR depth and a band pair ratio. This is essentially a technique to extrapolate the broadly spaced LIDAR depths over a finer grid and, as such, is analogous to using depth information from conventional acoustic sounding to calibrate the model. The processing method used was capable of almost completely separating the depth information from the 'dry' bottom reflectance (Lysenga, 1985).

### 2.6.2 The Daedelus 1260 AMSS

Possibly the most widely flown commercially available airborne multispectral scanners are the Daedelus 1260 instruments. Experiments in Canada in the early 1980's involved the simultaneous collection of data from a 1260 scanner, an aerial camera and the acquisition of ground control data.

In an initial analysis, using five bands, the imagery was corrected for sensor look angle and atmospheric effects. Depths were extracted using radiative transfer models to assess the utility of those models. The depths derived from a modified two-flow model were then compared to the ground truth observations and found to agree well (correlation coefficient of 0.89) for depths up to 10 m (Weidmark et al., 1981). It was noted, however, that a depth offset of 0.3 m was present between the data sets.

Further work using the same data (Jain et al., 1981) extended these results

to eight of the available spectral bands. This, combined with the use of a more accurate atmospheric correction method, resulted in an accuracy of depth estimation quoted as 0.15 m.

Work in Australia using a Daedelus 1260 for sand movement monitoring was undertaken in 1986. This was a pilot project and used a depth determination model based on the calibration of image data by conventional soundings. The depths were determined to a reported RMS accuracy of 0.435 m up to a maximum depth of 15 m (Danaher and Smith, 1988).

### 2.6.3 The Fluorescent Line Imager

A two dimensional array imager of 'pushbroom' type, programmed to provide a bandset similar to that of the NIMBUS Coastal Zone Colour Scanner, was tested for its applicability to bathymetric work in the Gulf of Mexico. The data were first processed to provide a bottom cover classification. A subsequent processing pass used a depth dependant algorithm to generate a look up table, from which depths at individual pixels could be estimated. Comparison with available soundings suggests that systematic errors of up to 2 m in depth exist in the resulting chart, although a relative accuracy of 0.5 m was claimed (Hollinger et al., 1985).

## 2.7 Studies Using SPOT

The French SPOT satellite seems to be less well suited to bathymetric work than the Landsat Thematic Mapper, due to its lack of a blue band. Nevertheless a number of workers have used SPOT multispectral data for seabed studies.

Working with data from the Cook Islands (19° S,160° W), a French Pacific team proposed the use of a method intermediate between the physical model and the regression methods. This approach segments the bottom into luminance classes based on the physical model and then establishes a regression relationship within those classes. Mean errors were reported as high (21 percent) for depths less than 3 m but better ($\approx$10 percent) in the range 3 to 10 m. A segmented image map was produced with segments at 1 m intervals down to a depth of 8 m. (Lemaire et al., 1990 ; Loubersac et al., 1991).

## 2.8 Theoretical studies

A considerable amount of work has been done using theoretical and simulated data sets for the testing of depth extraction algorithms. Some recent studies suggest potentially viable methods for processing the data used in this research.

Spitzer and Dirks (1987) considered the implications, for a number of potential algorithms, of variations in water quality and bottom type for data from a wide range of scanners. O'Neill and Miller (1989) suggest the use of a spatial iteration of the multi-band regression methods developed for Landsat TM and AMSS data. This is intended to cope with environmental parameters such as bottom type, which can be expected to vary at a different spatial frequency from depths. Philpot (1989), using a synthetic data set, surmised that not only spatial but temporal information would be of use in solving for varying environmental parameters.

## 2.9 Summary

The development of techniques for the extraction of water depth information from multispectral data may be traced over the past 23 years. It progresses, from beginnings in the late 1960's, through a series of experiments and applications using both satellite and airborne data acquisition systems.

Early techniques range from work using photographic products generated from Landsat MSS imagery through to the use of digital Landsat MSS data for charting waters, to depths of 20 m, around the Great Barrier Reef. The advent of Landsat TM data, with its improved spatial and spectral resolution provided impetus for further work. Successful use was made of TM data for charting in the Bahamas with depths to 21 m being measured with an RMS accuracy of one metre. Airborne sensors have also been used for bathymetric work, with some studies reporting an RMS accuracy of 0.5 m, or better, for measurements of water depths up to 15 m.

Some recent theoretical studies postulate techniques, such as the use of spatial modelling to overcome changing environmental parameters, which may be candidates for the processing of the TM data to be used in this study.

# CHAPTER 3

# SENSORS AND SENSOR PLATFORMS

## 3.1 Accuracy and Resolution

In its Standards for Hydrographic Surveys (IHO, 1987), The International Hydrographic Bureau lays down a series of acceptable scales and accuracies for hydrographic surveys. These may be considered in relation to the potential of various remote sensing systems.

### 3.1.1 Scale

For ports and pilotage waters a chart scale of 1:10000 is stipulated. This increases to 1:25000 for harbour approaches and to 1:50000 for coastal waters to 30 m depth (40 m under special circumstances). Surveys in deeper waters to 200 m may be conducted at a scale of 1:100000.

It is recommended that survey lines be spaced such that the plotted distance between lines on the chart is not greater than 10 mm, at the scale of the survey. It should be noted that, for soundings collected by a conventional echo sounder, the soundings that appear on the chart are the least depths that occur in the swath swept, on the sea bed, by the echo sounder beam. A typical beam width is 30 degrees. Swath width is therefore depth dependant, but at a depth of 10 m would be 5 m.

Taking the scales above as a guide, soundings on a chart require to be spaced at a minimum of 100 m for harbour work. In practice the spacing of the

sounding lines is closer and governed by the echo sounder beam width and the nature of the sea bed.

### 3.1.2 Positional and Depth Accuracy

In the same IHO standards document, positional accuracies for individual soundings are specified as being such that there is a 95 percent probability of a sounding falling within 1.5 mm, at plotted scale, of its true position. This translates to $\pm$ 15 m at 1:10000.

Depth accuracy is specified more stringently. A 90 percent probability is required that the error does not exceed 0.3 m for depths to 30 m. An error of one percent of depth is allowed for deeper water.

## 3.2 Ability of Remote Sensing to Meet Requirements

### 3.2.1 Spatial Considerations

The signal received by the detector of a remote sensing instrument is, discounting any atmospheric or other transmission effects, an integrated function of the radiance received from all that is within its instantaneous field of view (IFOV).

Unlike an echo sounder, a remote sensing detector does not pick up the extreme value of the imaged surface. Instead, as a first approximation, which assumes a linear mixture model, it detects the area-weighted mean of that which falls within the IFOV.

Under the assumed condition of a uniform seabed cover, with only

moderate relief, this could provide a good estimate of the mean depth in the IFOV. In cases of sudden changes in depth, such as presented by reef edges and particularly by isolated coral pinnacles, the estimate of mean depth may be of little value to the hydrographer or mariner.

Clearly the size of the IFOV is of considerable importance in the matching of a remote sensing system to a particular offshore mapping application.

### 3.2.2 Effect of Data Quantisation

The digital nature of remotely sensed data means that the data which are available for processing are in integer form. The exponential nature of the transmission of light through water means that the depth change represented by each digital number increases as depth increases.

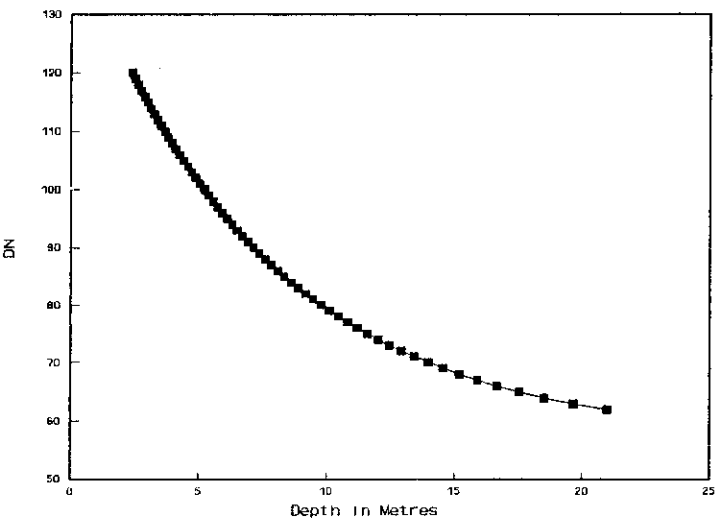


Figure 3.1 : Depth versus digital number (DN)

Using the physical model of light transmission through water, and data from a study in the Bahamas (Hallada, 1984), the relationship between depth and digital count and between depth and depth resolution for 8 bit data may be plotted. These are shown in Figures 3.1 and 3.2.

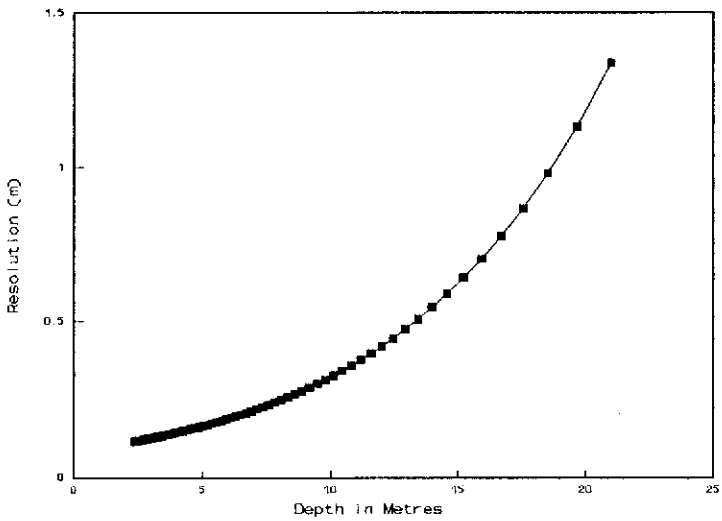


Figure 3.2 : Depth versus resolution per DN

It may be seen from these figures that, if the signal quantisation is increased to 10 bits, the resolution per digital count at 18 m depth increases from 1.2 m to a more acceptable 0.3 m.

A study aimed at determining the optimum design characteristics for a bathymetric sensor (Tanis and Byrnes, 1985) determined that noise components in the signal become a problem with 12 bit quantisation and 10 bit is therefore recommended.

### 3.2.3 Spectral Considerations

As most of the effective methods of depth extraction rely on the use of multiple water penetrating bands for resolution of bottom cover type problems, it is desirable that a sensor has a number of narrow wavebands within the blue - green region of the spectrum. The relationship between the spectral transmittance and wavelength for clear water at a range of depths is shown in Figure 3.3.

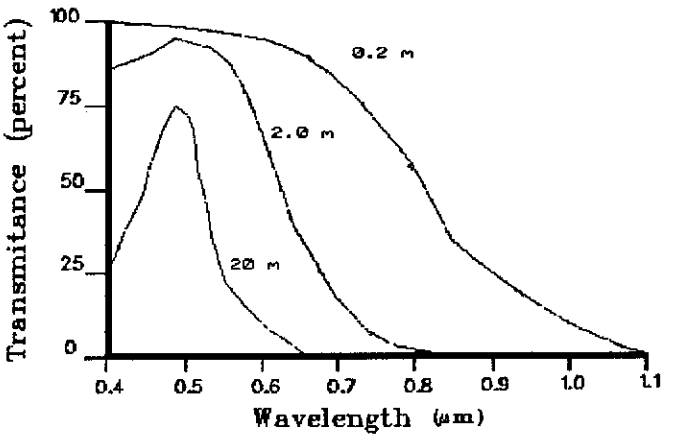


Figure 3.3 : Relationship between wavelength and transmittance for clear water at a range of depths (After Lusch, 1989)

Figure 3.3 indicates that the optimal spectral range to position sensors is between 0.45 and 0.55 $\mu$m.

### 3.3 Potential Satellite Sensors

A number of satellite sensors, and several airborne instruments, exist which may be considered as sources of suitable data. Satellite systems have fixed spatial, spectral and radiometric characteristics, but allow the selection of data from a considerable archive if required. Data from these systems can be obtained at moderate cost.

Airborne systems are more flexible but require the mounting of special data acquisition missions with attendant higher costs and the dangers of down time due to bad weather.

The following satellite sensors, which have the potential to provide data for bathymetric work are reviewed here :

(a) Landsat Thematic Mapper (TM)

(b) Landsat Multispectral Scanner (MSS)

(c) System Probotoire pour Observation du Terre (SPOT)

### 3.3.1 Landsat Thematic Mapper

The most widely available data source for multispectral bathymetry is Landsat Thematic Mapper (TM) data.

The Thematic Mapper has been carried on Landsat satellites since the launch of Landsat 4 in 1982. Reception facilities for Australia were not available until 1986 when a joint CSIRO/AMIRA signal pre-processing experiment began data acquisition. Data from this period are not of as high quality as those which is currently provided by the Australian Centre for Remote Sensing (ACRES). ACRES, who have reception facilities at Alice Springs and a processing centre in Canberra, have been responsible for the collection and distribution of TM data in Australia since 1988.

TM Band 1 (blue, 0.45-0.52 $\mu$m) is centred near the wavelength for theoretical maximum depth penetration of clear water. Additional wavelengths of use in the TM data set include Band 2 (green, 0.52-0.60 $\mu$m) and Band 3 (red, 0.63-0.69 $\mu$m) both of which penetrate water to some degree and can be used in a multi-band model. The near infrared bands, Band 4 (0.76-0.9 $\mu$m) and Band 5 (1.55-1.65 $\mu$m), are of use in delineating land/water boundaries. Spatial

resolution for all bands on the Thematic Mapper is 30 m except for the thermal band, Band 7 (10.4-12.5 $\mu$m) for which resolution is 120 m.

The Landsat satellites, currently represented by Landsat 5, which is deployed at an altitude of 705 km, are in sun-synchronous orbit with a descending node (daytime) overpass at a local time of 09:30 hrs. The repeat period for any one location is 16 days.

The scanning system of the Thematic Mapper uses an oscillating mirror to produce an optical swath across a track 185 km wide. This swath is projected onto a detector bank which has 16 detectors for each of the visible and near infrared bands and four for the thermal band. The effect of this swath method of data collection can be seen as periodic stripping in some images. This is particularly noticeable on imagery of homogenous areas such as deep water.

The TM detectors produce analogue signals, which are measures of the radiance received. These signals, which are quantised to 8 bits by the on board analogue to digital converter, are multiplexed prior to transmission to the ground station. The eight bit quantisation results in data which have 256 levels.

### 3.3.2 Landsat MultiSpectral Scanner

Data from the Landsat Multispectral Scanner (MSS) lack both the Blue and Thermal bands that are present in data from the Thematic Mapper instrument. In the years from 1972 to 1982 the MSS was the only routinely available source of multispectral data.

The MSS has four wavebands, all in the reflective part of the spectrum.

They are green (0.5-0.6 $\mu$m), red (0.6-0.7 $\mu$m), and two near infrared bands at 0.7-0.8 $\mu$m and 0.8-1.1 $\mu$m. The nominal field of view for each ground resolution cell is 79 m square but resampling geometry means that the actual pixel area is 56 m across track by 79 m along track.

MSS systems have been carried on all satellites of the Landsat series and data have been received in Australia since 1980. The orbital details are as for the TM instrument for Landsat 4 and 5. The first three satellites in the series were similar but had a repeat cycle of only 18 days.

The scanner is an oscillating mirror system but data is only recorded during scans in a left to right direction. The track width is the same as for the TM but the optical swath is projected onto a bank of only six detectors. This results in a stripping effect with a period of six lines being visible on some MSS imagery. The instrument has 6 bit quantisation on board giving 64 levels, which are converted by the receiving station to 128.

### 3.3.3 SPOT

The French satellite System Probotoire pour Observation du Terre (SPOT) has been in orbit since 1986. Data are received in Australia using the same ACRES facilities as are used for Landsat Thematic Mapper data. So far two satellites in a planned series of four have been launched.

The satellite carries the High Resolution Visible (HRV) imaging system. This instrument has green (0.50-0.59 $\mu$m), red (0.61-0.68 $\mu$m) and near infrared (NIR) (0.79-0.89 $\mu$m) bands in addition to a panchromatic band. The spatial resolution is 20 m for the multispectral bands and 10 m for the panchromatic

band. In terms of the system's suitability for water penetration work it has been suggested that the lack of a blue band is in some measure compensated for by the later data acquisition time of 10:45 hrs with its attendant higher sun angle. (Hick and Scoones, 1988).

The satellite is deployed in a sun-synchronous near polar orbit at an altitude of 830 km. The repeat cycle over any one location is 26 days but the system is equipped with steerable mirrors which mean that any one scene can be imaged, off nadir, several times during the orbital cycle. This mirror capability also permits the acquisition of stereo images.

The sensor on the HRV is a 'pushbroom' array of 6000 charge-coupled devices (CCD). This reduces the dependence on mechanical systems and all pixels in an image line are sensed simultaneously. The detector signal is quantised to 8 bits (256 levels) prior to transmission.

### 3.4 Airborne Systems

Airborne systems have some advantages for bathymetric work if suitable ground control points to allow their geometric rectification can be found.

Their principal advantages are that the data acquisition time can be controlled and that the number of available bands is generally greater. The former allows maximisation of sun angle or choice of tidal state, whilst the latter has obvious advantages in the application of multi-band algorithms. In addition airborne systems, being flown at lower altitudes, generally have considerably better spatial and radiometric resolution and do not suffer as greatly from atmospheric effects.

A number of systems are suitable for bathymetric work. The following three systems are considered here :

(a) Geoscan Mark II

(b) Compact Airborne Imaging Spectrometer

(c) CSIRO Ocean Colour Scanner

### 3.4.1 Geoscan Mk II Scanner

This is a West Australian owned and operated scanner designed primarily for mineral exploration work. The system records 18 channels, selected out of 32, in the wavelength range 0.45 - 2.50 $\mu$m and a further six channels in the thermal infrared region. The system has an IFOV of 3.0 milliradians and a total field of view of $\pm$ 45 degrees from nadir. At 3000 m above ground level this gives a pixel size of 6 m for an imaged strip 6 km wide. The instrument incorporates corrections for roll, pitch and yaw. The scanner is mounted in a twin engined aircraft and may be interfaced to a navigation system. Data are quantised to 8 bits and recorded on optical disks.

### 3.4.2 Compact Airborne Imaging Spectrometer (CASI)

The CASI is a Canadian built instrument which utilises 'pushbroom' CCD technology. In a typical configuration for oceanographic use, the optics project an imaged strip onto a CCD array 512 elements wide by 288 elements deep. Each of these 288 strips acts as a simultaneous set of detectors for one 0.0014 $\mu$m wide band between 0.4 and 0.8 $\mu$m. Due to data recording constraints only 40 channels of these data can be recorded. Alternatively the instrument may be operated to provide full 288 channel information for a selected number of spatial

positions.

The instrument fore-optics have a field of view of 30 degrees and provide an IFOV of 1.4 mrad. At a flying height of 3000 m this gives an effective imaged width of 1.6 km and a pixel size of 3 m. The system is lightweight and has low power consumption requirements making it suitable for mounting in light aircraft or helicopters. Data are quantised to 12 bits and recorded on helical scan tape.

### 3.4.3 CSIRO Ocean Colour Scanner

This research system is a rotating mirror scanner designed principally for ocean colour work. It was built for mounting in the CSIRO F27 research aircraft. There are nine channels available of which six span the spectral range 0.44 to 0.4 $\mu$m with band widths of 0.2 $\mu$m. The fore-optics provide a field of view of 90 degrees and an IFOV of 4 mrad. This provides for an imaged area of 6 km at 3000 m flying height with a pixel size of 12 m. Data are quantised to 12 bits and recorded on helical scan tape. Data from this instrument have been used in studies of chlorophyll concentration in Western Australian waters (Hick, 1992).

## 3.5 Summary

Scale and accuracy considerations are of importance in assessing the suitability of any remotely sensed bathymetry system. The International Hydrographic Bureau lays down strict guidelines covering these issues. For chart production at 1:10000 scale depths must be measured with an accuracy of $\pm$ 0.3 m and located within 15 m of their true position. The ability of remote sensing systems to meet these guidelines must be considered from the standpoints of

production at 1:10000 scale depths must be measured with an accuracy of $\pm$ 0.3 m and located within 15 m of their true position. The ability of remote sensing systems to meet these guidelines must be considered from the standpoints of spatial and spectral resolution as well as data quantisation.

A review of a number of potential satellite systems indicates that, none is capable of meeting the requirements for detailed charting. Several may be capable of use as broad scale mapping tools in a reconnaissance role. Among the airborne systems some, particularly the CASI, may be capable of operation as survey tools, if flown at an appropriate altitude. Of the satellite systems reviewed, the Landsat Thematic Mapper offers the best combination of accessible data, spectral and spatial resolution for investigation as a reconnaissance tool.

# CHAPTER 4

# PHYSICAL PRINCIPLES

The use of remotely sensed data for the determination of water depth relies as its central principle on the fact that, for any given wavelength, the attenuation of light with water depth is an exponential function, assuming a homogenous water column. In the case of passive remote sensing the light in question is natural sunlight and the wavelengths in question are determined by the sensor design. Essentially the signal received at a sensor contains a number of components which are illustrated in Figure 4.1.

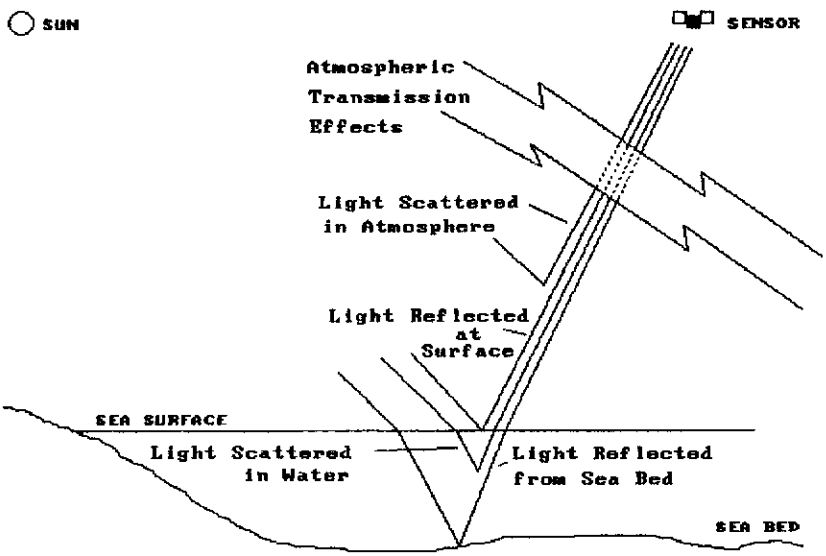


Figure 4.1 : Ray paths to a sensor

## 4.1 Radiative Transfer Model

A simple reduction of the elements illustrated in Figure 4.1 breaks them

down into components related to atmospheric transmission, sea surface components, and components related to transmission through the water column. Jupp (1988) describes the radiance received at the sensor (***Lrec***) for any waveband ***j*** as being:

$$Lrec_j = Ta_j\ (L_j + Ls_j) + La_j \qquad (4.1)$$

where $Lrec_j$ is the signal recorded

$Ta_j$ is an atmospheric transmission factor

$L_j$ is the radiance from the water column

$Ls_j$ is the radiance reflected from the water surface

$La_j$ is the radiance due to atmospheric scattering

In Equation 4.1 the term ***Lj*** , the radiance received from the water column, essentially comprises two further components, signal reflected from the bottom and water body signal. Their relationship may by expressed as :

$$L_j = Tw_j \times Lb_j + (1-Tw_j)\ Lw_j \qquad (4.2)$$

where $Tw_j$ is a water transmission factor

$Lb_j$ is the radiance of wet bottom material (with no water cover)

$Lw_j$ is the radiance of infinitely deep water

That is to say, for completely opaque water conditions ($Tw_j = 0$), all signal is deep water signal and, for completely transmissive water ($Tw_j = 1$), all

signal is from wet bottom. The exponential nature of the transmission of light though water means that the term $Tw_j$ may be represented in terms of a further constant $K_j$ thus:

$$Tw_j = e^{(-2K_jZ)} \tag{4.3}$$

where $K_j$ is a water-type transmission constant for wavelength $j$

$Z$ is the water depth

## 4.2 Atmospheric Transmission Effects

In cases where the data to be used are of one date and the whole area of interest is covered by one image, it is possible to ignore the atmospheric effects in Equation 4.1. This assumes atmospheric homogeneity over the extent of the image. If data from more than one date are used, some further modelling of atmospheric parameters must be undertaken.

Under the assumption that imagery is cloud free, and of a single date, with the further assumption of an optically homogenous atmosphere, Equation 4.2 may essentially be reduced to :

$$L_j = Lw_j + (Lb_j - Lw_j)\, e^{(-2K_jZ)} \tag{4.4}$$

Rewriting Equation 4.4 to solve for depth gives :

$$Z = -\frac{1}{(2K_j)}[\ \ln (L_j - Lw_j) - \ln (Lb_j - Lw_j)\ ] \qquad (4.5)$$

For any given water column $Lw_j$ and $K_j$ are constants and for any given bottom type $Lb_j$ is a constant. Hence under an assumption, for a particular area, of uniform water type and bottom cover, the equation may be reduced to a simple linear expression whose coefficients represent water type and bottom type.

$$Z = a_0 + a_1 X_j \qquad (4.6)$$

where $X_j = ln\ (L_j - Lw_j)$

In Equation 4.6, $L_j$ and $Lw_j$ are related to the digital number recorded for each pixel by a gain and offset, enabling the use of the digital numbers as surrogates for the radiances.

### 4.3 Transmission Effects in the Water Column

The term $-2\ K_j$ in the above discussion is related to the optical extinction properties of the water column. The constant 2 implies a round trip condition. Factors affecting the magnitude of the term $K_j$ may loosely be described as those pertaining to water clarity and combine the processes of absorption and scattering that occur within the water column.

4.3.1 Absorption and Scattering - the Two Flow Model

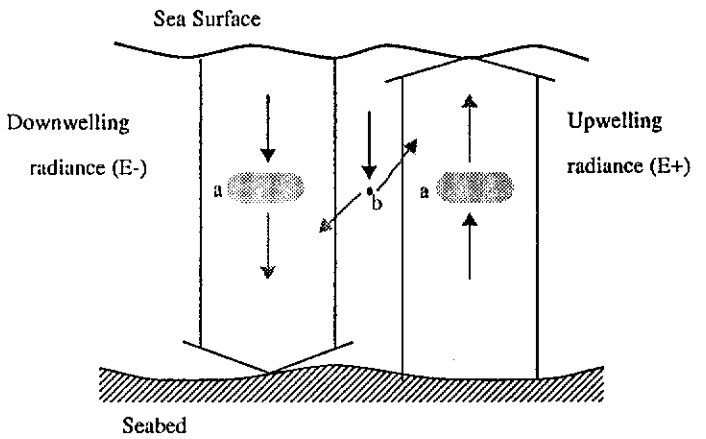


Figure 4.2 : Light paths in a water column

Figure 4.2 details a breakdown of light paths within the water column. The components may be divided into the downwelling *(E-)* and upwelling radiances *(E+)*. For an infinitely deep water column there is no reflected component from the sea bottom. Joseph (1950), cited in Doerffer (1979), derived a formula which relates $R$, the ratio of upwelling and downwelling radiances, to the absorption coefficient $a$ and backscattering coefficient $b$:

$$R = \frac{(E+)}{(E-)} = \frac{\sqrt{1 + 2\frac{b_j}{a_j}} - 1}{\sqrt{1 + 2\frac{b_j}{a_j}} + 1} \qquad (4.7)$$

From Equation 4.7 the diffuse irradiance attenuation coefficient $K_j$ may be calculated as :

$$K_j = \sqrt{a_j\ (a_j+2b_j)} \qquad (4.8)$$

where $a_j$ and $b_j$ are the absorption and scattering coefficients at wavelength j. It may also be shown (Jupp, 1988) that the emerging radiance at the surface of infinitely deepwater ($Lw_j$ in Equations 4.2 et seq.) is :

$$L_{wj} = \frac{(a_j+b_j-K_j)}{b_j} \qquad (4.9)$$

4.3.2 The Diffuse Attenuation Coefficient

The diffuse attenuation coefficient of seawater has been the subject of much research. Models other than the two-flow example outlined above have been suggested (Jain and Miller, 1977 ; Philpot, 1987). A number of workers have conducted measurements of this coefficient for various water types. An extremely comprehensive account of these measurements is presented by Jerlov (1976). That work classified sea water on the basis of optical clarity into Ocean Types I (the clearest) to III and Coastal Types 1 to 9 in order of increasing effective attenuation coefficient. Table 4.1 shows the diffuse attenuation coefficient for some of these water types at a range of wavelengths.

The potential exists to use the two flow and other attenuation models to determine information about the chlorophyll concentrations and sediment loads of offshore water masses, and a body of literature exists concerning these applications. Where the signal contains some reflected bottom component it may

be used for bathymetry. If an assumption is made that within a limited area the optical parameters will vary little, then a bathymetric model based on Equation 4.6 may be calibrated by the use of known depths. Alternatively, if the parameters $a_j$ and $b_j$ can be measured or estimated, the possibility exists to extract depth information directly from the remotely sensed signal. This research will use a depth calibrated method.

| Water Type | I | II | III | 1 | 3 |
|---|---|---|---|---|---|
| Wavelength (μm) | Attenuation coefficient ($m^{-1}$) | | | | |
| 0.310 | 86 | 69 | 50 | 16 | 9 |
| 0.350 | 94 | 84 | 71 | 32 | 19 |
| 0.375 | 96.3 | 89 | 79 | 54 | 34 |
| 0.400 | 97.2 | 92 | 84 | 69 | 53 |
| 0.425 | 97.8 | 93.5 | 87 | 79 | 66 |
| 0.450 | 98.1 | 94 | 88.5 | 84 | 75 |
| 0.475 | 98.2 | 94 | 89 | 87.5 | 80 |
| 0.500 | 97.2 | 93.5 | 89 | 88.8 | 82 |
| 0.525 | 96.1 | 92.5 | 88.5 | 88.5 | 82 |
| 0.550 | 94.2 | 90.5 | 86.5 | 86.5 | 81 |
| 0.575 | 92 | 87.5 | 82.5 | 82.5 | 78 |
| 0.600 | 85 | 80 | 75 | 75 | 71 |
| 0.625 | 74 | 71 | 68 | 68 | 65 |
| 0.650 | 70 | 67.5 | 65 | 65 | 62 |
| 0.675 | 66 | 63.5 | 61 | 61 | 57 |
| 0.700 | 59 | 56 | 54 | 54 | 51 |

Table 4.1 : Diffuse attenuation coefficient for five water types (after Jerlov,1976)

### 4.3.3 Internal Reflection

In shallow waters, the possibility exists that some internal reflection may take place between the underside of the sea surface and the seabed. This may cause the relationship between received radiance leaving the water column and

depth to diverge from that which pertains in deeper waters. A possible strategy to address this problem is the segmentation of the image, such that different model coefficients can be developed for use in shallow water areas.

### 4.4 Summary

The basic physical principles governing the attenuation of light within water bodies allow a model to be developed which relates depth to radiance leaving the water column. That radiance is subsequently modified by atmospheric transmission effects and is also subject to variations caused by non-uniform optical properties in the water body. If assumptions are made about the spatial distribution of atmospheric effects, and some means is provided to take account of spatial variations in optical characteristics, it is then possible to develop algorithms for the extraction of depth information from the signals received at a remote sensing platform. Chapter 5 looks at the development of some of these algorithms.

# CHAPTER 5

# DATA PROCESSING ALGORITHMS

Several algorithms for the extraction of depth information from remotely sensed data have been published. In essence they are all related by their dependence on the basic physical principles presented in Chapter 4. The symbols and abbreviations used in this discussion of potential algorithms follows those used in Chapter 4.

## 5.1 Depth of Penetration Methods

Depth of penetration methods in their simplest form may be regarded as a simplification of methods that rely entirely on observed spectral data. The depth of penetration (DOP), of any wavelength in a given water type, is the depth at which the signal is attenuated by some fraction of the input signal. This fraction is frequently regarded as 90 percent.

Measurements have been made for a variety of water types ranging from clear ocean water to turbid coastal waters. The standard reference for these parameters is the work of Jerlov (1976). Gordon and McCluney (1975) and Jupp (1988) derive, using different methods, a maximum theoretical penetration depth of 55 m for the clearest ocean water type ( Type I ).

Figure 5.1 is a plot of DOP against wavelength using Jupp's method from Jerlov's data for ocean Water Type I and for coastal Water Types 1 and 3. In practice this depth of penetration will be reduced due to less than optimal sun

angles. Depth of penetration zones are those to which the respective

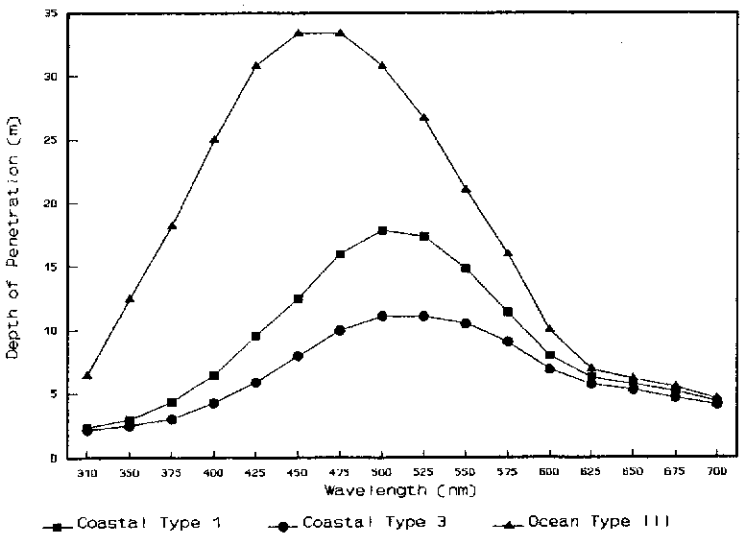


Figure 5.1 : Theoretical depth of penetration against wavelength

bands of a multispectral scanner will theoretically penetrate. It is not possible to make precise measurements of DOP zones directly from multispectral data, but the image may be segmented into representative zones if some assumptions are made. These assumptions are that the sea bed (wet but uncovered) is significantly brighter than the deep water radiance, that the water type is homogenous, and that there are no significant variations in bottom cover in the area under investigation.

The basic algorithm for DOP work may be described as follows:

Step 1: Mask the image to exclude land areas based on infrared band data.

Step 2: Obtain histograms and statistics for a deep water area for all bands.

Step 3: Take maxima and minima from these statistics such that:

Max band i = $Bmax_i$ Max band j = $Bmax_j$

Step 4: Segment image as follows:

FOR $K_i > K_j$

IF $L_j > Bmax_j$ AND Li $<= Bmax_i$

THEN pixel is in DOP zone j.

Care must be exercised in cases where $K$ does not increase with wavelength. Typically this only occurs with data sets possessing more than one band whose central wavelength is 0.475 $\mu$m or less.

Extensions to this method allow interpolation within the zones and a degree of calibration using some known depths.

## 5.2 Regression Methods

Essentially all methods for which some known depth data are available may be described as regression methods. The basic vehicle for the regression is provided by Equation 4.6 above. A number of refinements of the method exist, which endeavour to take into account variations in bottom type and water quality. For all these methods it is necessary to be able to link each sounding used as control to a pixel in the image.

### 5.2.1 Single Band Method

The simplest form of regression method is the single band method in which, for an area of known uniform bottom cover, the coefficients of Equation 4.6 above are derived by the relationship of known depths to the relevant pixel digital counts. The appropriate depth for all other pixels is then computed by

application of those coefficients. This method has recently been reported as providing depth information to 37 m from Landsat MSS data of Penang, Malaysia (Ibrahim and Cracknell, 1990). Unfortunately no error analysis for that study is presented.

The single band method algorithm proceeds as follows:

Step 1: Compute coordinate transformations between control soundings and image data.

Step 2: Determine deep water threshold ( $Lw_j$ ) for relevant band.

Step 3: Extract pixel values for relevant band from image.

Step 4: For each extracted pixel value determine the value

$$X_j = Ln(L_j - Lw_j)$$

Step 5: Perform regression of depth vs. $X_j$ for each control sounding.

Step 6: Assign depth values to other pixels based on coefficients from regression.

5.2.2 Ratio Methods

The use of ratios in remote sensing removes the effects of components in the signal that are common to all wavelengths and highlights components that are not. The presence, in any area under consideration of more that one bottom type, renders the assumptions made by the single band and DOP methods invalid. The basic ratio algorithm relies on the assumption that a pair of wavelengths exist, such that the ratio of the bottom reflectances in these bands is the same (Lysenga, 1978).

Mathematically expressed, the ratio method assumes that, for bottom types *1,2,3* etc. and wavebands *i* and *j* :

$$RB = \frac{R_{1_i}}{R_{1_j}} = \frac{R_{2_i}}{R_{2_j}} = \frac{R_{3_i}}{R_{3_j}} \quad etc \tag{5.1}$$

This ratio assumption allows the rewriting of Equation 4.5 as :

$$Z = \frac{1}{2(K_i - k_j)} \times \left[ \ln\left(\frac{K_i}{K_j}\right) - \ln\left[\frac{(L_i - Lw_i)/(L_j - Lw_j)}{RB}\right]\right] \tag{5.2}$$

where $K_i$, $K_j$ are attenuation constants for the two bands

$L_i$, $L_j$ are received radiance at the sensor

$Lw_i$, $Lw_j$ are deep water radiances

$RB$ is the ratio of bottom reflectances

Combining all constant or assumed constant terms a regression of the natural log of the ratio of signals in the two bands against depth may be performed. The simplified expression is :

$$Z = a_0 + a_1(X_i - X_j) \tag{5.3}$$

where $X_i = ln(L_i - Lw_i)$

$X_j = ln(L_j - Lw_j)$

The algorithm for the ratio method is similar to that for the single band method:

Step 1: Compute coordinate transform between control soundings and image data.

Step 2: Determine deep water threshold ($Lw_j$) for each band to be used.

Step 3: Extract pixel values for each band from image.

Step 4: For each extracted pixel value determine the values

$$X_i = ln(L_i - Lw_i) \ , \ X_j = ln(L_j - Lw_j)$$

Step 5: Perform regression of depth vs. $(X_i - X_j)$ for each control sounding.

Step 6: Assign depth values to other pixels based on coefficients from regression.

5.2.3 Multi-band Methods

Multi-band methods operates under a generalised ratio assumption with a derivation that is an extension of that for the ratio model. This method has been reported in the work of Paredes and Spero (1983). The essential equation reduces to one similar to Equation 5.4 above, but having as many coefficients as there are bands and hence as many discriminable bottom types.

$$Z = a_0 + a_1X_1 + a_2X_2 + ..... a_nX_n \qquad (5.4)$$

In practice for satellite imagery the maximum value for $n$ is three and the depth to which the higher wavelength band penetrates may be less than one metre. The method would have greater potential if applied to airborne data of higher spectral dimension. The algorithm is essentially the same as for the two band ratio model except in the form of the equation used in the regression.

### 5.2.4 Multi-band Method with Spatial Iteration

It has been suggested (O'Neill et al., 1987 ; O'Neill and Miller, 1989) that an improvement to the multi-band method may be made if the spatial context of the pixels is considered. The principle is that environmental changes such as water quality and bottom type will occur at a different, lower, spatial frequency than depth changes. Work by O'Niell and Miller (1989) used a simulated data set and assumed a one dimensional case for spatial variation.

Essentially the method solves the regression equation, expressed here in matrix form:

$$Z = A\ X \tag{5.5}$$

The relationship is then made in the spatial domain between the depth residuals resulting from the solution of Equation 5.5 and their position. This may be expressed in matrix notation as :

$$\delta Z = Z_{calc} - Z_{true} = Y\ B \tag{5.6}$$

where $\boldsymbol{Y}$ is a matrix of spatial positions

$\boldsymbol{B}$ is a vector of coefficients

Equation 5.6 may be solved by matrix inversion to give the coefficient vector $\boldsymbol{B}$. These coefficients are spatially dependant and may be applied to the other pixels in the image. A potential algorithm would proceed as for a multi-band regression and then as follows :

Step 6: Perform spatial regression to establish spatially dependant coefficients

Step 7: Apply waveband dependant coefficients and spatially dependant coefficients to image pixels to produce depth surface

### 5.2.5 Multi-band Ratio Model

Workers using a synthetic TM data set (Spitzer and Dirks, 1987) found that the best measure of $\boldsymbol{X}$ for use in the regression method was obtained from a three band ratio. This ratio is expressed as follows :

$$X = \ln\left[\frac{(L_1 - Lw_1 + L_2 - Lw_2)}{(L_3 - Lw_3)}\right] \qquad (5.6)$$

An implementation of this follows the same process as for a multi-band method except in the method of calculation of the variable $\boldsymbol{X}$.

### 5.2.6 Hybrid Methods

Some workers have used a combination of techniques in their development

of methods. One such method for three bands of TM data uses a multi-band model for depths that can be penetrated by all bands, reducing to a single band model for depths that can be penetrated only by band 1. This method has been used for work in the Bahamas with depths to 16 m being measured with an accuracy of a little over 1 m (Tanis and Hallada, 1984).

### 5.3 Classification Methods

Another solution to the problem of varying bottom cover type is to first use a 'classical' classification technique to segment the bottom into cover classes and to then run regression models for each cover class. This method has merit if some information is available on the likely bottom classes to be found.

A similar approach has been tried with some success on SPOT HRV data of Pacific atolls. In that case the image was subdivided into 'luminance classes' in an image space, formed by rotation of the data in response to the ratio of waveband attenuation coefficients (Lemaire et al.,1990).

### 5.4 Multi-temporal Methods

In situations where suspended sediment is likely to be a problem, a multi-temporal algorithm may be appropriate. The principal disadvantage of multi-temporal methods in general is that radiometric transfer parameters, as well as illumination factors, such as sun angle, will not be the same for both images. Therefore it is necessary to apply some form of radiometric standardisation to the images used. This is a complex process in itself and is still the subject of research (Hill and Sturm, 1991).

Multi-temporal data have been digitally processed in two ways: firstly, to enhance depth penetration by temporal averaging (Polcyn and Lysenga, 1979) and, secondly, to produce depth data relating to two or more dates for quality control and morphological studies (van Hengel and Spitzer, 1991).

On the assumption that radiometric standardisation has been carried out, a possible multi-temporal algorithm would compare values on a pixel by pixel basis and produce a composite, sediment minimising, set of bands as input to one of the algorithms described above.

### 5.5 Summary

A number of potential algorithms suitable for the processing of Thematic Mapper data have been published in recent years. They cover a considerable range of complexity. Some have been published as part of case studies using real data and some have been postulated as theoretical but validated using synthetic data. They can be broadly categorised as either calibrated methods that use known depth points as input to a regression, or uncalibrated methods which derive depth estimates directly from remotely sensed data. An adaptation of a spatially iterated multi-band regression method, previously tested with synthetic data, has the potential to enhance the accuracy of reconnaissance charting using Landsat TM data. This method was chosen for application in this study.

# CHAPTER 6

# DATA ACQUISITION AND REGISTRATION

## 6.1 Choice of Study Area

During the early stages of this work, the possibility of using airborne multispectral imagery was considered. At that time the only airborne instrument available in Western Australia was the Geoscan Mark I scanner. It was arranged that data from this 13 channel device be collected for a coastal swath covering Warnbro and Cockburn Sounds (Figure 6.1). The choice of these areas was partly governed by the fact that the scanner was being flown in those areas, partly by their geographical location and partly by the bottom topography.

Cockburn Sound has a good range of depths down to 22 m whilst Warnbro Sound extends down to 19 m. Both areas are partly enclosed by islands which facilitates geometric rectification of imagery. Cockburn Sound has areas of sea bed covered by calcareous sand with a high albedo. Such is the purity of this sand that it is commercially extracted as raw material for the Cockburn Cement plant.

Initial work with the Geoscan data was generally disappointing. There were considerable problems of rectification despite the presence of adequate control points. This, together with problems of data noise and sun glint, essentially rendered the data unusable for bathymetric purposes.

A decision was taken to restrict the study to the use of Landsat Thematic Mapper imagery. This imagery has coarser spatial resolution than the Geoscan

MKI data, but has similar spectral resolution in the visible wave bands. As TM data are routinely available it is possible to select scenes with optimal environmental conditions.

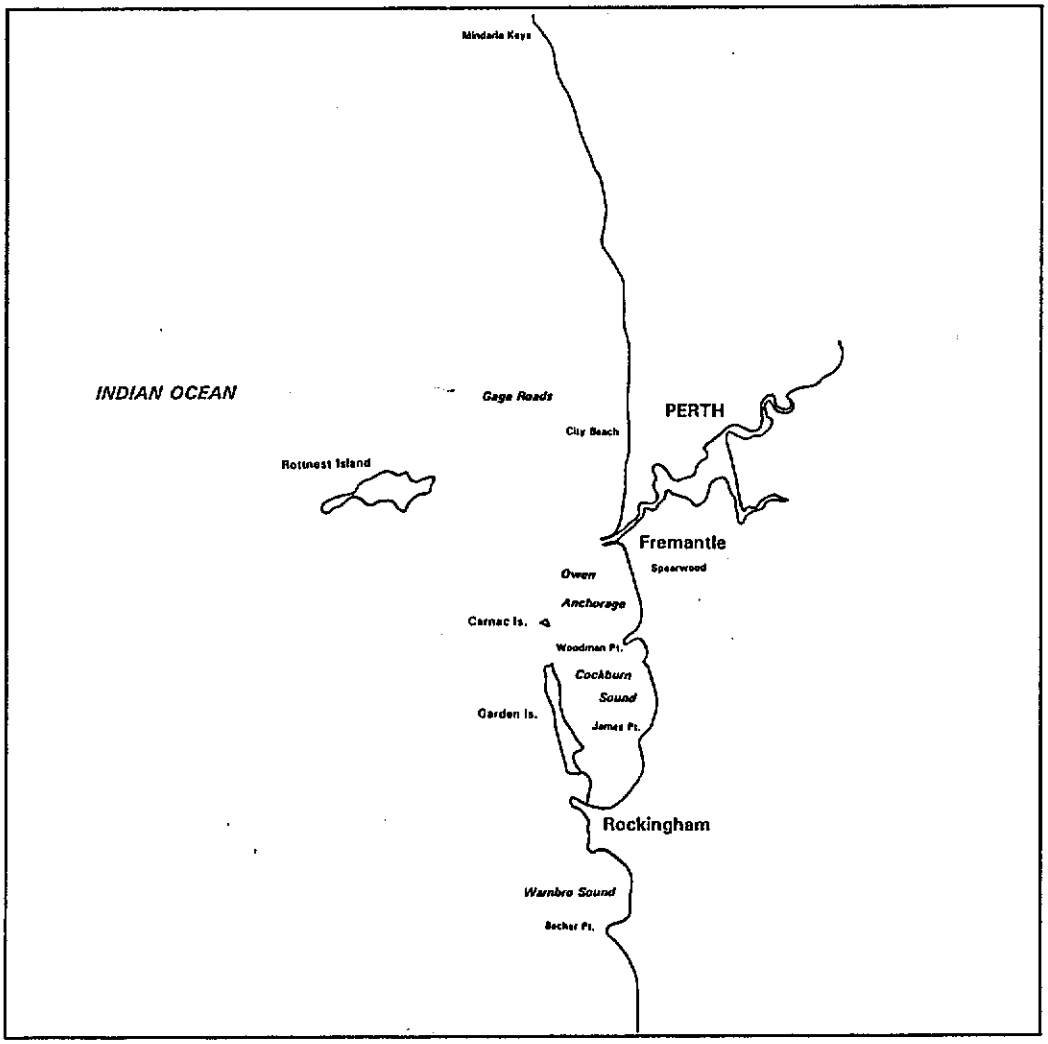


Figure 6.1 : The coastline of metropolitan Perth

## 6.2 TM Data Acquisition

Permission was obtained from the Remote Sensing Applications Centre (RSAC) of the Western Australian Department of Land Administration (DOLA) to gain access to data purchased by them on behalf of other projects. This permission was granted on the understanding that the data were to be used solely

for research purposes. The quick-look prints for a number of images were inspected at RSAC and the image for 25 th February 1990 was selected as the best available.

### 6.2.1 Image Characteristics

The image comprises path 112 row 82 in the Landsat Worldwide Reference System (WRS) and is centred on 31° 46' S, 116° 37' E. The sun elevation for this image is 42 degrees with an azimuth of 70 degrees. The maximum achievable sun elevation for this latitude, at the time of Landsat overpass, is 53 degrees. The data chosen represents the best combination of availability, overall image quality, cloud cover and sun angle.

### 6.2.2 Data Transfer

The data were available at RSAC on two 9 track 1/2 inch magnetic tapes as delivered from ACRES. In order to minimise the effort required by RSAC personnel, the entire scene, including header and trailer information was transferred to 'Exabyte' high density storage tape as a series of anonymous files. This tape was the read onto the CSIRO remote sensing system using the Unix 'dd' command. This command allows reading from a block device to a named file. The data values for the block of data from the second tape, which covers the area from just north of Mindarie Keys to just south of Becher point, were then converted to DISIMP format. The DISIMP utility INHDD was used for this conversion. Once in the DISIMP environment the data could be inspected and subsetted using the DISIMP routines SUBSET and IMPCPY. Details of the DISIMP image processing system and modules used in this study can be found in

Appendix A.

## 6.3 Area Selection and Description

The image data were inspected, whilst referring to hydrographic charts, to determine a suitable sub-area for detailed analysis. A 1000 pixel square sub-image covering the coast from City Beach to James Point was selected. This sub-image extends seaward to include the eastern end of Rottnest Island, Carnac Island and the northern part of Garden Island. The area of Parmelia Bank was selected for the testing of the multi-band spatial iteration algorithm identified in Chapter 5. A further sub-image of 330 lines by 500 samples was identified for this detailed work, whilst the 1000 by 1000 pixel image, having areas of deep water, was retained for noise removal work. Figure 6.2 shows this study area.

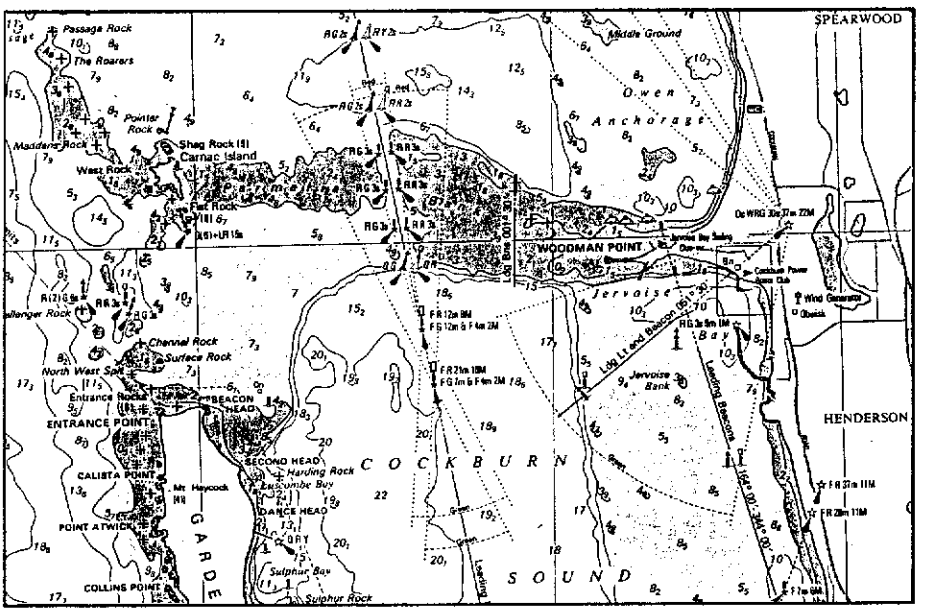

Figure 6.2 : Parmelia Bank study area

The coastline of south-west Western Australia has a number of sub parallel ridges representing stages in the marine transgression of the coast. These ridges

are separated by depressions. Cockburn Sound lies in depression between the Spearwood Ridge and the Garden Island Ridge. Over the past 10,000 years changes in sea level have resulted in cycles of erosion and accretion. These have resulted in a land bridge between the two ridges at Rockingham and in the production of two submerged sills, the Parmelia and Success Banks (DCE, 1979). In addition, wave action on the eastern side of the sound has cut a shelf of depth six to eight metres into the Spearwood Ridge. On the south side of the Parmelia Bank the sea bed shelves gradually at the western end of the bank but more abruptly at the eastern end. A dredged channel has been cut through the bank to connect the two harbours of Cockburn Sound and Owen Anchorage.

The landward end of the Parmelia Bank forms Woodman Point. The eastern extremity of the bank forms Carnac Island. The sea bed on the Parmelia Bank is a predominantly calcareous sand with patches of seagrass (Posedonia sp). The Cockburn Cement operation to mine calcareous sand for cement production has shore facilities at Woodman Point. During a site visit to the study area it was ascertained that the area currently being dredged for production purposes is in the Success Bank. Material is brought from there in hopper barges and discharged into a suction sump at a jetty on the north side of the point. Figure 6.3 is a view westwards across Parmelia Bank from Woodman Point.

### 6.4 Bathymetric Data

The ideal bathymetric data set for a study such as this would be one collected at the same time as the satellite overpass. This would allow some estimate of water quality to be made. The data set would ideally consist of digital easting/northing/depth triplets as recorded by the navigation and

sounding equipment on a vessel. Similar data from an airborne LIDAR system would also serve. Given the constrains of this project, funding among them, the acquisition of a data set contemporaneous with a satellite overpass was not possible.

In areas that are relatively sheltered, and not at the mouths of major rivers, there is likely to be little natural change in sea bed topography in the short to medium term. Consequently, data collected at a time other than that of the overpass may be used with some degree of confidence.

Figure 6.3 : View westwards from Woodman Point

Enquires among the hydrographic community failed to produce any suitable digital data. Fremantle Port Authority was able to make available some

digital easting/northing/depth data for sounding lines run directly out from the mouth of the Swan River. These soundings, which are along the main navigation approach to the Port of Fremantle, have a very small range of values. This rendered them unsuitable for this study.

The best published source of soundings for the Parmelia Bank is the Admiralty 1:25000 Chart AUS 117. The soundings, in the area used, range from less than one metre down to a little over 22 m and are fairly well distributed throughout the range.

### 6.4.1 Digitising

Soundings covering an A3 section of the chart were digitised using the DIGITIZE module of the raster GIS program IDRISI. As the chart graticule is in latitude and longitude, the soundings were digitised onto an arbitrary XY grid for later registration to the Australian Map Grid. A total of 318 soundings was digitised. The soundings were digitised in a stratified random order. That is, they were randomly selected within the boxes formed by the chart graticule, which were taken in a regular order of increasing easting and northing. Due to an operational problem it was necessary to digitise the soundings in two sessions. This required the digitisation of the set up points for each session. Sixteen intersection points on the chart graticule were used as set up points. These intersections were taken at intervals of one minute in latitude and two minutes in longitude. Details of the IDRISI software may be found in Appendix A.

### 6.4.2 Tidal Correction

Soundings published on Admiralty Charts are reduced to a Tidal Datum. The height of the sea surface at the time of a satellite overpass will vary from this datum. Tidal information for the Port of Fremantle, for the date on which the image data were acquired, 25 th February 1990, was obtained from the Australian National Tide Tables. High water at 11:23 hrs was 0.7 m and had been preceded by low water of 0.4 m at 05:08 hrs. By interpolation, using the sinusoidal grid method in the Tide Tables, the tidal height at 09:30 hrs, the time of the Landsat overpass was determined to be 0.63 m. This value was added to the depth value of all digitised soundings.

## 6.5 Co-registration of Data

In order that accurate relationships may be made between the pixels in the imagery and the geographical features to which they relate, imagery must be registered to a suitable map grid.

### 6.5.1 Australian Map Grid

The map grid used for this study is the Australian Map Grid (AMG), which is conventionally used for all mapping in Australia. This grid is based on the Universal Transverse Mercator projection and holds to the same zone numbering conventions. Zones are six degrees in longitude from east to west with the origin being the point of intersection of the Central Meridian and the Equator. Coordinates are defined in relation to a false origin 500,000 m west and 10,000,000 n south of the true origin (NMCA, 1972).

### 6.5.2 Warping and Resampling

The data received at a satellite sensor for each pixel represent the reflected radiation for a particular area of the earth's surface, modified by its passage through the atmosphere. If the data are not changed in any way prior to analysis, then the maximum amount of spectral information may be extracted from them. Unfortunately it is not practicable to work with data that are both geometrically and radiometricaly 'raw'. It is, however, desirable to keep alterations to the data to an absolute minimum.

The geometric characteristics of the satellite orbit and the curvature and rotation of the earth all affect the geometry of the satellite image. The pixels are, by their very nature, recorded in a rectangular fashion. The recording takes place in such a way that the geographical location of each 16 line swath of data is offset from the preceding swath by approximately one pixel across track. Corrections for this are applied by the ground station receiving the data. There is some along-line resampling at this stage using a damped eight point sinc function. In addition some radiometric corrections are applied. The image delivered from the receiving station to a client is therefore not the raw data as received from the satellite. It has had some preprocessing applied to it that is outside the control of the client.

Some workers warp an image to fit a suitable map grid, prior to the comparison of image and ground truth data. This requires further resampling of the data. Even in the case of a nearest neighbour resampling scheme it is possible for artefacts to be included in the data at this stage. This study adopted the alternative approach of mapping the ground truth to the image pixels. The ground truth, being represented as real vector coordinates, is much more amenable to

transformation than the raster data representation of the image.

This mapping comprised four principal steps. Firstly, the transformation between the AMG and the digitiser coordinates of the soundings was determined. Secondly, the soundings coordinates were converted to AMG. Thirdly, the transformation between the AMG and the image data was determined, and finally the soundings were allocated to the appropriate image pixels.

### 6.5.3 Transformation Software

Two separate programs were used in the calculation of transformation parameters. The first of these (UTM) was written by a fellow post-graduate student and is designed to convert between geographical coordinates and the Universal Transverse Mercator projection, of which the AMG is a subset. Transformations may be carried out in either direction. The program uses the Australian National Spheroid as a default but offers the option of entering any spheroidal parameters.

The second program (RTRANS), written by a staff member at Curtin, is designed to calculate and apply transformations between rectangular coordinate systems. The program compares two control point files and calculates the transformation parameters between the systems using any of the following transformations:

(a) Conformal

(b) Affine

(c) Projective

(d) Second order polynomial

(e) Second order conformal

(f) Third order polynomial

The program displays and writes to an optional file the transformation parameters and residuals for both a forward and inverse transformation. If the appropriate input file contains, in addition to the control points, a number of X,Y,Z points in one system these will be converted and written to the output file.

Some modules from the DISIMP image processing system were also used in the registration process.

## 6.6 Registration of Soundings to AMG

As described in Section 6.4.1 the graticule of the chart from which the soundings were taken is referenced in latitude and longitude. AMG coordinates for these graticule intersection points were calculated using UTM. Transformation parameters between these AMG coordinates and the appropriate digitiser coordinates were calculated using RTRANS for each of the two digitiser setups. Due to differences in the x and y scaling of the arbitrary coordinate system adopted for the digitiser tablet, a projective transformation was used. The RMS of the transformation residuals was 3.5 metres in both eastings and northings. Tables 6.1 and 6.2 list the residuals in easting and northing for the transformation between digitiser coordinates and AMG.

RTRANS was then used to convert the digitised soundings to AMG coordinates. In order to provide both an experimental and a control set of soundings, a simple C language routine was written to separate the raw digitiser

file into two files each containing alternate soundings from the input stream. Figures 6.4 and 6.5 show the frequency distribution of the two sets of soundings.

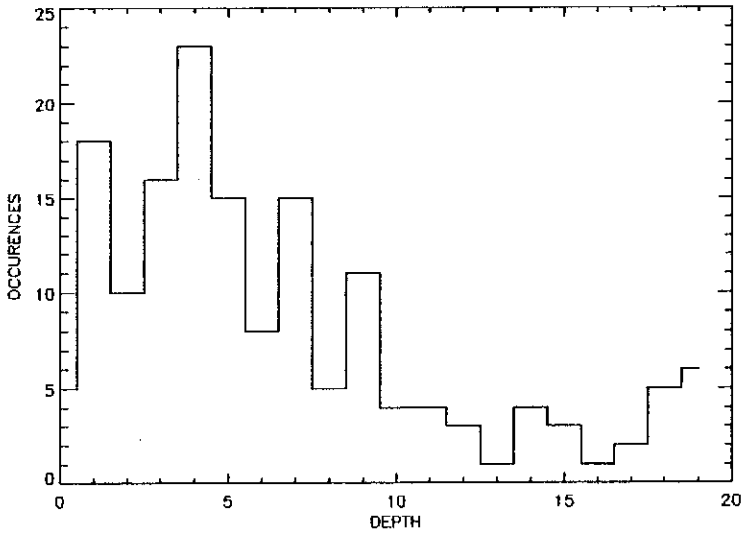


Figure 6.4 : Frequency distribution of control sounding set

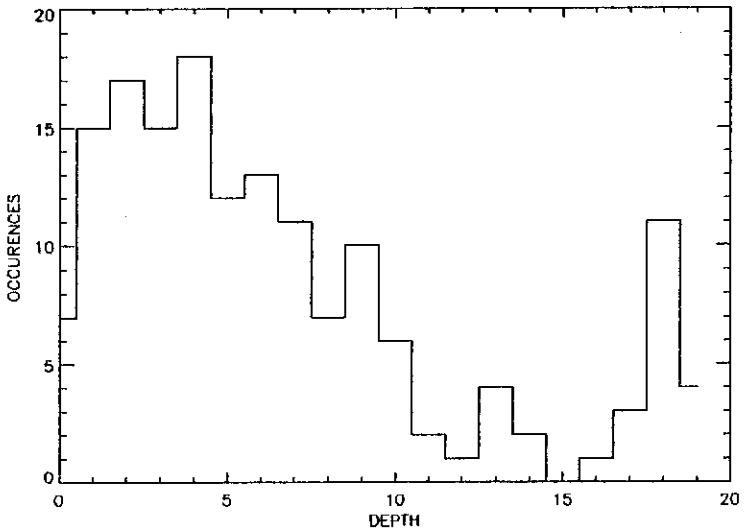


Figure 6.5 : Frequency distribution of check sounding set

| Point No | Digitiser coords. | | AMG (m). | |
|---|---|---|---|---|
| | X | Y | E | N |
| 1 | 0.615 | -0.263 | 0.1 | 5.7 |
| 2 | 0.259 | -0.147 | -2.1 | 1.2 |
| 3 | -0.114 | -0.079 | -5.1 | -1.7 |
| 4 | -0.764 | -0.097 | 0.2 | -1.7 |
| 5 | -0.005 | 0.138 | 5.5 | 4.2 |
| 6 | 0.052 | 0.267 | -0.3 | -0.2 |
| 7 | -0.095 | 0.269 | -0.5 | -0.5 |
| 8 | -0.373 | 0.418 | 2.5 | -5.6 |
| 9 | -0.401 | 0.42 | 3.5 | -5.6 |
| 10 | -0.006 | 0.365 | -3.5 | -3.6 |
| 11 | -0.039 | 0.222 | 2.8 | 1.3 |
| 12 | 0.057 | 0.226 | 3.4 | 1.3 |
| 13 | -0.795 | -0.006 | 1.3 | -4.7 |
| 14 | 0.014 | -0.205 | -9.4 | 2.4 |
| 15 | 0.129 | -0.181 | 2.3 | 2.3 |
| 16 | 0.637 | -0.242 | -0.7 | 4.9 |
| RMS Error | 0.388 | 0.248 | 3.6 | 3.5 |

Table 6.1 : Residuals from digitiser to AMG transformation (first setup)

| Point No | Digitiser coords. | | AMG (m) | |
|---|---|---|---|---|
| | X | Y | E | N |
| 1 | 0.641 | -0.757 | -0.5 | 2.3 |
| 2 | 0.164 | -0.790 | 0.9 | 2.8 |
| 3 | -0.253 | -0.709 | -0.7 | -0.3 |
| 4 | -0.843 | -0.514 | 2.2 | -6.9 |
| 5 | 0.071 | -0.449 | 2.8 | 4.2 |
| 6 | 0.166 | -0.278 | -4.2 | -1.3 |
| 7 | -0.109 | -0.361 | -0.3 | 1.1 |
| 8 | -0.246 | -0.412 | -2.1 | 2.5 |
| 9 | -0.382 | -0.167 | 2.3 | -5.1 |
| 10 | 0.013 | -0.242 | -4.2 | -2.6 |
| 11 | -0.082 | -0.284 | 3.8 | -1.1 |
| 12 | 0.157 | -0.376 | 0.0 | 1.9 |
| 13 | -0.912 | -0.650 | 4.3 | -2.7 |
| 14 | -0.022 | -0.765 | -8.1 | 1.4 |
| 15 | 0.141 | -0.807 | 1.7 | 3.4 |
| 16 | 0.560 | -0.692 | 2.1 | 0.4 |
| RMS Error | 0.408 | 0.558 | 3.2 | 3.0 |

Table 6.2 : Residuals from digitiser to AMG transformation (second setup)

## 6.7 Registration of Image Data to AMG

For the 330 by 500 pixel sub-image covering the Parmelia Bank, six well defined control points were located in the image. The DISIMP utility LOCATE was used for point selection. The ground points representing these image pixels were identified on large scale maps and charts. Coordinates were scaled off the maps directly as AMG values. For points on offshore islands the Latitude and Longitude values were converted to AMG using UTM. The transformation between the two systems was calculated using the DISIMP WARP utility and confirmed using RTRANS. In both cases, due to the inherently good satellite geometry an affine transformation was used and resulted in residuals with an RMS error of less than 0.7 metres in both eastings and northings. Table 6.3 shows the residual output from the DISIMP utility WARP. The soundings from both the control and check sets were then transformed using RTRANS to image pixel coordinates.

| Seq | Error | | Calculated | | Actual | |
|---|---|---|---|---|---|---|
| | X | Y | X | Y | X | Y |
| 1 | 0.7 | 0.3 | 728.3 | 1668.7 | 729.0 | 1669.0 |
| 2 | -0.5 | -0.3 | 744.5 | 1790.3 | 744.0 | 1790.0 |
| 3 | -0.1 | 0.1 | 829.1 | 1983.9 | 829.0 | 1984.0 |
| 4 | 0.2 | 0.4 | 1113.8 | 1984.6 | 1114.0 | 1985.0 |
| 5 | 0.8 | -1.2 | 1056.2 | 1831.2 | 1057.0 | 1830.0 |
| 6 | -1.1 | 0.7 | 1035.1 | 1756.3 | 1034.0 | 1757.0 |
| Mean square error (x,y,xy): | | | 0.6578 | | 0.6174 | 0.9022 |

Table 6.3 : Residuals from image to AMG transformation

## 6.8 Summary

A study area, the Parmelia Bank in Cockburn Sound, was selected on the basis of availability of data and of suitability of bottom topography. Disappointing results from an early investigation of some airborne scanner data led to the decision to limit this study to the use of satellite data. Digital Landsat Thematic Mapper data were acquired, and soundings from a portion of an Admiralty Chart were digitised. Figure 6.6 shows the progress of these data through the processes described in this chapter.

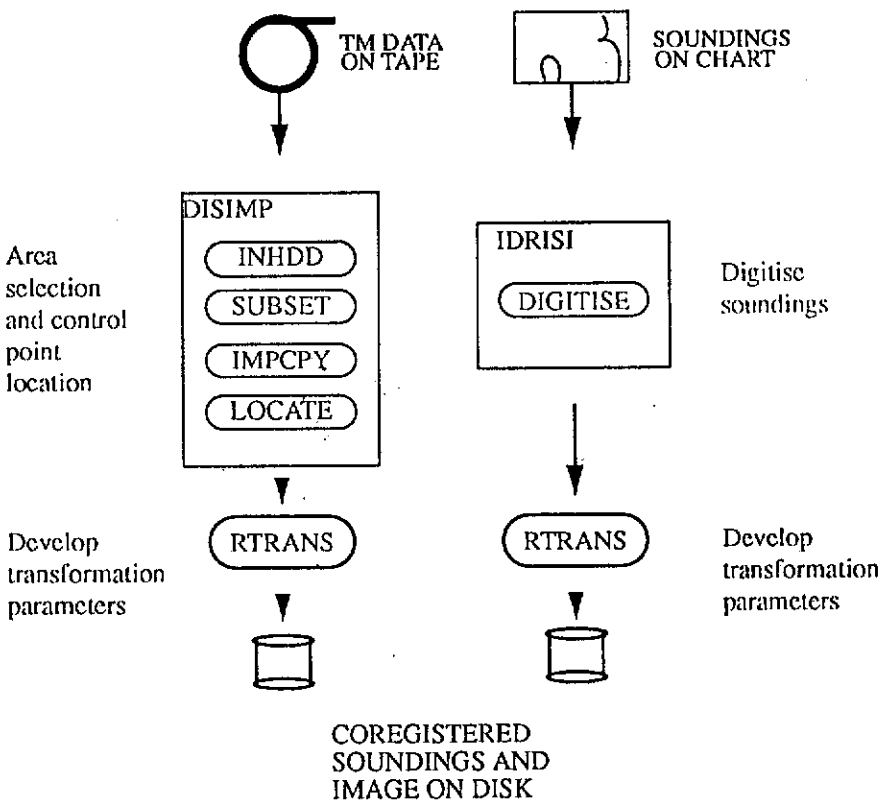


Figure 6.6 : Flowchart - Data input and coregistration

The need for a common spatial reference frame between remotely sensed data and ground truth was addressed by the co-registration of both datasets

through the common medium of the Australian Map grid. This approach, rather than the warping of the image data to fit the map grid, allows spatial resampling to be kept to a minimum. Some unavoidable resampling of the data has already been applied by the signal reception facility. A transformation was established so that each sounding can be related to a particular image pixel.

# CHAPTER 7

# SIGNAL PREPROCESSING AND NOISE REMOVAL

All digital satellite data contain some noise. In work using statistical classification methods for information extraction, this noise may be regarded as being sufficiently random as to not bias the outcome. In a study such as this, where an attempt is being made to relate the magnitude of a physical parameter to a remotely sensed signal, the noise may be significant. There is therefore some merit in trying to reduce the effects of such noise.

## 7.1 Noise Characteristics

Two forms of noise are likely to be present in multispectral satellite imagery used for bathymetric work. One, periodic striping, is physical in nature and is entirely sensor dependent. The other is environmental in nature and includes sunglint, atmospheric variations and water quality variations. Periodic striping and sunglint may be removed in a preprocessing phase prior to the application of a depth extraction. Atmospheric and water quality variations are among the spatial effects which the proposed spatial iteration of the multi-band algorithm is seeking to model.

### 7.1.1 Periodic Striping

The principal form of noise present in multispectral imagery is striping. This is caused by unmatched detectors in the sensor. As described in Chapter 3, the Landsat TM instrument records data in 16 line swaths. For each line in that

swath, each waveband has a unique detector. As each of the detectors within a swath has slightly different physical characteristics and response to incident radiation, a striping pattern is visible even over a homogenous surface. This difference in response is due principally to the detector transfer function between incoming raw radiance and outgoing signal. Even if this function is assumed to be linear, the gains and offsets used will vary between detectors (Richards, 1986).

If no further radiometric processing of the signal takes place, then the striping will have similar characteristics for each swath. However processing of the signal does take place, firstly on board the satellite and again at the receiving station before the data are distributed to the end user. Among these preprocessing steps is the conversion of the analogue signal generated by the detector to a digital signal with eight bit quantisation. This has the potential to cause two adjacent detector readings that differ by less than half of the magnitude of one digital count to be recorded as differing by one count.

The receiving station also applies an image wide destriping correction. This appears to have the effect of modifying the nature of the striping pattern in response to the surface that the detectors have recently been scanning. This is particularly noticeable at a land water interface, where changes in striping pattern may be seen to coincide with features such as headlands and bays. Figure 7.1 shows the effect of this on imagery of the Warnbro sound area.

### 7.1.2 Sunglint

Sunglint may be present in two forms in over-water images. The presence of either of them depends on the geometric relationship between the sun, the

sensor and the surface of the water.

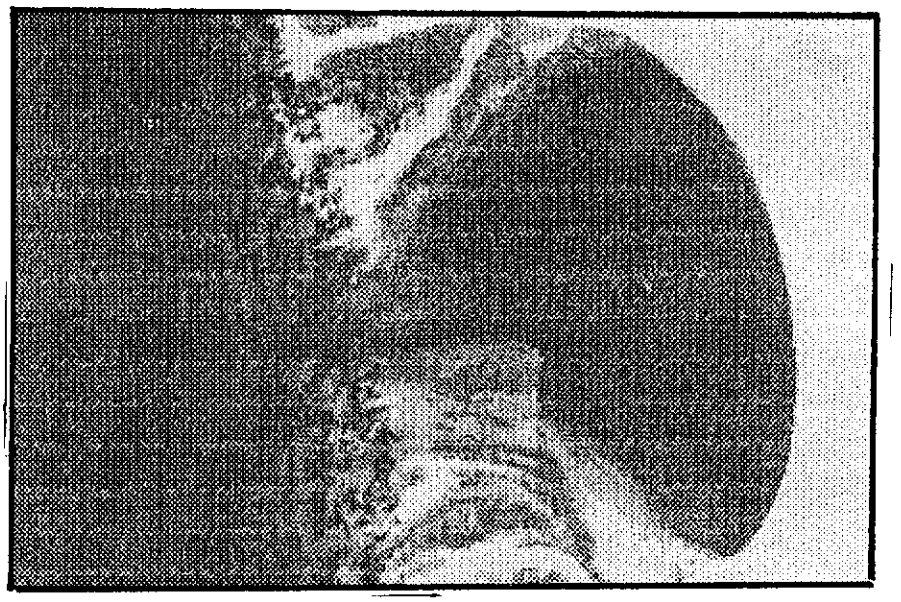

Figure 7.1 : Striping in a TM Band 1 image of Warnbro Sound

The water surface will behave in part as a specular reflector and will, for a certain proportion of incident light, obey the basic physical law that, for a plane specular reflector, the angle of incidence and angle of reflection of light are equal. If the sea surface is flat then, under some sun angle conditions, a greater amount of radiation will be reflected into the sensor than under others. Since the angle at the sea surface between the sun and the sensor changes across the image, so will the degree of sunglint.

In addition, where the surface of the sea is disturbed by waves, wave facets may present a surface at a suitable angle so as to induce sunglint. This will vary across an image with wave direction, magnitude and relative geometry. Sunglint from waves has been used to deduce sea surface wind parameters using Advanced High Resolution Radiometer data from the TIROS range of satellites (Wald and Monget, 1983).

## 7.2 Image Inspection

Each band of the 1000 pixel by 1000 pixel subarea described in Section 6.3 was displayed using the COLOR85 option in IDRISI. The default IDRISI colour palette was used. This has the effect of mapping 16 consecutive digital counts, in the band under inspection, to different colours. It is possible to step thought the image in groups of 16 counts. This very effectively highlights the small differences caused by striping. The characteristics of striping and other noise in the signal were noted for each band from Band 1 to Band 4. Examples of the striping patterns are shown in Figure 7.2.

### 7.2.1 Band 1

In Band 1 periodic striping is evident, with the same pattern for each swath. The west side of the image appears lighter than the eastern, coastal, area. This could be due either to sunglint or to the presence of plankton in the surface layer. This latter is more probable, as the Leeuwin current provides a southwards stream of nutrient rich warm water down the coast (Cresswell, 1991). The coastal area with bays and headlands is somewhat protected from this current. Some areas of deep water show a range of eight digital counts from a supposedly homogenous target.

### 7.2.2 Band 2

In Band 2 severe striping is present with two distinct swath patterns being discernible. These patterns are not alternate but occur in blocks varying in size from one to 27 swaths. The range within stripes in assumed homogenous areas is five DN.

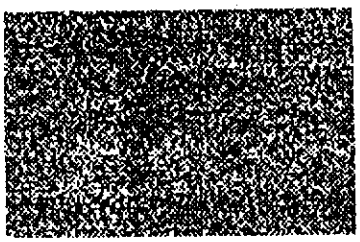

(a) Band 1

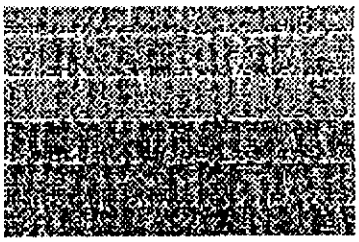

(b) Band 2

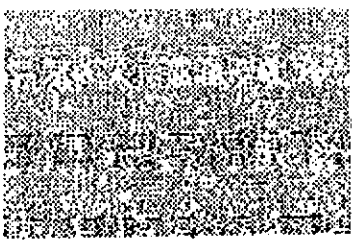

(c) Band 3

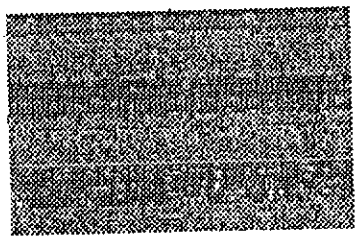

(d) Band 4

Figure 7.2 Striping patterns

### 7.2.3 Band 3

Band 3 has striping visible at very low DN. All sea surface values are approximately 15 DN. Four types of striping pattern are evident. These occur in blocks which alternate between pairs of patterns. The changes between these blocks are at the same row positions as the block changes in Band 2.

### 7.2.4 Band 4

Despite the fact that there is little water penetration in Band 4, the image was inspected as it may be of use in the application of a sunglint correction. Striping was evident with two patterns being seen. These alternate throughout the image.

## 7.3 Potential Methods of Noise Correction

Methods have been developed to compensate for both periodic striping and sunglint. They are not necessarily all applicable under all circumstances.

### 7.3.1 Periodic Striping

Imagery acquired over water has a rather different structure to imagery acquired over land. An image over deep water may be expected to have areas of homogenous reflectance due to the lack of bottom reflection. Imagery over shallow water will have areas of uniform bottom in which the reflectance values change relatively slowly and smoothly with depth. Large and sudden changes in reflectance may occur at changes in bottom type. This contrasts with imagery acquired over urban areas, where reflectance may change rapidly from pixel to pixel and where homogenous areas are rare. Imagery over a rural area falls

somewhere between these extremes. Periodic striping in imagery over water will generally be more apparent than it would be over land.

The destriping algorithms implemented in most image processing systems are designed for use with imagery acquired over land and approach the gain and offset correction by normalisation. An alternative method, more suited to use over water, applies an offset only.

(a) Normalisation Method

The basis for this method is the assumption that the signals produced by the detectors for any band will be statistically similar, i.e. their means and standard deviations will be the same. A second assumption that scene detail does not change significantly within the along track dimension of a swath (480 m) is also made. The usual algorithm calculates the mean and standard deviation for each detector and then sets the means and standard deviations of all detectors to the same, standard, values (Richards, 1986). The value used as standards may either be the mean and standard deviation for the entire image, as implemented by IDRISI, or may be those of one of the scan line detectors.

(b) Offset Method

The offset method, proposed by Gee and Forster (1984), requires that there be areas within the image with an assumed homogenous response. The further assumption is made that the gain differences between detectors are small in relation to offset differences. Over the low range of DNs presented by typical over-water imagery, this assumption is reasonable. The areas of assumed homogenous response are provided by areas of deep water.

The method is implemented by taking the mean signal for each line in the swath over a deep water area. One mean is set as a standard and the offset required to level the area for the other lines is calculated. The offsets are then applied throughout the image.

### 7.3.2 Sunglint

Since sunglint is caused by reflection at the sea surface, when it occurs there is some sunglint signal present in wavelengths higher than the visible. Lysenga (1985) has suggested that a suitable test for the presence of sunglint is to examine the correlation between the visible signals and those in a near infrared band, for a deep water area. A high correlation coefficient indicates the presence of sunglint. The sunglint in any one visible channel may be corrected by obtaining the covariance between the signals in that channel and a near infrared channel. Since the NIR channel is not water-penetrating its signal comprises only sunglint and atmospheric effects. If the atmospheric affects are ignored the sunglint correction for each pixel is :

$$\Delta L_i = \frac{\sigma_{ij}}{\sigma_{jj}}(L_j - L_{sj}) \qquad (8.1)$$

where $i, j$ are indices for visible and NIR bands respectively

$\Delta L_i$ is the correction applied to pixels in band $i$

$\sigma_{ij}$ is the covariance between bands $i$ and $j$ for deep water

$\sigma_{jj}$ is the variance of band $j$

$Ls_j$ is the mean deepwater signal in band $j$

$L_j$ is the signal in band $j$

## 7.4 Application of Offset Destriping Method

The offset method for destriping has advantages when working with imagery over water and was used in this study. No software implementation of the algorithm was available. The offset corrections were determined by extracting digital counts into a spreadsheet template and a C language routine was written to apply the corrections throughout the image.

### 7.4.1 Determination of Offsets

The 1000 pixel square sub-scene described in Section 6.3 was displayed as indicated in Section 7.2 above. The number of patterns of striping was noted and an area of occurrence for each pattern in a deep water area was found. Deep water areas were identified with reference to Admiralty charts.

For each pattern type, a representative section of 16 rows by 100 columns was extracted from the deep water sections of the image. The IDRISI routine WINDOW was used for the data extraction and the images were converted into ascii listings using the IDRISI CONVERT routine. These listings were read into a template file prepared using the spreadsheet program Lotus 123.

The spreadsheet calculations produced a mean value for each line in the 16 line swath and a mean value for the whole swath. Offsets to set each of the line means to the swath integer mean were also determined. The offset values were output to files for further processing. Typical output from a spreadsheet session is shown in Table 7.1 and Figure 7.3. All files used in the destriping process are

listed in Appendix C, which also contains plots of detector offsets for all striping patterns.

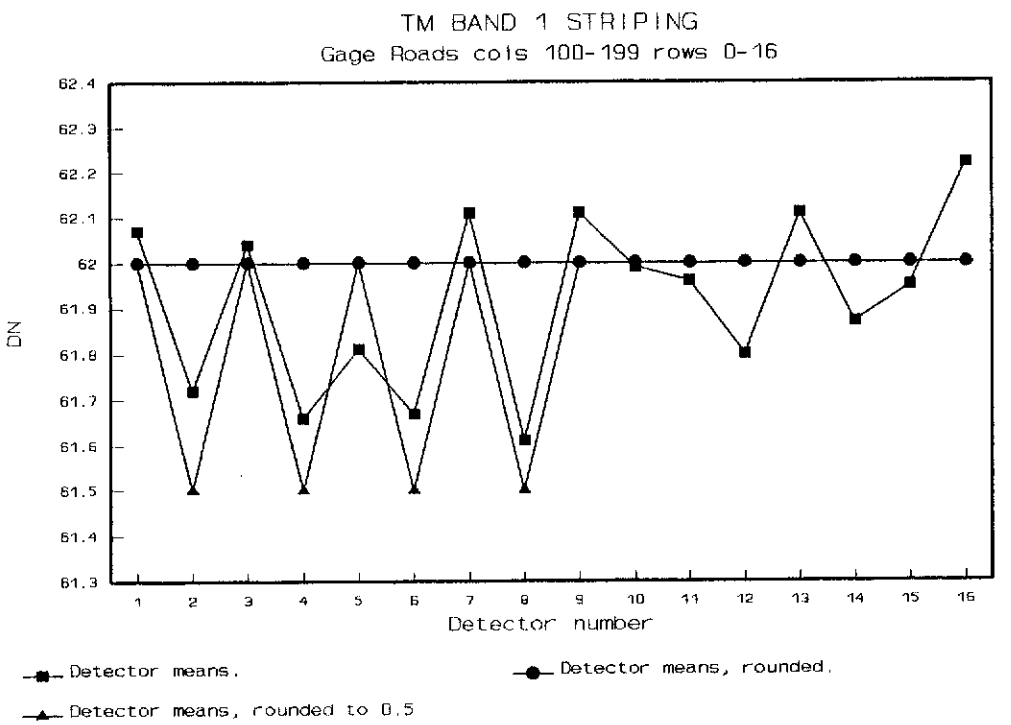


Figure 7.3
Plot of detector offsets for Band 1

### 7.4.2 Application of Corrections

The offset corrections were applied using a custom written program DSOFFSET. This program was written in C for use on a Sun Sparcstation. A full program listing is contained in Appendix B.

Since the offset corrections to bring each line in the deep water areas to an integer mean are real numbers, the output image is necessarily real. In addition to the original byte image the software requires two other input files. These are a list file containing the sequence in which patterns occur in a particular band and a file containing the appropriate offset corrections for each of the striping patterns.

Printouts of the files used in the correction of the sub-image are contained in Appendix C.

Corrections were applied to the three visible bands and to the NIR band 4 of the 1000 by 1000 pixel sub-scene using DSOFFSET. The resulting images were kept as single band files for further processing using custom software and also converted to a four band real image in DISIMP format. The DISIMP utility INHDD was used for image conversion.

| Line | Raw Mean | Rounded Mean | Half int. Mean | Offset |
|---|---|---|---|---|
| 1 | 62.07 | 62 | 62 | -0.07 |
| 2 | 61.72 | 62 | 61.5 | 0.28 |
| 3 | 62.04 | 62 | 62 | -0.04 |
| 4 | 61.66 | 62 | 61.5 | 0.34 |
| 5 | 61.81 | 62 | 62 | 0.19 |
| 6 | 61.67 | 62 | 61.5 | 0.33 |
| 7 | 62.11 | 62 | 62 | -0.11 |
| 8 | 61.61 | 62 | 61.5 | 0.39 |
| 9 | 62.11 | 62 | 62 | -0.11 |
| 10 | 61.99 | 62 | 62 | 0.01 |
| 11 | 61.96 | 62 | 62 | 0.04 |
| 12 | 61.80 | 62 | 62 | 0.20 |
| 13 | 62.11 | 62 | 62 | -0.11 |
| 14 | 61.87 | 62 | 62 | 0.13 |
| 15 | 61.95 | 62 | 62 | 0.05 |
| 16 | 62.22 | 62 | 62 | -0.22 |
| Overall means | 61.8937 | 62 | | |

Table 7.1 : Offsets for Band 1 destriping

## 7.5 Determination of Sunglint Correction Factors

The correction method suggested by Lysenga (1985) and outlined in Section 7.3.2 above, requires a knowledge of the covariance matrix between the visible and NIR bands. This was calculated for 1283 pixels in a deep water area of the 1000 by 1000 pixel sub image, after destriping. The DISIMP utility DSPSIG was used for this operation. The correlation matrix for the area was calculated from the covariance matrix. The correlation and covariance matrices are presented in Tables 7.2 and 7.3.

| Band | 1 | 2 | 3 | 4 |
|---|---|---|---|---|
| 1 | 1.770 | -0.016 | 0.038 | 0.034 |
| 2 | -0.016 | 0.614 | -0.063 | 0.001 |
| 3 | 0.038 | -0.063 | 0.685 | 0.058 |
| 4 | 0.034 | 0.001 | 0.058 | 0.293 |

Table 7.2 : Covariance matrix for deep water area

| Band | 1 | 2 | 3 | 4 |
|---|---|---|---|---|
| 1 | 1.000 | -0.015 | 0.034 | 0.047 |
| 2 | -0.015 | 1.000 | -0.097 | 0.002 |
| 3 | 0.034 | -0.097 | 1.000 | 0.025 |
| 4 | 0.047 | 0.002 | 0.025 | 1.000 |

Table 7.3 : Correlation matrix for deep water area

Given the low correlations between bands in the deep water areas and the low correction values that would consequently be used in Equation 7.1 no sunglint correction was applied to the image.

## 7.6 Summary

Satellite imagery over water is subject to a number of forms of noise. The chief amongst these, periodic striping may be compensated for using either a gain and offset correction or, as was done for this study an offset only correction. The application of this correction required the writing of custom software. The other major noise component frequently present in such imagery is sunglint. Although apparently effective algorithms exist to compensate for its effects, a simple test indicated that, in the imagery under consideration, sunglint was present to a negligible extent. The removal of noise forms a necessary pre-processing step to the more analytical work described in subsequent chapters. Figure 7.4 shows the progress of the image data through this process.

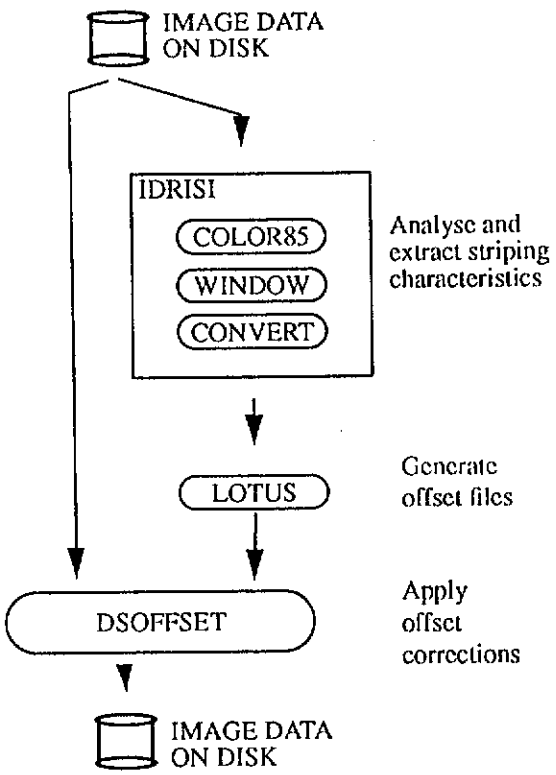


Figure 7.4 : Flowchart of de-striping process

# CHAPTER 8

# IMAGE SEGMENTATION

The method of bathymetric data extraction described by O'Neill and Miller (1989) as a multi-band model with spatial iteration is outlined in Section 5.2.4. This method requires the generation of a surface of residuals throughout the area for which the multi-band model has been generated. Due to the abrupt changes in both bottom type and depth in the Parmelia Bank area, the generation of one overall surface as suggested by O'Neill is possibly not applicable. The area may be effectively divided into zones within which environmental parameters may be assumed to be more homogenous than in other zones. Surfaces may then be developed within those zones.

It seems therefore appropriate to divide the image into sections within which a number of surfaces of residuals may be interpolated. Natural zone boundaries that offer themselves for segmentation are those created by changes in bottom types and those caused by the different depth extinction characteristics of the spectral wavebands used.

## 8.1 Depth of Penetration (DOP) Zones

Depth of penetration zones have been used as a simple form of bathymetric mapping and the concept has been extended to a more sophisticated level (Jupp, 1988). The procedure for their derivation, which is described in Chapter 5, may be summarised as being the labelling, with a value representing a particular zone, of all those pixels in an image which fall between suitable thresholds.

A semi-automated implementation of the algorithm may take the form of either a parallelepiped classification in multispectral space or a decision tree. Both implementations are described by Jupp (1988) and generate the same number of zones as there are water penetrating bands, and at least one class of anomalous pixels.

The decision tree method may also be implemented manually using the pixel reclassification and overlay capabilities afforded by raster based Geographic Information Systems such as IDRISI. The manual approach was used in this study.

### 8.1.1 Derivation of Zones

Cut off levels for the zones were derived from statistics for deep water areas. The deep water areas used in the noise removal process described in Chapter 7 were used again for this process. The reclassification was carried out on byte images that had not been destriped.

| TM Band | Mean | Std. Dev. | Mean + 2SD |
|---|---|---|---|
| 1 | 61.31 | 1.33 | 63.96 |
| 2 | 15.45 | 0.78 | 17.02 |
| 3 | 11.58 | 0.83 | 13.23 |
| 4 | 5.63 | 0.54 | 6.71 |

Table 8.1 : Band means and standard deviations for deep water area

Statistics for the deep water area are listed in Table 8.1. Cut off values used were the mean plus two standard deviations. This upper part of the distribution was used in an attempt to minimise noise. The reclassification

procedure for the three water penetrating bands proceeded as follows:

(a) Pixels in Band 1 with values lying above 63 were assigned a value of 1.

(b) Pixels in band 2 with values in excess of 17 were assigned a value of 2.

(c) Pixels in band 3 with values in excess of 13 were assigned a value of 4.

An additional data layer was created by setting to zero all pixels in band 4 which exceed 15 and setting to 1 all other pixels in that band. This latter process had the effect of generating a binary mask delineating land and water. The data were manipulated using the IDRISI module RECLASS.

The three images produced from the water penetrating bands were added and then masked by multiplication with the binary image from Band 4. Finally, for display purposes, the binary mask was inverted, multiplied by 10 and added to the masked sum of the other bands. The values produced by these operations are detailed in Table 8.2. All algebraic operations were carried out using the IDRISI module OVERLAY.

### 8.1.2 DOP Image Smoothing

Images produced by multispectral classifications typically contain a degree of noise. This manifests itself as isolated pixels or small areas assigned to particular classes and surrounded by pixels of a different class. This noise is an indication of the limitations of spectral classification and its effects may be somewhat ameliorated by consideration of the spatial context of the pixels. It is

reasonable to assume a degree of spatial homogeneity within the image and within the classes.

| Image value | DOP zone | Pixels in smoothed image | Comments |
|---|---|---|---|
| 0 | None | 48216 | Water too deep to return bottom signal in any waveband. |
| 1 | 1 | 11573 | Signal in Band 1 only above threshold. Pixel is in DOP zone 1. |
| 2 | Anomaly | 1130 | Signal in Band 2 only above threshold. Pixel is anomalous. |
| 3 | 2 | 36500 | Signal in Bands 1 and 2 above threshold. Pixel is in DOP zone 2. |
| 4 | Anomaly | 1889 | Signal in Band 3 above threshold. Bands 1 and 2 below. Pixel is anomalous. |
| 5 | Anomaly | 1287 | Signal in Bands 1 and 3 above threshold. Band 2 above. Pixel is anomalous. |
| 6 | Anomaly | 478 | Signal in Bands 2 and 3 above threshold. Band 1 below. Pixel is anomalous |
| 7 | 3 | 18180 | Signal in Bands 1,2 and 3 above threshold. Pixel is in DOP zone 3 |
| 10 | Land | 45747 | Signal in Band 4 greater than 15. |

Table 8.2 : Values resulting from generation of DOP zones

A smoothing technique based on this assumption is the majority or modal filter (Schowengerdt, 1983). This filter is ideally suited to classified data where the pixel values are labels representing class membership rather than expressions of the magnitude of some property. A modal filter assigns, to the central pixel of a filter box, the most frequently occurring value within that box. The IDRISI FILTER routine used on these data operates in a 3 x 3 pixel neighbourhood. The smoothed DOP image is shown in Figure 8.1

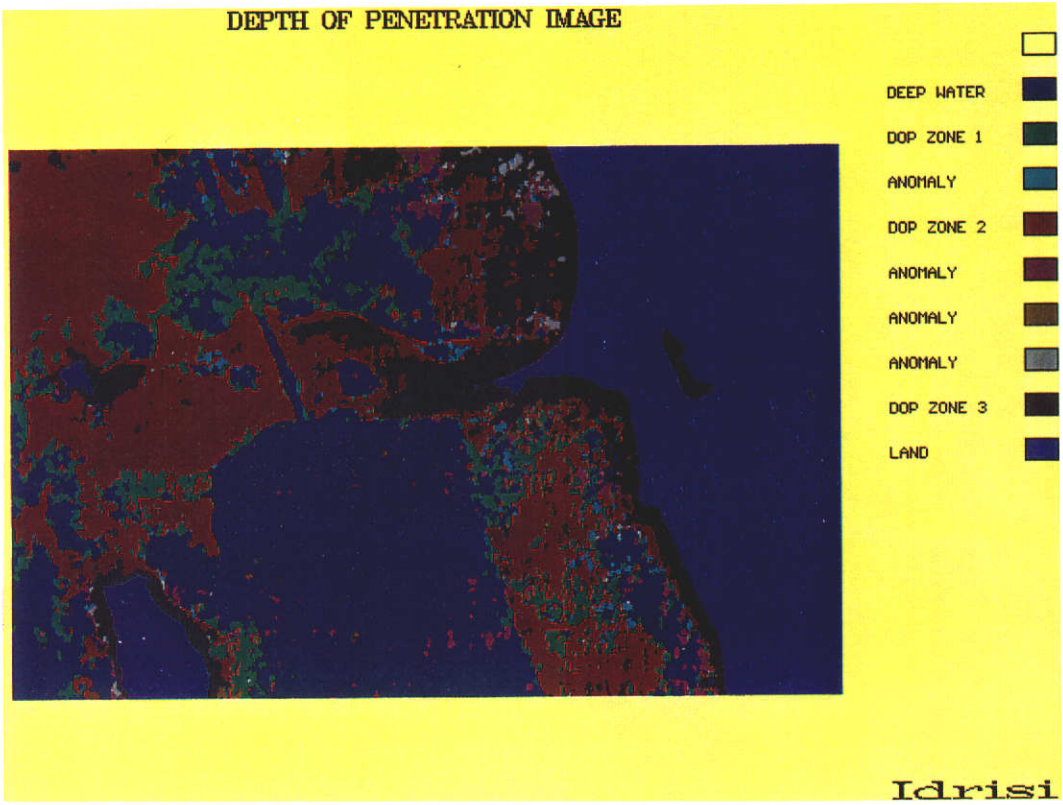


Figure 8.1 : Smoothed DOP image

## 8.2 Bottom Cover Classes

### 8.2.1 Training Site Selection

Bottom cover classes which can be expected in the Parmelia bank area vary between the two extremes of bright sand and dark green seagrass. Two other classes which are apparent in the imagery may be taken as representing more muddy sands. In order to assist in the selection of training areas for a multispectral classification of the image, a vertical air photograph of the area just north of Woodman point was obtained from The W.A. Department of Land Administration. On this photograph, part of which is reproduced in Figure 8.2, it is possible to distinguish shallow weed areas from deep water areas with other types of bottom.

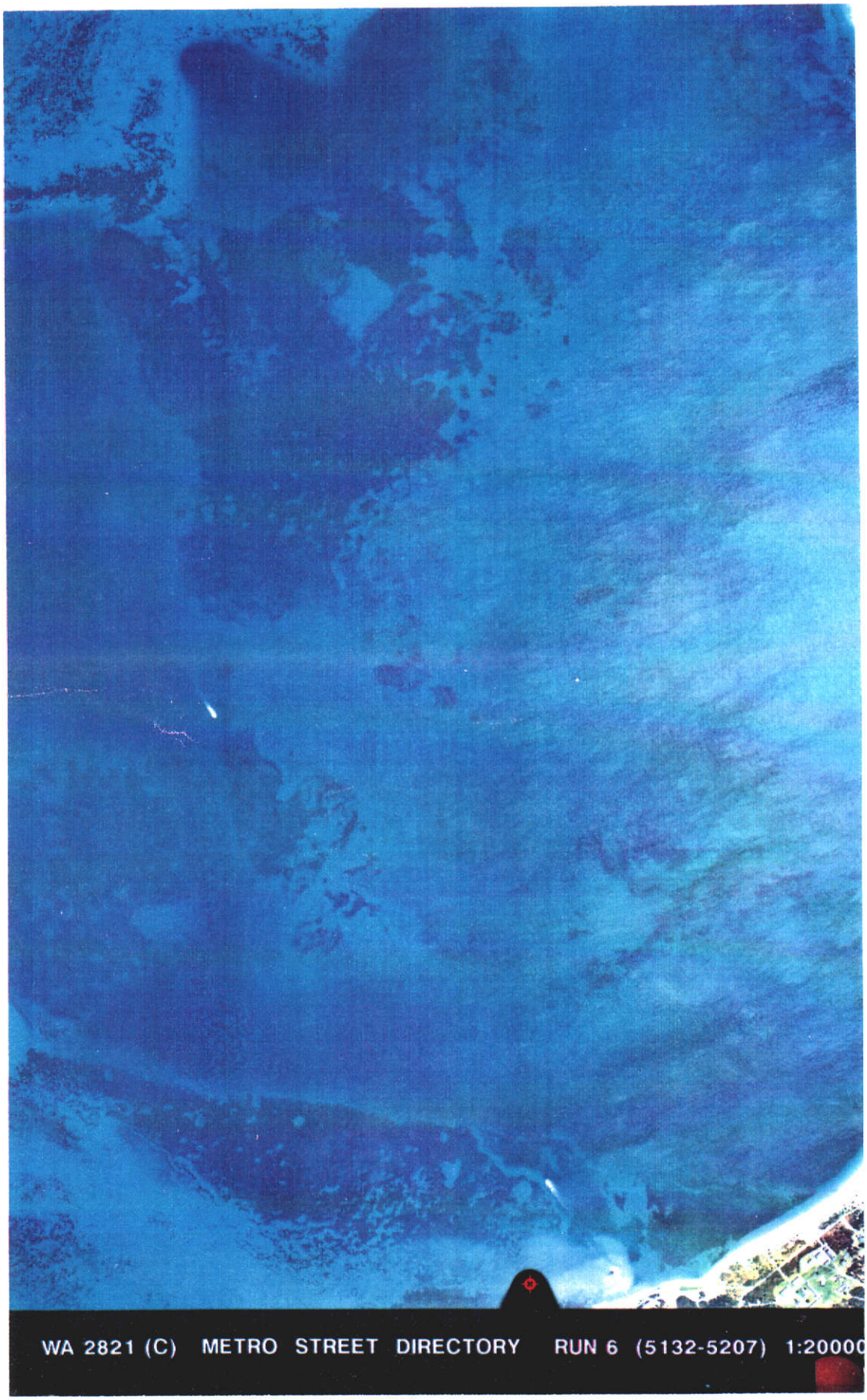


Figure 8.2 : Part of vertical air-photo. North of Woodman Point

```
IDENT S1 BOTTOM CLASS SIGNATURES

 IMAGE    parmr.dat

 NO. CHN   3
 CHANNEL   1  2  3

 CATEGORY     1  sand1
 SIGNATURE          90.053    32.530    16.417
 NUM. OBS.   151
 COVAR    1    32.318    21.385    12.771
 COVAR    2    21.385    15.797     9.398
 COVAR    3    12.771     9.398     6.991

 CATEGORY     2  sand2
 SIGNATURE          69.975    22.325    12.700
 NUM. OBS.    80
 COVAR    1     3.063     0.818     0.182
 COVAR    2     0.818     0.982     0.086
 COVAR    3     0.182     0.086     0.795

 CATEGORY     3  weed
 SIGNATURE          61.308    17.154    12.128
 NUM. OBS.    39
 COVAR    1     .798    -0.128    -0.067
 COVAR    2    -0.128     0.818    -0.020
 COVAR    3    -0.067    -0.020     0.694
```

Table 8.3 : Training site statistics

Proximity to the shore and reference to bottom type codes on Admiralty Chart AUS 117 were also used as indicators of probable class. The image of the Parmelia Bank area was displayed using the DISIMP image processing system and training sites were selected using the routine DSPSIG. Signature, sample size and signature covariances for the training areas are listed in Table 8.3

### 8.2.2 Classification

The image was classified using the DISIMP routine CLMXL. This is an implementation of the maximum likelihood classification algorithm (Richards,

1986). The resulting image exhibits the same isolated pixels and noise effects as the DOP image. These are caused by noise and by category overlap in multispectral space.

The category overlap in its turn reflects the difficulty of picking suitable training sites. Detailed site investigation of bottom types at particular locations, which would be of use in resolving some misclassifications, lay beyond the resource base of this study. A modal filter, operating in a 3 x 3 pixel neighbourhood, was applied to the classified image using the DISIMP routine MODTRN. The resulting bottom classification map is shown in Figure 8.3.

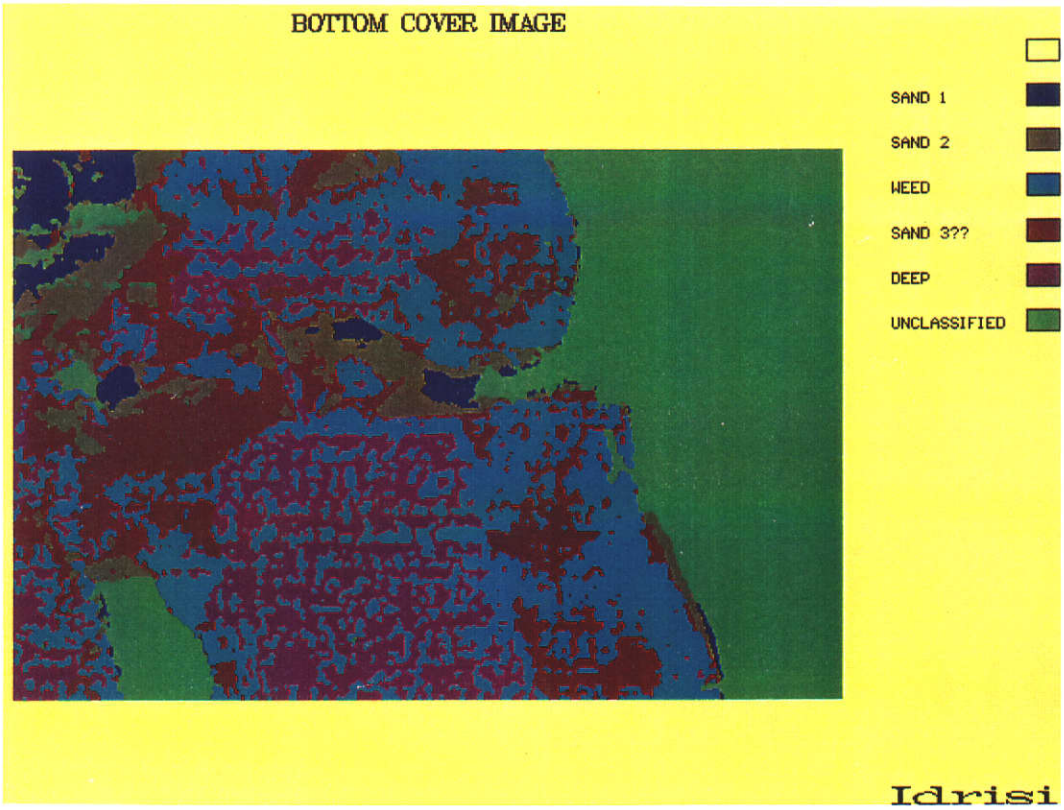


Figure 8.3 : Smoothed bottom class image

The numbers of pixels assigned to each class in the smoothed image are listed in Table 8.4. The large number of pixels assigned to Class 2 (weed), is probably more indicative of the difficulties of spectrally separating weed and deep water than of the actual proportions of the two cover types.

| Class No. | Description | No. of pixels |
|---|---|---|
| 0 | Unclassified | 5221 |
| 1 | Sand1 | 9735 |
| 2 | Weed | 46558 |
| 3 | Sand2 | 28605 |
| 4 | Sand3 | 24754 |
| 5 | Deep water | 50127 |

Table 8.4 : Pixel count for smoothed bottom class image

### 8.3 Summary

In order to provide limited spatial fields in which to develop residual surfaces, two approaches to image segmentation were attempted. The first divided the image on the basis of the depth to signal extinction in three optical wave bands. This resulted in an image comprising three major classes and a number of very much smaller classes with anomalous values. The second divided the image into perceived bottom classes using training sites chosen with the aid of aerial photography and a hydrographic chart. This classification produced five classes and a number of anomalous and unclassified pixels. Both segmented images were smoothed using a modal filter. This filter was applied to improve the classification prediction by taking account of the spatial context of each pixel. Figures 8.4 and 8.5 show the paths taken by the data during the generation of the two classified images.

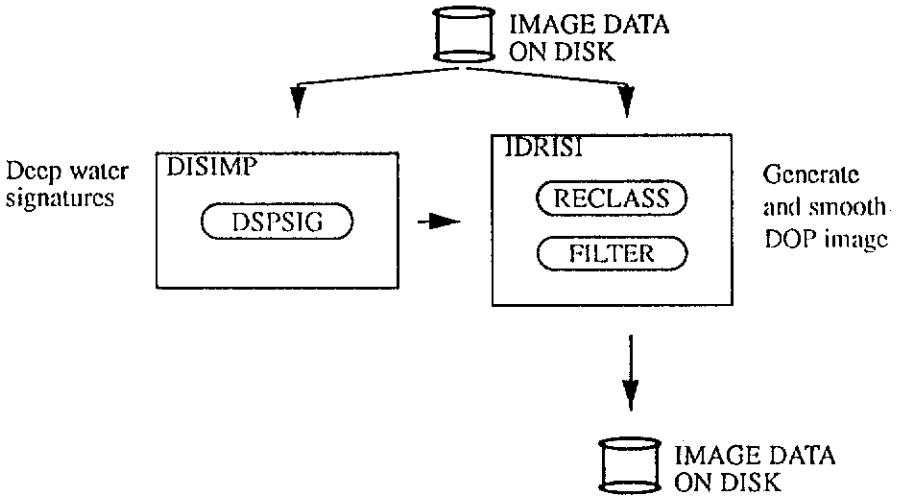


Figure 8.4 : Flowchart for generation of DOP image

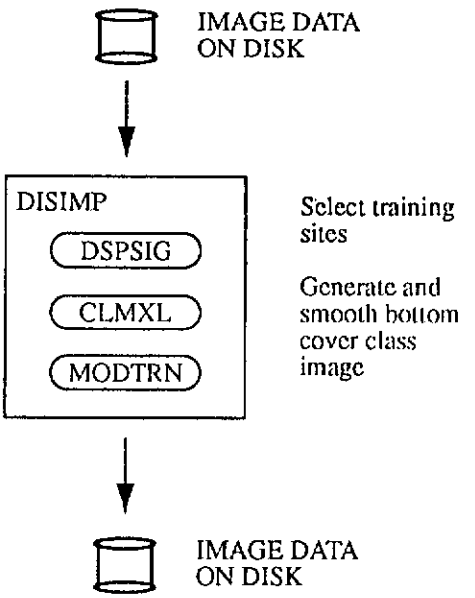


Figure 8.5 : Flowchart for generation of bottom cover image

# CHAPTER 9

# DATA FITTING BY REGRESSION

After passing through the noise minimisation and data segmentation stages described in the preceding two chapters the data were now ready for further analysis. The first process established a regression relationship between the image data and the surveyed depths in the experimental dataset. This was then followed by a spatial modelling of the residuals from that relationship.

## 9.1 Extraction of Image Data

As described in Chapter 6 the soundings digitised from the Admiralty chart are related to individual image pixels through transformation equations. The first part of the multi-band depth extraction algorithm requires the solution of Equation 5.4. This equation, restated here as Equation 9.1 takes as input the values $X_1$ to $X_n$ where n is the number of bands whose signal contains a bottom return component.

$$Z = A_0 + A_1 \times X_1 + A_2 \times X_2 \ldots\ldots + A_n \times X_n \qquad (9.1)$$

The terms $X_1$ to $X_n$ are defined (as general term $X_j$) in Equation 5.2 as being the natural log of the received signal minus the deep water mean signal for that band (Equation 9.2).

$$X_j = Ln\ (L_j - Lw_j) \qquad (9.2)$$

### 9.1.1 Data Extraction Software

A software routine was written to extract, from nominated images, the relevant pixel values and to perform the logarithmic transformation. Pixels for which the logarithm could not be calculated were assigned a value of -999 as a flag to further processing. These are pixels whose reflectance values are lower than the deep water mean. Deepwater means used in this process were the same as those used in the generation of the DOP image and are listed in Table 8.1. The software routine also extracts, from a nominated classified image, the class label for each pixel. The routine, named SOUNDER, is written in the C language and is listed in full in Appendix B.

### 9.1.2 Data Extraction and Sorting

Values for Bands 1, 2 and 3 were extracted, for each sounding in the experimental data set, from the real valued destriped images. Coincident values were extracted from the byte valued classified images representing depth of penetration zones and bottom cover classes. Output files from this process, were input to a Lotus 123 spreadsheet template and sorted according to DOP zone or bottom class, as appropriate. The files were then subdivided on the basis of class or DOP membership and passed to a Unix workstation for further processing.

## 9.2 Regression Models

The data analysis functions of the Interactive Data Language (IDL) package were used to perform multiple regressions on the data sets to determine the coefficients of Equation 9.1. A brief description of IDL and the routine used appears in Appendix A.

### 9.2.1 Choice of Regression Variables

It is reasonable to assume that the water quality in Cockburn Sound resembles more closely that of Jerlov's Coastal Types than any of the three Clear Oceanic Types. The peak penetration wavelength for Coastal Types 1 to 3, at around 0.50 $\mu$m is a little higher than the 0.475 $\mu$m of Oceanic Type I. This wavelength falls between the central wavelengths of TM Bands 1 and 2. However the TM sensors have responses which are spread over a range of wavelengths. These detector response functions are approximately gaussian in shape. It is possible to predict the response of such a detector to a wavelength continuum, such as a spectrum, by convolving the two waveforms. The program CONVOL, made available by the CSIRO W.A. Remote Sensing Group, carries out this process. The depth of penetration curves for Coastal Type 1 and 3, as shown in Table 4.1 and Figure 5.1 were convolved with the TM detector functions for Bands 1, 2 and 3. The resulting theoretical depths of penetration are shown in Table 9.1.

| Band | Water Type 1 | Water Type 3 |
|---|---|---|
| 1 | 16.2 m | 10.2 m |
| 2 | 12.0 m | 9.0 m |
| 3 | 5.5 m | 5.0 m |

Table 9.1 : Theoretical depths of penetration for coastal water types

These depth of penetration figures support the presumption that Band 1 penetrates further than Band 2, which in turn penetrates further than Band 3. In

this case, if the image is segmented on the basis of DOP zones, it is valid to use the Bands appropriate to each zone as input to the regression.

For an image segmented on the basis of bottom cover classes any of the potentially water penetrating bands may contribute to the relationship. It is therefore valid to use all bands for all cover classes, at least in an initial regression analysis.

### 9.2.2 Depth of Penetration Dataset

The transformed DN (TDN) values for each depth point were visually inspected. Within DOP zone 1 there are six points, which is insufficient to develop a meaningful regression relationship. In DOP zone 2 there are 53 candidate values and in DOP zone 3 there are 43 candidate values. A further seven points are either in anomalous zones or associated with pixels classed as land, while 50 points fall in the deep water zone. The deep water points represent soundings too deep to have bottom return in this data set.

Any depth points for which a logarithmic transformation could not be obtained, in any band appropriate to their zoning, were discarded. The spatial filtering process used in the generation of the DOP image introduced a neighbourhood effect into the allocation of pixels to particular zones. It is, therefore, a reasonable assumption that any individual pixel, in an unfiltered image, that presents an anomalous value, be regarded as noise affected. After weeding out such noise affected pixels, 52 pixels remained in zone 2 and 41 in zone 3.

For depth points falling in DOP zone 2, regressions were carried out of

depth against TDNs for Bands 1 and 2 and of depth against TDN for Band 2 only. For points falling in DOP zone 3, regressions were carried out of depth against TDNs for Bands 1, 2 and 3 and of depth against TDNs for Bands 2 and 3.

### 9.2.3 Bottom Cover Dataset

Table 9.2 summarises the distribution of points in the data set segmented on the basis of bottom cover classes. The assumption that data affected by noise in any one band be regarded as suspect was also applied to this dataset. After deleting suspect soundings, the subdivided datasets were input to the IDL regression routines. For all classes regressions were carried out between depth and the TDN for all three bands.

| Cover Class | Total points | Points used |
|---|---|---|
| 1 | 8 | 7 |
| 2 | 15 | 14 |
| 3 | 57 | 43 |
| 4 | 48 | 42 |
| 5 | 18 | 10 |
| 6 | 13 | 13 |

Table 9.2 : Data points in each bottom class

## 9.3 Regression Results

### 9.3.1 DOP Zone 2

The results for the zone 2 regression using TDNs for Bands 1 and 2 are shown in Table 9.3. The multiple regression correlation coefficient has a low value of only 0.38. This indicates that the relationship is rather weak. However

the F statistic from the analysis of variance is significant at a level of 2 percent. This means that the hypothesis that no relationship exists between the dependant variable, depth, and the independent variables, the TDNs, can be rejected. The magnitude of the significance level indicates that this rejection may be made with 98 percent confidence. Investigation of the coefficients suggests that the principal contribution to the relationship comes from the Band 2 TDN with a much smaller contribution from the Band 1 TDN.

Regression results for DOP zone 2. Using bands 1,2

Regression: Correlation Coeff = 0.387467

| VARIABLE | COEFFICIENT | STDDEV | T | P |
|---|---|---|---|---|
| Constant | 9.726981 | | | |
| Var0 | 0.1190854 | 0.5336249 | 0.2231632 | 0.8244 |
| Var1 | -2.750659 | 1.117268 | -2.461950 | 0.0175 |

ANALYSIS OF VARIANCE

| SOURCE | SUM OF SQUARES | DF | MEAN SQUARE | F | p |
|---|---|---|---|---|---|
| Regression | 34.91789 | 2 | 17.45895 | 4.2397 | 0.0202 |
| Residual | 197.7 | 48 | 4.118 | | |

Table 9.3 : Regression results for zone 2 using Bands 1 and 2

Table 9.3 shows the regression results for DOP zone 2 using only the TDNs for Band 2. There is little change in either the magnitude of the correlation coefficient or in the offset and slope coefficient for the TDN. The F value of 8.59 is significant at a level of 0.5 percent which represents an apparent improvement on the two-band regression. This must be considered against the higher multiple correlation coefficient for the two-band model. The F value is not independent of the multiple correlation coefficient, being derived from it and the number of degrees of freedom associated with the fitted equation (Daniel and

Wood, 1971). It appears, from the coefficients in the two-band model, that there is some small contribution to the model from both bands, as theory would suggest. This two-band model is therefore acceptable as input to a spatial iteration process, which seeks to explain spatial variation in parameters which will affect all bands.

Regression results for DOP zone 2 using band 2

Regression: Correlation Coeff = -0.386322

| VARIABLE | COEFFICIENT | STDDEV | T | P |
|---|---|---|---|---|
| Constant | 9.686254 | | | |
| Var0 | -2.601718 | 0.4415912 | -5.891688 | 0.0000 |

ANALYSIS OF VARIANCE

| SOURCE | SUM OF SQUARES | DF | MEAN SQUARE | F | p |
|---|---|---|---|---|---|
| Regression | 34.71280 | 1 | 34.71280 | 8.5962 | 0.0051 |
| Residual | 197.9 | 49 | 4.038 | | |

Table 9.4 : Regression Results for zone 2 using Band 2

### 9.3.2 DOP Zone 3

Table 9.5 shows the results of a multiple regression run using all three, potentially contributing, independent variables for DOP zone 3. The correlation coefficient for this regression of 0.62, although still low, is a considerable improvement on that for the zone 2 relationship. The F test in the analysis of variance indicates that the relationship is significant at the 0.4 percent level. Inspection of the coefficients shows that the dominant contribution to the depth relationship is still being made by the Band 2 TDN.

Further regressions analyses were carried out to test the strength of the relationship between depth and various combinations of TDNs. Table 9.6 shows the results using TDNs for bands 2 and 3 while Table 9.7 shows those for the TDNs of Bands 1 and 2. The results for a simple regression using Band 2 TDNs only as a single variable are shown in Table 9.8.

Regression results for DOP zone 3 using bands 1,2,3

Regression: Correlation Coeff = 0.625737

| VARIABLE | COEFFICIENT | STDDEV | T | P |
|---|---|---|---|---|
| Constant | 10.06106 | | | |
| Var0 | 1.534429 | 0.8592621 | 1.785752 | 0.0826 |
| Var1 | -4.827497 | 1.409622 | -3.424675 | 0.0016 |
| Var2 | 0.5511131 | 0.6191656 | 0.8900899 | 0.3793 |

ANALYSIS OF VARIANCE

| SOURCE | SUM OF SQUARES | DF | MEAN SQUARE | F | p |
|---|---|---|---|---|---|
| Regression | 116.7680 | 3 | 38.92266 | 7.7221 | 0.0004 |
| Residual | 181.5 | 36 | 5.040 | | |

Table 9.5 : Regression results for zone 3 Using Bands 1, 2, and 3

These latter three regression models show a slight decrease in multiple correlation coefficient with a linked increase in both F statistic and its significance. Nevertheless the significance of the three-band model at 0.4 percent is satisfactory, and coupled with the magnitude of the multiple correlation coefficient, suggests that this model be used as input to the spatial iteration phase.

Regression results for DOP zone 3 using 2,3

Regression: Correlation Coeff = 0.581076

| VARIABLE | COEFFICIENT | STDDEV | T | P |
|---|---|---|---|---|
| Constant | 9.014282 | | | |
| Var0 | -2.755102 | 0.8234772 | -3.345694 | 0.0019 |
| Var1 | 0.5194565 | 0.6369562 | 0.8155295 | 0.4200 |

ANALYSIS OF VARIANCE

| SOURCE | SUM OF SQUARES | DF | MEAN SQUARE | F | p |
|---|---|---|---|---|---|
| Regression | 100.6946 | 2 | 50.34728 | 9.4308 | 0.0005 |
| Residual | 197.5 | 37 | 5.339 | | |

Table 9.6 : Regression results for zone 3 using Bands 2 and 3

Regression results for DOP zone 3 using 1,2

Regression: Correlation Coeff = 0.614944

| VARIABLE | COEFFICIENT | STDDEV | T | P |
|---|---|---|---|---|
| Constant | 9.642044 | | | |
| Var0 | 1.512532 | 0.8564951 | 1.765956 | 0.0857 |
| Var1 | -4.249093 | 1.247388 | -3.406393 | 0.0016 |

ANALYSIS OF VARIANCE

| SOURCE | SUM OF SQUARES | DF | MEAN SQUARE | F | p |
|---|---|---|---|---|---|
| Regression | 112.7747 | 2 | 56.38736 | 11.250 | 0.0002 |
| Residual | 185.4 | 37 | 5.012 | | |

Table 9.7 : Regression results for zone 3 using Bands 1 and 2

Regression results for DOP zone 3 using only band 2

Regression: Correlation Coeff = -0.570737

| VARIABLE | COEFFICIENT | STDDEV | T | P |
|---|---|---|---|---|
| Constant | 8.633085 | | | |
| Var0 | -2.237364 | 0.2270023 | -9.856129 | 0.0000 |

ANALYSIS OF VARIANCE

| SOURCE | SUM OF SQUARES | DF | MEAN SQUARE | F | p |
|---|---|---|---|---|---|
| Regression | 97.14392 | 1 | 97.14392 | 18.358 | 0.0001 |
| Residual | 201.1 | 38 | 5.292 | | |

Table 9.8 : Regression results for zone 3 using Band 2

### 9.3.3 Bottom Cover Classes

The dataset subdivided on the basis of bottom cover class was used as input to the IDL regression routines. Summary results from these regression analyses are listed in Table 9.9.

| Class | Desc. | Const | Coeff 1 | Coeff 2 | Coeff 3 | R Mult | F | p | Points |
|---|---|---|---|---|---|---|---|---|---|
| 1 | Sand 1 | -13.81 | 7.99 | -1.67 | -1.48 | .79 | 1.70 | .33 | 7 |
| 2 | Sand 2 | 9.29 | 3.09 | -5.97 | -0.89 | .80 | 5.90 | .01 | 14 |
| 3 | Sand 3 | 9.65 | -.45 | -.75 | -.76 | .21 | .64 | .58 | 43 |
| 4 | Weed | 8.05 | 1.56 | -2.84 | .08 | .37 | 2.04 | .121 | 42 |
| 5 | Deep | 14.35 | -1.64 | 3.51 | -.65 | .48 | .60 | .63 | 10 |
| 6 | Un'class. | 4..08 | 5.39 | -2.20 | -4.02 | .61 | 1.86 | .20 | 13 |

Table 9.9 : Summary of regression results for bottom cover classes

The multiple correlation coefficients for bottom cover Types 1 and 2 , two types of sand, seem at first inspection to indicate good relationships. In the case of Type 1 the F statistic, which is significant at the 33 percent level, strongly

argues against the use of such a model. Inspection of the coefficients of this model indicates that it is markedly different from those developed using depth of penetration as an image segmentation tool. The figures for the Type 2 bottom cover are better and suggest that this would be a useful model for this cover type, even though it is based on only 14 observations.

The results for cover types classes 3, 4, 5 and 6 are disappointing, with low F values and consonant high p values, indicating that these models represent virtually no improvement on a random distribution. Taking this into consideration there is little to support the use of spectrally derived bottom classes as a means of image segmentation in this case.

### 9.4 Summary

Data values relevant to each sounding in the experimental set were extracted from the preprocessed images and the classification images. Regression relationships were established between the surveyed depths and the transformed DNs (TDN) using suitable combinations of independent variables. This operation was performed on data sets segmented using both DOP zones and bottom cover classes. The results for the bottom cover segmentation mitigate against the use of that method in this case. Relationships within the DOP zones, although weak, offer suitable coefficients as input to the spatial modelling stage of the spatially iterated multi-band depth extraction algorithm. Figure 9.1 illustrates the processes of data extraction and regression.

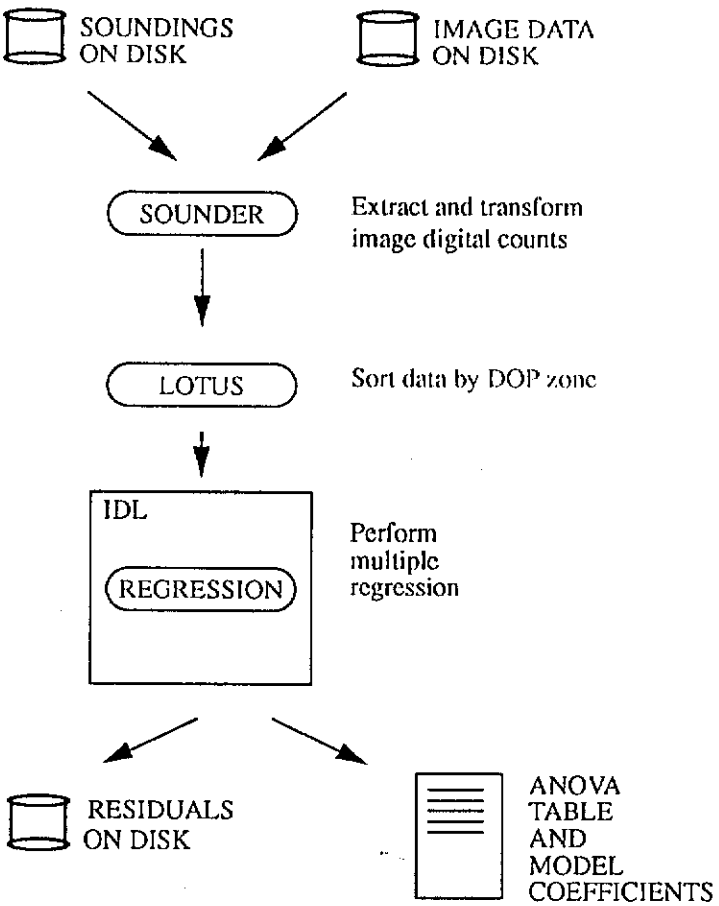


Figure 9.1 : Flowchart illustrating data extraction and analysis

# CHAPTER 10

# SPATIAL ITERATION AND MODEL TESTING

## 10.1 Spatial Modelling

Accepting the regression relationships developed for the two depth of penetration zones as being a first approximation, it is possible to generate spatial models of the deviation of fitted values from the observed values. These models can then be used to correct fitted values at other locations within the image. Spatial modelling of this nature may be carried out in raster Geographic Information Systems such as IDRISI and GRASS. Descriptions of these systems, both of which were used in this study, can be found in Appendix A.

## 10.2 Selection of Surface Generation Method

A residual surface may be generated using a number of methods. Earlier, theoretical, work by O'Neill and Miller (1989) suggests the use, for a one dimensional case, of high order polynomials. The order of polynomial suggested is the same as the number of points to be used in its generation. This has the advantage that, since the number of coefficients is the same as the number of input data points, there is an exact fit to the input data. The two dimensional analogue of this is the fitting of a trend surface. However, if extended to high orders, trend surfaces present a number of potential problems. If the data are not well distributed in the spatial domain, such surfaces are prone to distortion (Davis, 1986). There is also a tendency for the polynomial fit to wave the edges of the data in an attempt to fit points closer to the centre (Ripley, 1981). Other

difficulties arise due to the propagation of errors when estimates are raised to extremely high powers.

Since the residuals being spatially modelled have optimum values at the input data points, it is desirable that the surface generated should honour the data at the input points. This cannot be achieved by the use of polynomials of order lower than the number of input points. Possible methods of surface interpolation, which do honour the input data, include the generation of Thiessen polygons and the use of inverse distance weighting techniques.

### 10.2.1 Thiessen Polygons

The polygonal approach requires the assumption that each data point has an area of influence, in which the property being interpolated is invariant (Ripley, 1981). This assumption may be partially true for the data set in question. If deviations from the fit are principally due to changes in bottom type, they may indeed be constrained within hard boundaries. However, other factors causing deviation from the fit, such as changes in water quality, may change more gradually in the spatial domain.

### 10.2.2 Distance Weighted Interpolation

The inverse distance weighting technique (Isaaks and Srivastava, 1989) allows the influence, on a spatial mean, of any one input data point to be a maximum locally. This influence then falls off at a rate proportional to some power of distance, for more remote interpolated points. The choice of a power of two is common in implementations of this algorithm. The size of search neighbourhood around each interpolated point is frequently governed by the

selection of the number of neighbouring input data points to be used in the generation of the spatial mean.

### 10.3 Data Masking

Although the two depth of penetration zones are mutually exclusive in the spatial domain, each nevertheless contains inclusions of the other. A surface generated by simple interpolation from the residuals of points falling in either zone would also cover the other zone. The GRASS routine **r.mask** enables the generation of a geographic mask, to the inside of which the action of any spatial process can be limited. Masks were generated, from the smoothed DOP image, for each of the two DOP zones.

### 10.4 Residual Surface Generation

Files comprising position and depth residual triplets were written out from the IDL regression routines. These were converted to raster image files using the program SIT2IMG. This program, which is listed in full in Appendix B, was written specifically to generate integer valued raster data layers from point information. The resulting data layers essentially comprise just those image pixels from which values had originally been extracted. The values thus assigned to those pixels, are those of the residuals from the regressed fit. To avoid problems associated with negative values, a scalar value of 10 was added to the residuals for all points, giving them all positive values. The data were further scaled by a factor of 100 to reduce losses due to roundoff in the conversion from real tabular values to integer image cell values.

### 10.4.1 Distance Weighted Interpolation

In order to determine the optimum number of neighbour points to be used in the distance weighted interpolation, tests were carried out using the unmasked residuals from DOP zone 2. Surfaces generated using 12, six and three neighbours are illustrated in Figure 10.1. Examination of these surfaces suggested that there is little to support the use of 12 neighbours in preference to six. The spatial distribution of the input data points for both DOP zones, as indicated by Figures 10.2 and 10.3, also supports the use of six neighbours to avoid the inclusion of inappropriate points in the interpolation.

The geographic masks generated from the DOP zones were now applied to the data. Surfaces generated within the appropriate masks, using six neighbours, were then combined to provide one surface covering the image area. Figure 10.4 illustrates the combined masked surface.

### 10.4.2 Generation of Thiessen polygons

The models used for the relationship between depth and TDN for each of the DOP zones are essentially independent. It is therefore reasonable to construct sets of Thiessen polygons for the whole area from the residual points for each model. This may be carried out, using the rasterised residual point files as input, by the IDRISI routine THIESSEN. The boundaries for polygons at the edge of the data for each model extend towards the edge of the image along the perpendicular bisector of a line joining the data points to which they refer. For each model surface, these polygons were truncated using the, mutually exclusive, geographic masks from GRASS. The two polygonal surfaces were then combined

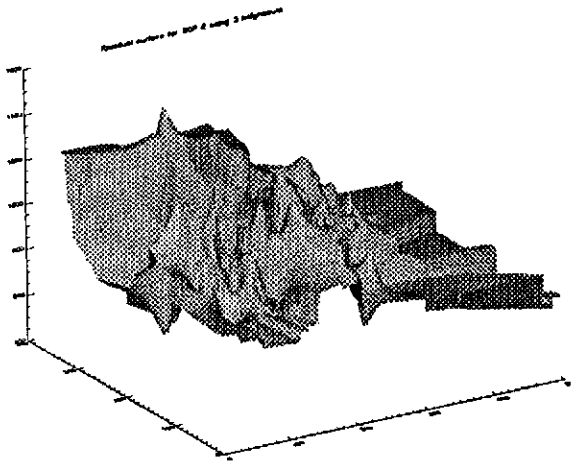

(a) Using 3 neighbours

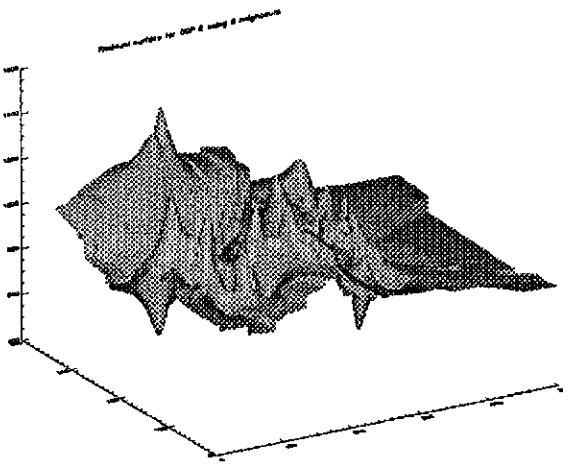

(b) Using 6 neighbours

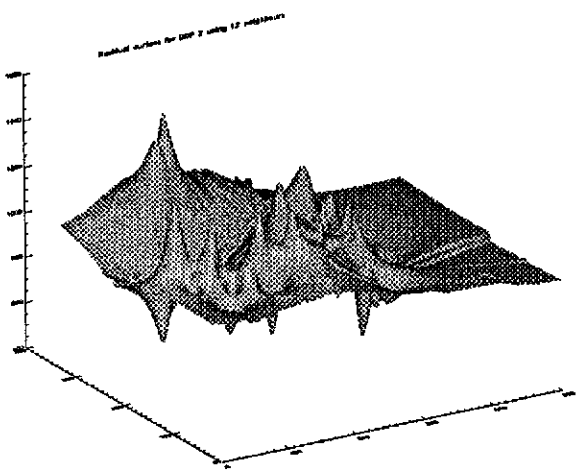

(c) Using 12 neighbours

Figure 10.1 : Test Residual Surfaces for DOP zone 2

using the IDRISI OVERLAY module. The polygonal surface is illustrated in Figure 10.5.

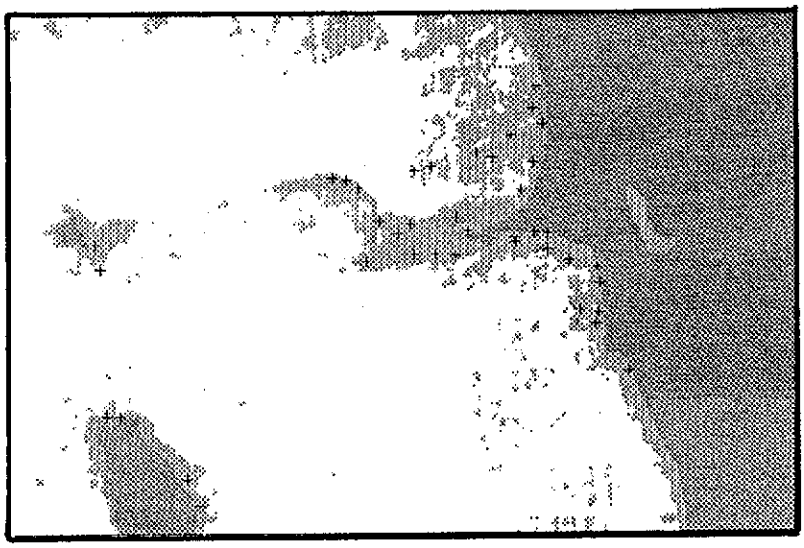

Figure 10.2 : Spatial distribution of points in DOP zone 2

Figure 10.3 : Spatial distribution of points in DOP zone 3

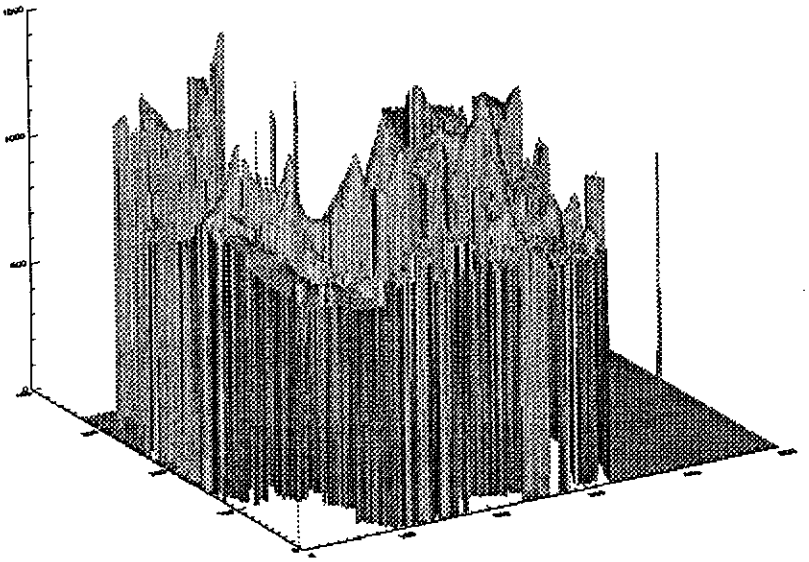

Figure 10.4 : Combined residual surface using inverse distance weighting

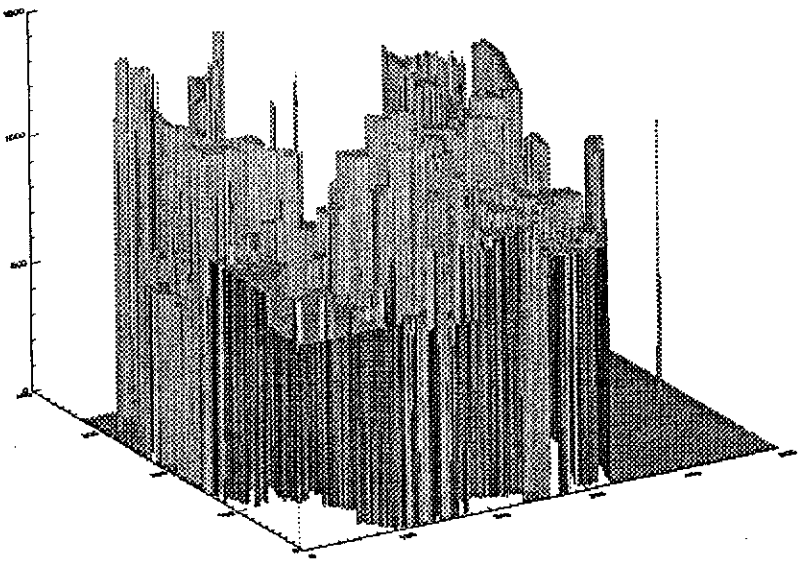

Figure 10.5 : Combined residual surface using Thiessen polygons

## 10.5 Testing the Models

Having generated residual surfaces it is now possible to use those surface to improve the estimation of depth from transformed DNs at other locations.

### 10.5.1 Data Extraction

The reserved control set of soundings described in Chapter 6 was used as input to the program SOUNDER. The procedure used was the same as that described in Section 9.1.2. In addition to data being extracted from the three image data files and the DOP image it was also extracted from the residual surface images. Out of 159 possible soundings, 48 fell into no DOP zone, 10 fell in zone 1, 45 in zone 2, 45 in zone 3 and 11 in anomalous zones or in area classed as land. The output files from this process were input to a spreadsheet template and sorted according to DOP zone. Within the spreadsheet the regression models developed for the two DOP zones were applied to the appropriate TDNs to give sets of estimated depths.

### 10.5.2 Comparison of Results

The values extracted from the residual surface for the check data points may then be applied to the depth estimates. Comparisons can now be made between the estimated depths, before and after application of mapped residuals, and the original surveyed depths. Table 10.1 shows the deviation of uncorrected and corrected depths from surveyed depths for the distance weighted surface. Table 10.2 shows the same information for the Thiessen polygon surface. Table 10.3 shows the correlation coefficients between the surveyed depths, the uncorrected depth estimates and the corrected estimates.

The very poor relationship in DOP zone 3 led to a re-examination of the dataset. It was found that five pixels used in this dataset lay in a near shore area where recent breakwater construction work has taken place. These five pixels

were edited out of the dataset.

| | ZONE | DOP 2 | DOP 3 | DOP 3 (edited) |
|---|---|---|---|---|
| Using Residual Mapping | Min | -3.63 m | -11.00 m | -4.27 m |
| | Max | 3.63 m | 7.88 m | 4.72 m |
| | Mean | 0.09 m | 0.47 m | 0.51 m |
| | Std. Dev. | 1.57 | 3.46 | 2.56 |
| Without Residual Mapping | Min | -4.09 m | -9.80 m | -4.34 m |
| | Max | 4.31 m | 5.10 m | 4.27 m |
| | Mean | -0.01 m | 0.29 m | 0.86 m |
| | Std. Dev. | 1.90 | 3.22 | 2.35 |

Table 10.1 : Comparision of check values using distance weighted residual mapping

| | ZONE | DOP 2 | DOP 3 | DOP 3 (edited) |
|---|---|---|---|---|
| Using Residual Mapping | Min | -5.49 m | -10.95m | -4.17 m |
| | Max | 4.71 m | 9.43 m | 6.33 m |
| | Mean | -0.40 m | 0.72 m | 0.67 m |
| | Std. Dev. | 2.49 | 4.16 | 2.86 |
| Without Residual Mapping | Min | 4.09 m | 9.80 m | -4.34 m |
| | Max | -4.31 m | -5.10 m | 4.27 m |
| | Mean | -0.12 m | 0.19 m | 0.86 m |
| | Std. Dev. | 1.99 | 3.15 | 2.34 |

Table 10.2 : Comparision of check values using polygonal residual mapping

| | Uncorrected Depth Estimates | Corrected Depth Estimates | |
|---|---|---|---|
| | | Distance Weighted | Theissen Polygons |
| DOP Zone 2 | 0.45 | 0.68 | 0.45 |
| DOP Zone 3 | 0.26 | 0.29 | 0.27 |
| DOP Zone 3 (edited) | 0.42 | 0.46 | 0.45 |

Table 10.3 : Correlation between uncorrected and corrected depth estimates

## 10.6 Discussion of Results

### 10.6.1 Distance Weighted Surface

From Table 10.1 and Table 10.3 it can be seen that the use of the distance weighted surface has reduced the error in estimation for DOP zone 2 but slightly increased the error in DOP zone 3. This is illustrated in Figure 10.6, which shows plots of the estimated depths versus the surveyed depths for DOP zone 2, with and without the use of residual mapping. Figure 10.7 shows the same plots for DOP zone 3.

These results indicate that a two-band model is capable of estimating depths in DOP zone 2 with a standard deviation of 1.9 m and that this may be improved by the use of distance weighted mapping. Despite the apparently better multiple correlation coefficient in the generation of the initial fit, the results for points in DOP zone 3 are disappointing. This may be interpreted more as a failure of the three-band model to estimate the depths, than of the spatial modelling to improve the precision of those estimates. Recently published work (Ji et al., 1992) has addressed the problem of shallow water depth estimation and

postulates a different model for depths down to about 5 m.

### 10.6.2 Thiessen Polygon Surface

Table 10.2 and Table 10.3 do not offer any support for the use of a polygonal method of residual interpolation. Figures 10.8 and 10.9 show what amounts to a randomisation of the depth estimates when these mapped residuals are applied. The failure of the method of surface generation would tend to suggest that the variations that contribute to the residuals are not controlled by hard boundaries. This observation is, however, possibly prejudiced by the relatively coarse spatial sampling of the surveyed depths. The development of a polygonal surface within areas of known bottom cover might be worth investigation, should a bottom cover map of sufficient spatial accuracy be available.

## 10.7 Summary

Residuals from fitted depth points may be spatially interpolated to cover a whole image. This enables the correction of depth estimates at other locations. In order to honour the data at the initially fitted points a surface generation method such as Thiessen polygons or inverse distance weighting can be used. Figure 10.10 shows the data flow during the generation and testing of such surfaces.

A comparison of these two methods shows that distance weighting offers some improvement in depth prediction in DOP zone 2. There is no apparent improvement in DOP zone 3 which may be attributable to the use of an inappropriate depth estimation model. The use of Thiessen polygons offers no improvement in either DOP zone.

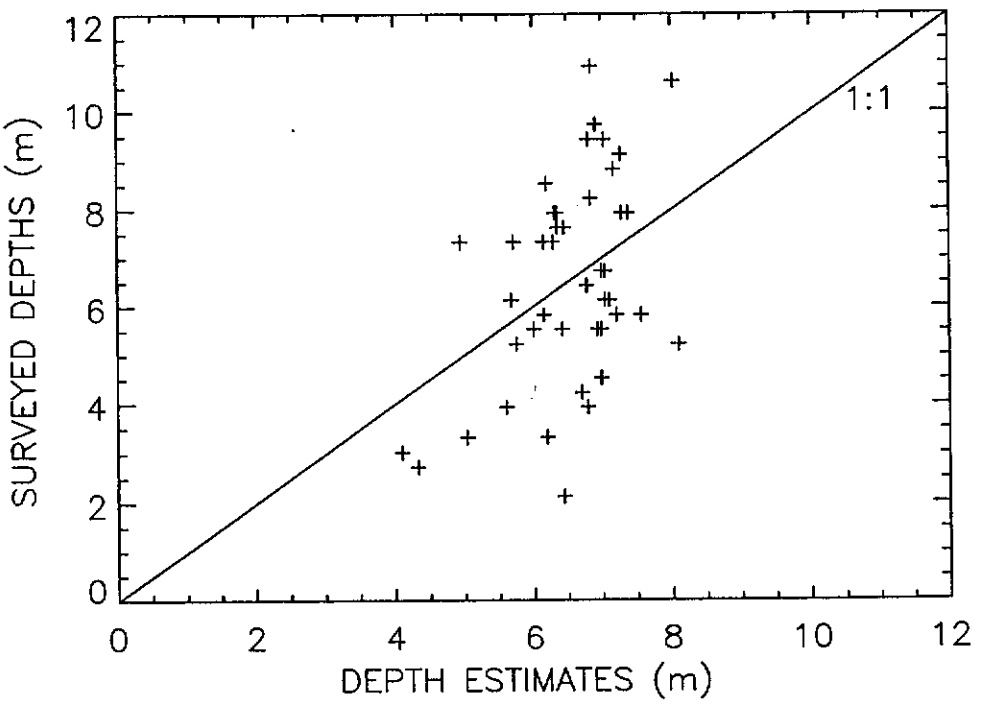


(a) Uncorrected

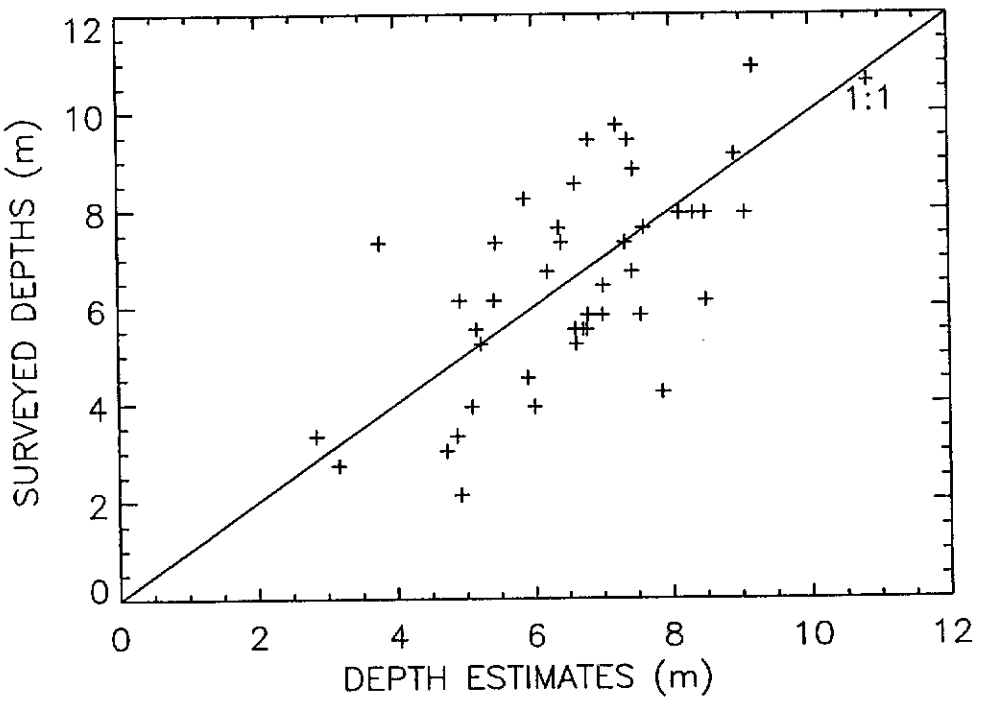


(b) Corrected

Figure 10.6 : Comparison of results - distance weighted residuals - DOP zone 2

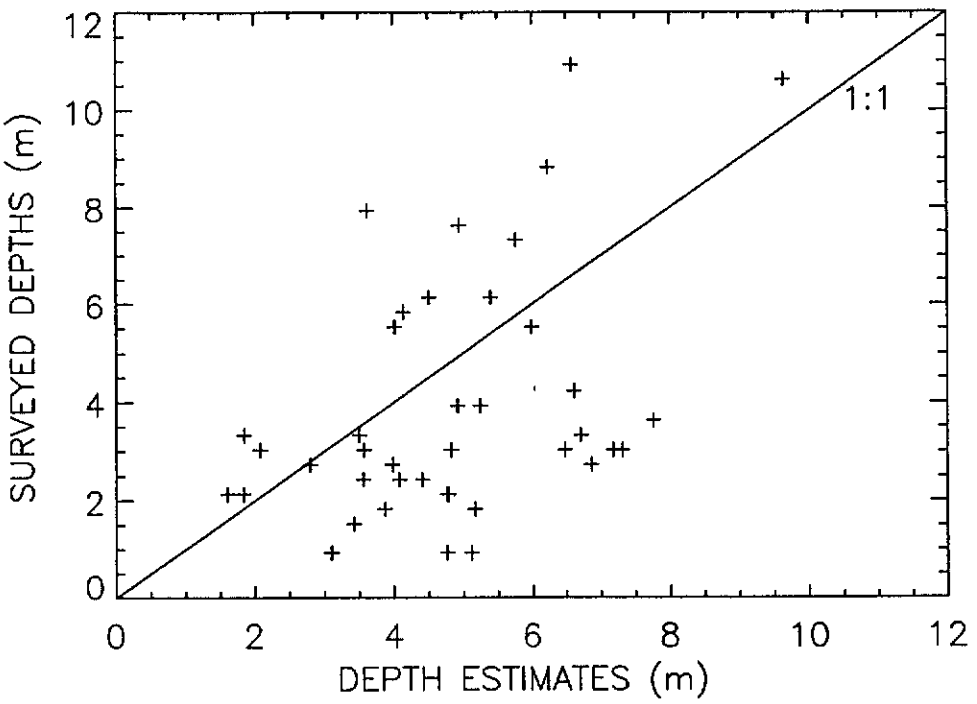


(a) Uncorrected

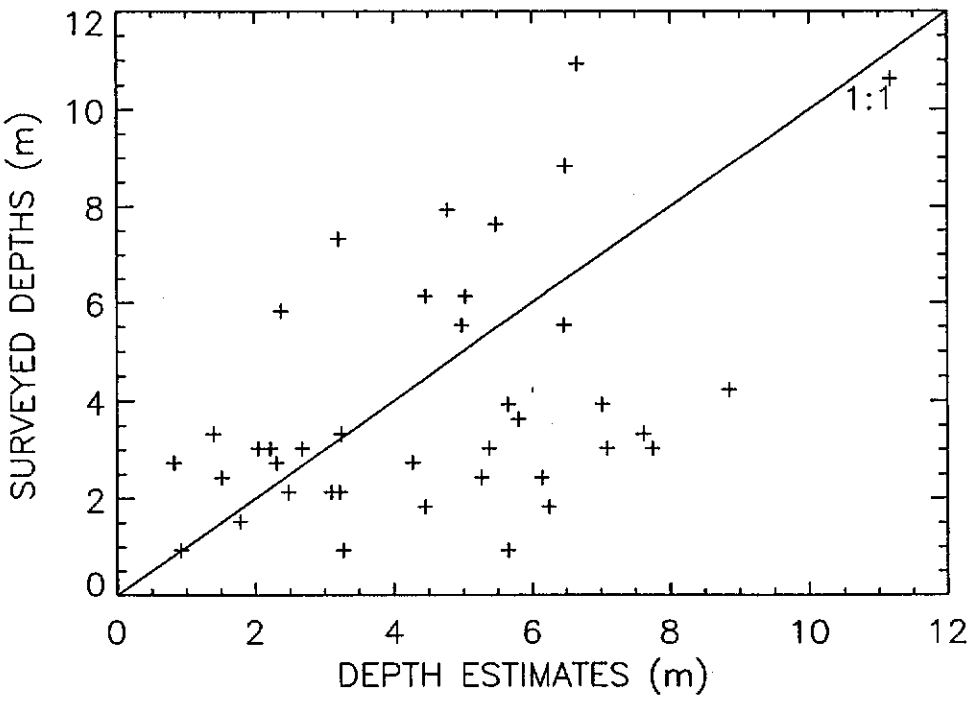


(b) Corrected

Figure 10.7 : Comparison of results - distance weighted residuals - DOP zone 3

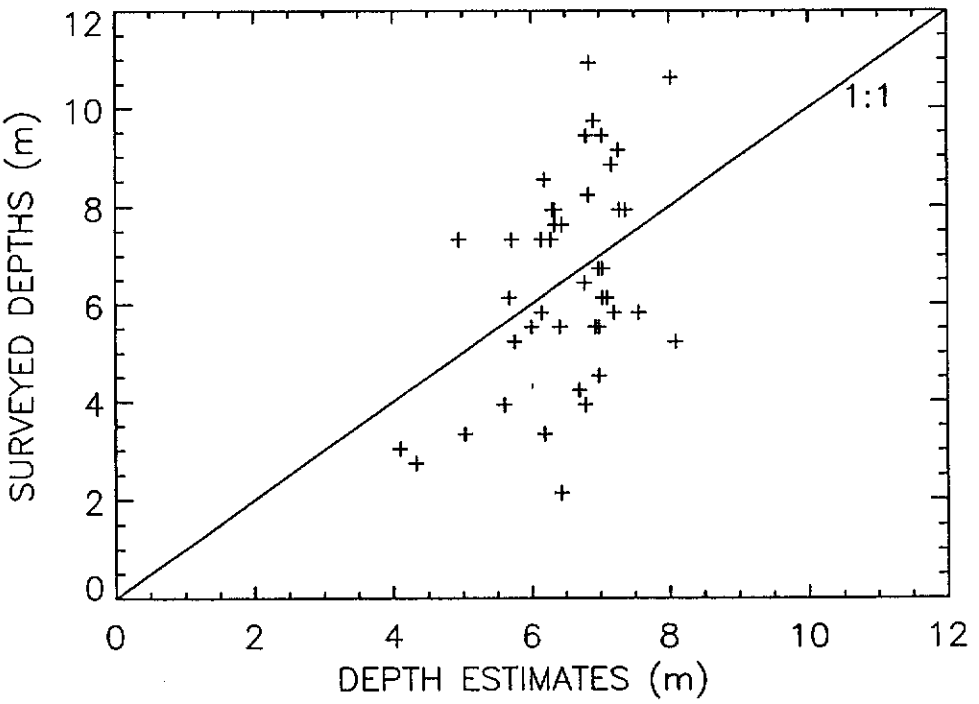


(a) Uncorrected

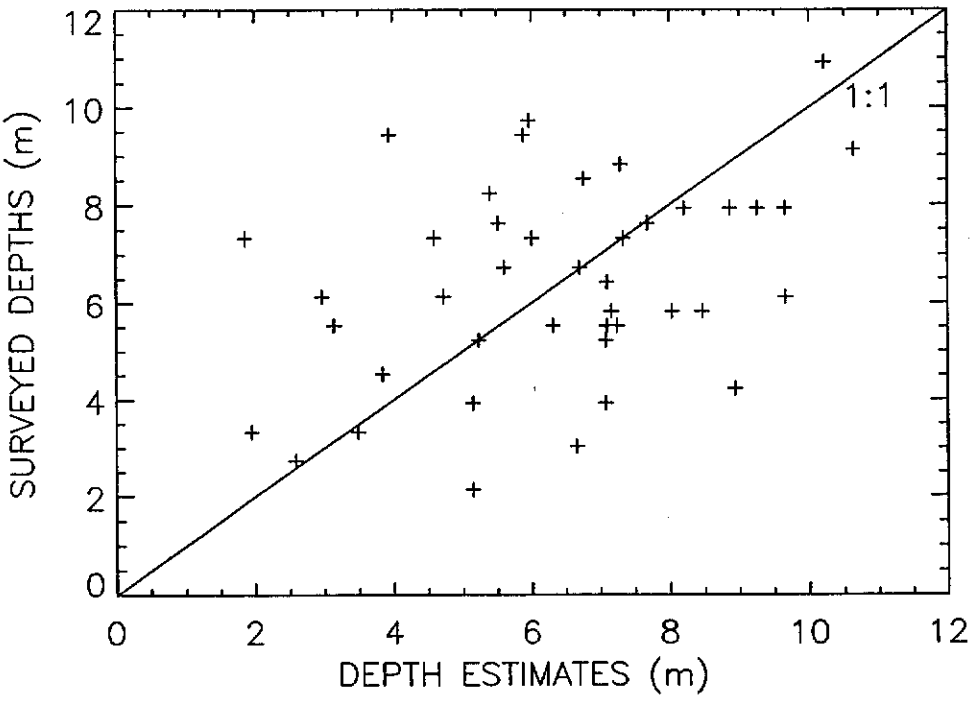


(b) Corrected

Figure 10.8 : Comparison of results - polygonal residuals - DOP zone 2

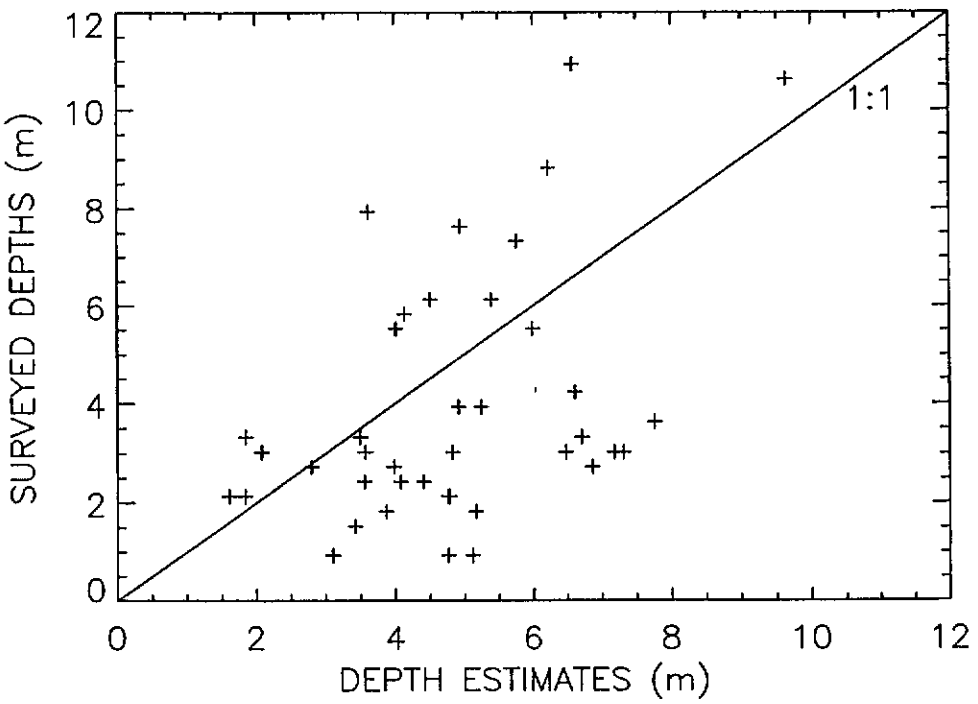


(a) Uncorrected

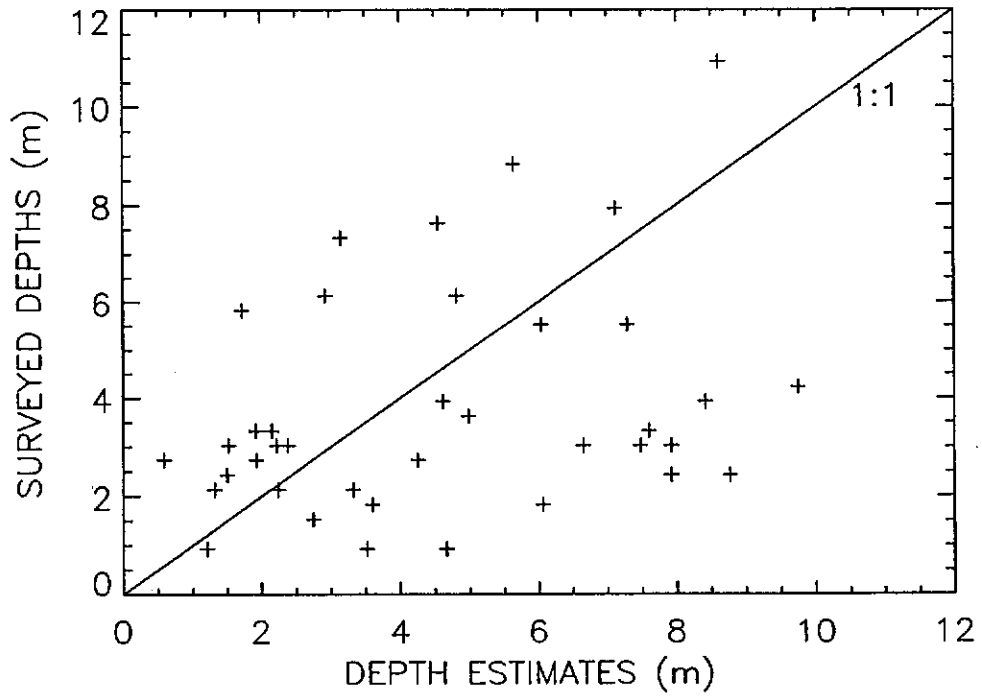


(b) Corrected

Figure 10.9 : Comparison of results - polygonal residuals - DOP zone 3

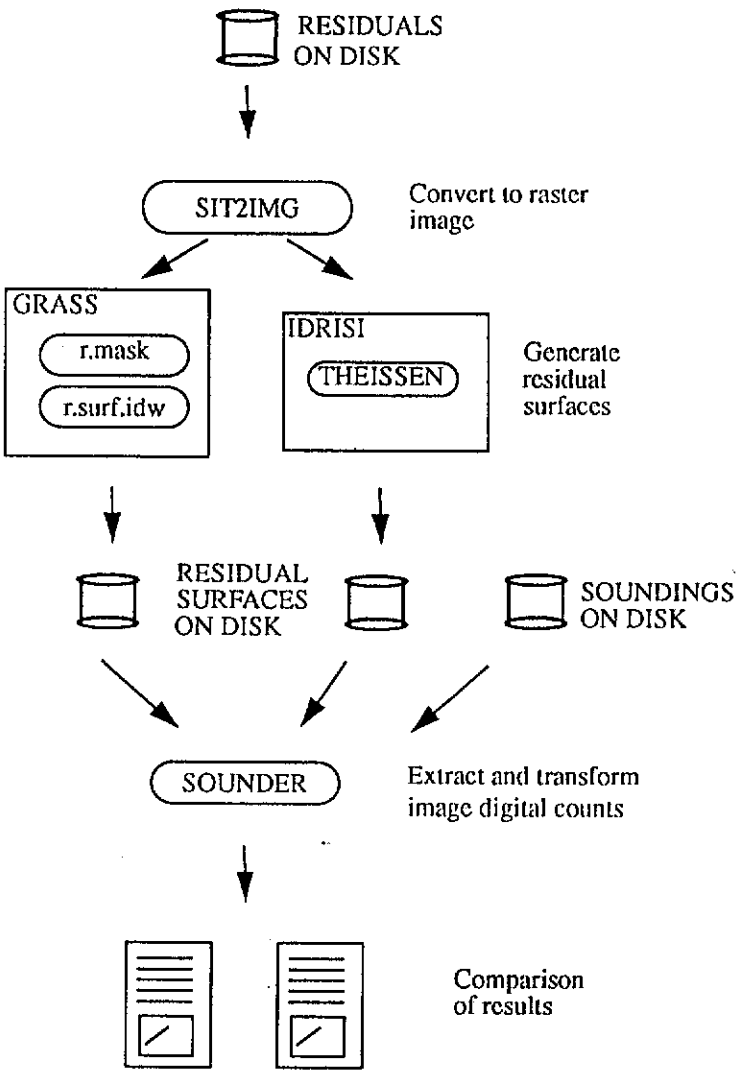


Figure 10.10 : Flowchart for generation and testing of residual surfaces

# CHAPTER 11

# CONCLUSIONS AND RECOMMENDATIONS

## 11.1 Conclusions

This research set out to demonstrate the use of remotely sensed multispectral data as a reconnaissance tool for bathymetric surveying. It was intended that a review of existing techniques be followed by the application of a suitable algorithm to Landsat Thematic Mapper data for a test site off the Perth metropolitan coastline.

The development of techniques for the extraction of water depth information from multispectral data may be traced over the past 23 years. It progresses, through a series of experiments and demonstrations using both satellite and airborne data acquisition systems. Satellite systems have been shown to be capable, under optimum conditions, of estimating depths down to 21 m with an RMS one metre, whilst airborne systems have achieved an RMS depth accuracy of 0.5 m.

These accuracy of these depth measurements, and the spatial resolution of the sensors, may be compared with IHO guidelines for bathymetric surveys. Those guidelines recommend that, for 1:10000 scale charting, depths be determined to $\pm$ 0.3 m with a positional accuracy of $\pm$ 15 m. Whilst some airborne systems are capable of satisfying these requirements, satellite systems cannot. Nevertheless the Landsat TM instrument may be used effectively in a reconnaissance role.

The basic physical principles governing the attenuation of light within water bodies allow a model to be developed which relates depth to radiance leaving the water column. That radiance is subsequently modified by atmospheric transmission effects and is also subject to variations caused by non-uniform optical properties in the water body. If assumptions are made about the spatial distribution of atmospheric effects and some means is provided to take account of spatial variations in water column optical characteristics, it is then possible to develop algorithms for the extraction of depth information from the signals received at a remote sensing platform.

A number of potential algorithms suitable for the processing of Thematic Mapper data have been published in recent years. They cover a considerable range of complexity. Some have been published as part of case studies using real data and some have been postulated as theoretical, but validated using synthetic data. They can be broadly categorised as either calibrated methods that use know depth points as input to a regression, or uncalibrated methods which derive depth estimates directly from remotely sensed data. On consideration of these methods an adaptation of a spatially iterated multi-band regression method, previously tested with synthetic data, was chosen for demonstration by this study.

A study area, the Parmelia Bank in Cockburn Sound, was selected on the grounds of availability of data and suitability of bottom topography. Disappointing results from an early investigation of airborne scanner data led to the decision to limit this study to the use of satellite data. Digital Landsat Thematic Mapper data were acquired, and soundings from a portion of an Admiralty Chart were digitised.

The need for a common spatial reference frame between remotely sensed data and ground truth was addressed by the co-registration of both datasets through the common medium of the Australian Map Grid. This approach, rather than the warping of the image data to fit the map grid, allows spatial resampling to be kept to a minimum. Some unavoidable resampling of the data has already been applied by the signal reception facility. A transformation was established so that each sounding can be related to a particular image pixel.

Satellite imagery over water is subject to a number of forms of noise. The chief amongst these, periodic striping may be compensated for using either a gain and offset correction or, as was done for this study, an offset correction only. The application of this correction required the writing of custom software. The other major noise component frequently present in such imagery is sunglint. Although apparently effective algorithms exist to compensate for its effects, a simple test indicated that, in the imagery under consideration, sun glint was present to a negligible extent.

In order to provide limited spatial fields in which to develop residual surfaces, two approaches to image segmentation were attempted. The first divided the image on the basis of the depth to signal extinction in three optical wave bands. This resulted in an image comprising three major classes and a number of very much smaller classes with anomalous values. The second divided the image into perceived bottom classes using training sites chosen with the aid of aerial photography and a hydrographic chart. This classification produced five classes and a number of anomalous and unclassified pixels. Both segmented images were smoothed using a modal filter. This filter was applied to improve

the classification prediction by taking account of the spatial context of each pixel.

Data values relevant to each sounding in the experimental set were extracted from the preprocessed images and the classification images. Regression relationships were established between the surveyed depths and the transformed DNs (TDN) using suitable combinations of independent variables. This operation was performed on data sets segmented using both DOP zones and bottom cover classes. The results for the bottom cover segmentation mitigate against the use of that method in this case. Relationships within the DOP zones, although weak, offer suitable coefficients as input to the spatial modelling stage of the spatially iterated multiband depth extraction algorithm.

Residuals from fitted depth points may be spatially interpolated to cover a whole image. This enables the correction of depth estimates at other locations. In order to honour the data at the initially fitted points a surface generation method such as Thiessen polygons or inverse distance weighting can be used. A comparison of these two methods showed that distance weighting offers some improvement in depth prediction in DOP zone 2. There is no apparent improvement in DOP zone 3, which may be attributable to the use of an inappropriate depth estimation model. The use of Thiessen polygons offers no improvement in either DOP zone.

This research demonstrated that, under some conditions, the depth estimates, made using a weak calibrated regression relationship between transformed remotely sensed values and surveyed depths, can be improved. This improvement is brought about by mapping residuals from the regression. Improvement in estimation of depths at a check set of locations was effected using

a two waveband model in the spatial segment of the image appropriate to those wavebands (DOP zone 2). The residuals from the fit were modelled using inverse distance weighting.

In the case of a three waveband model, in the appropriate spatial zone (DOP zone 3), the apparently stronger regression relationship was not sustained by a check group of soundings, and the application of residuals modelled using distance weighting offered little improvement. It should be noted that the dominant waveband providing depth information, for this inshore study site, was Thematic Mapper Band 2.

In both cases an alternative method of residual mapping, the use of Thiessen polygons, was not appropriate. Image segmentation on the basis of assumed bottom cover classes prior to the development of regression relationships also proved unsuitable.

It should be noted that all the data used in this study were sourced on the basis of availability. This led to the use of a set of soundings whose spatial distribution, within the DOP zones, may be less than optimum and whose spatial and depth accuracy was be assumed correct. In addition, the lack of accurate bottom sampling for the development of cover classes led to the use of assumed cover types which contain a degree of spectral confusion.

### 11.3 Recommendations

Further work is required to address the apparent failure of the three waveband model in DOP zone 3. Investigation of a shallow water model recently postulated by other workers would be of use. In addition, segmentation of the

image into observed rather than assumed bottom classes would enable models employing appropriate wavebands to be developed within DOP zones, and also permit spatial modelling to be performed within regions of known like bottom cover. A number of conditions would be required for this work.

The spatial sampling of the ground truth data would need to be of appropriate design and would need to be accompanied by bottom sampling. The acquisition of ground truth at the time of imaging would enable water quality estimates to be made. Such work would require access to considerable physical resources. A survey vessel fitted with an echo sounder, positioning system and equipment for both water and bottom sampling, would need to be deployed to the study area coincidently with a satellite overpass.

Research is required on the development of spatial models appropriate to the generation of variable surfaces within boundaries constrained by some form of classification. The development of such models calls for the software tools provided by high powered raster Geographic Information Systems. A GIS such as GRASS or the raster modules of Arc-Info would be suitable. These systems also offer image processing and statistical analysis capabilities to support other facets of the work. There is considerable advantage in keeping all processing within one environment although the cost of the initial investment in software and hardware may be considerable.

Based on the overwhelming contribution to the regression models made by TM Band 2 and the probability that for coastal waters the maximum penetration depth is achieved at around 0.5 $\mu$m , the use of SPOT HRV Band 1 data (0.5 $\mu$m - 0.59 $\mu$m) should be considered. This data may also contain less noise than

that which seems to be prevalent in the visible bands of the Thematic Mapper.

If a bathymetric survey reconnaissance system based on satellite data and the spatial modelling of environmental parameters can be demonstrated, then the possibility exists to extend that system to survey work. This could be achieved through the use of an appropriate airborne system such as the CASI. The narrower swath width of such an airborne instrument would present challenges associated with the rectification of over-water image data. This would require research into the design and deployment of either floating or submersible tethered targets capable of remaining on station, in water up to 30 m deep, at all stages of the tide.

## REFERENCES

Benny, A.H. and G.J.Dawson (1983) Satellite Imagery as an Aid to Bathymetric Charting in the Red Sea, The Cartographic Journal, Vol. 20, No. 1, pp. 5 - 16.

Cresswell, G.R. (1991) The Leeuwin Current - Observations and Recent Models. Journal of the Royal Society of Western Australia. Vol. 74, p. 1 - 14.

Danaher, T. and P.Smith (1988) Applications of Shallow Water Mapping Using Passive Remote Sensing. Proceedings of a Symposium on Remote Sensing of the Coastal Zone, Gold Coast, Queensland, 7 - 9 September 1988, 7 pp.

Daniel, C. and F.S.Wood (1971) Fitting Equations to Data, John Wiley and Sons, New York, N.Y., 342 pp.

Davis, J. C. (1986) Statistics and Data analysis in Geology, John Wiley and Sons, New York, N.Y., 646 pp.

DCE (1979) Cockburn Sound Environmental Study. 1976-1979, Report Number 2, Department of Conservation and Environment (W.A.), October 1979, 103 pp.

Doerffer, R. (1979) Applications of a Two-flow Model for Remote Sensing of Substances in Water, in Passive Radiometry of the Ocean, J.F.R. Gower (ed), D.Reidel, Dordrecht, Netherlands, pp. 221 - 232.

Estep, L. (1990) Airborne Stereo Multispectral Sensor (ASMSS) - A Feasibility Study for the US Navy, The Hydrographic Journal, No. 56, pp. 5 - 7.

Gee, L. and B.C.Forster (1984) Landsat Data as an Aid to Hydrographic and Bathymetric Mapping in Shallow Seas, Proceedings of the Third Australasian Remote Sensing Conference, Gold Coast, Queensland, 21 - 25 May 1984, pp. 161 - 173.

Gordon, H.R. and W.R.McCluney (1975) Estimation of the Depth of Sunlight Penetration in the Sea for Remote Sensing, Applied Optics, Vol. 14, pp. 413 - 416.

Hallada, W.A. (1984) Mapping Bathymetry with Landsat 4 Thematic Mapper, Preliminary Findings, Proceedings of the Ninth Canadian Symposium on Remote Sensing, St John's, Newfoundland, 14 - 17 August 1984, pp. 277 - 285.

Hallada, W.A. (1989) Personal Communication.

Hammack, J.C. (1977) Landsat Goes to Sea, Photogrammetric Engineering and Remote Sensing, Vol. 43, No. 6, pp. 683 - 691.

Hick, P.T. (1992) Personal Communication.

Hick, P.T. and R.Scoones (1988) Satellite Derived Imagery for Water Penetration and its Relevance to Fisheries in the Kimberley Region of Western Australia, Restricted Report 122R, CSIRO Division of Exploration Geoscience, Perth, W.A., 29 pp.

Hill, J. and B.Sturm (1991) Radiometric Correction of Multi-temporal Thematic Mapper Data for Use in Agricultural Land-Cover Classification and Vegetation Monitoring, International Journal of Remote Sensing, Vol. 12, pp. 1471 - 1491.

Hollinger, A. B., N.T.O'Neill, J.D.Dunlop, M.T.Cooper, H.Edel, and J.R.F.Gower (1985) Water Depth Measurement and Bottom Type Analysis Using a Two-dimensional Array Imager, Proceedings of the Nineteenth International Symposium on Remote Sensing of Environment, Ann Arbor, Michigan, 21 - 25 october 1985, pp. 553 - 563.

Honey, F.M. and P.M.Byrne (1978) Air Survey and Satellite Imagery: Tools for Shallow Water Bathymetry. Proceedings of the 20th Australian Survey Congress, Darwin, N.T.

Hydrographer of the Navy (1965) Admiralty Manual of Hydrographic Surveying, Hydrographer of the Navy, London, U.K., 671 pp.

I.H.O. (1987) IHO Standards for Hydrographic Surveys, International Hydrographic Organisation Special Publication No. 44, International Hydrographic Bureau, Monaco, pp. 1 - 9.

Ibrahim, M. and A.P.Cracknell (1990) Bathymetry using Landsat MSS data of Penang Island in Malaysia, International Journal of Remote Sensing, Vol. 11, pp. 557 - 559.

Isaaks, E.H. and R.M.Srivastava (1989) Applied Geostatistics, Oxford University Press, New York, N.Y., 561 pp.

Jain, S.C. and J.R.Miller (1977) Algebraic Expression for the Diffuse Irradiance Reflectivity of Water from the Two-flow Model, Applied Optics, Vol. 16, pp. 202 - 204.

Jain, S.C., H.H.Zwick and R.A.Neville (1981) Passive Bathymetry with Airborne Multispectral Scanner, Proceedings of the Seventh Canadian Symposium on Remote Sensing, Winnipeg, Manitoba. 8 - 1 September 1981, pp. 513 - 519.

Jerlov, N. G. (1976) Marine Optics, Elselvier, Amsterdam, Netherlands, 231 pp.

Ji, W., D.L.Civco and W.C.Kennard (1992) Satellite remote Bathymetry: A New Mechanism for Modelling, Photogrammetric Engineering and Remote Sensing, Vol. 58, pp. 545 - 549.

Joseph, J. (1950) Untersuchungen uber Ober und Unterlightmessungen im Meere und uber ihren Zusammenhang mit Durchsichtigkeitmessungen, Deut. Hydrograph. Z., Vol. 3, pp. 324 - 335.

Jupp, D.L.B. (1988) Background and Extensions to Depth of Penetration (DOP) Mapping in Shallow Coastal Waters, Proceedings of a Symposium on Remote Sensing of the Coastal Zone, Gold Coast, Queensland, 7 - 9 September 1988, 19 pp.

Jupp, D.L.B, P.R.Guerin, K.K.Mayo, D.vanR.Claasen and R.A.Kenchington (1984) Landsat as a Support for Management of the Great Barrier Reef, Proceedings of the Third Australasian Remote Sensing Conference, Gold Coast, Queensland, 21 - 25 May 1984, pp. 706 - 716.

Jupp, D.L.B., K.K.Mayo, D.A.Kuchler, S.J.Heggen, S.W.Kendal, B. M. Radke and T. Ayling (1985) Landsat Based Interpretation of the Cairns Section of the Great Barrier Reef Marine Park, Natural Resources Series, 4, C.S.I.R.O. Division of Water and Land Resources, Canberra, A.C.T, 51 pp.

Kilbride, A.R. (1985) The Hydrographic Application of Spacelab Photography, Photogrammetric Record, Vol. 11, pp. 711 - 715.

Lemaire, O., L.Loubersac, H.Varet, P-Y.Burban and F.Chenon (1990) Bathymetric Modelling using SPOT Data: The Aitutki Example (Cook Is.). Proceedings of the Fifth Australasian Remote Sensing Conference, Perth, W.A. 8 - 12 October 1990, pp. 793 - 802.

Loubersac, L., P-Y. Burban, O. Lemaire, H. Varet and F. Chenon (1991) Integrated Study of Aitutaki's Lagoon (Cook Islands) Using SPOT Satellite Data and In Situ Measurements: Bathymetric Modelling, Geocarto, No. 2, pp. 31 - 36.

Lusch, D.P. (1989) Fundamental Considerations for Teaching the Spectral Reflectance Characteristics of Vegetation Soil and Water, in Current Trends in Remote Sensing Education, M.D.Nellis, R.Lougeay and K.Lulla (eds), Geocarto International Centre, Hong Kong, pp. 5 - 27.

Lysenga, D.R. (1978) Passive Remote Sensing Techniques for Mapping Water Depth and Bottom Features, Applied Optics, Vol. 17, No. 3, pp. 379 - 383.

Lysenga, D.R. (1981) Remote Sensing of Bottom Reflectance and Water Attenuation Parameters in Shallow Water Using Aircraft and Landsat Data, International Journal of Remote Sensing, Vol. 2, No. 1, pp. 71 - 82.

Lysenga, D.R. (1985) Shallow Water Bathymetry Using Combined Lidar and Passive MSS Data, International Journal of Remote Sensing, Vol. 6, No.1, pp. 115 - 125.

NMCA (1972) The Australian Map Grid Technical Manual, Special Publication No. 7, National Mapping Council of Australia, AGPS, Canberra, A.C.T., 78 pp.

O'Neill, N.T., A.R.Kalinauskas and J.R.Miller (1987) Passive Optical Bathymetry: Status Review and Perceived Role in Operational Hydrography, Proceedings of the Eleventh Canadian Symposium on Remote Sensing, Waterloo, Ontario, 22 - 25 June 1987, pp. 719 - 725.

O'Neill, N.T. and J.R.Miller (1989) On Calibration of Passive Optical Bathymetry Through Depth Soundings. Analysis and Treatment of Errors Resulting from the Spatial Variation of Environmental Parameters, International Journal of Remote Sensing, Vol. 10, No. 9, pp 1481 - 1501.

Paredes, J.M. and R.E.Spero (1983) Water Depth Mapping from Remotely Sensed Data Under a Generalised Ratio Assumption, Applied Optics, Vol. 22, No. 8, pp. 1134 - 1135.

Philpot, W.D. (1987) Radiative Transfer in Stratified Waters: A Single-scattering Approximation for Irradiance, Applied Optics, Vol. 26, No. 19, pp. 4123 - 4131.

Philpot, W.D. (1989) Bathymetric Mapping with Passive Multispectral Imagery, Applied Optics, Vol. 28, pp 1569 - 1578.

Polcyn, F.C. (1976) Final report on NASA/Cousteau Ocean Bathymetry Experiment, Remote Bathymetry Using High Gain Landsat Data, NASA-CR-ERIM-118500-1-F

Polcyn, F.C. and D.R.Lysenga (1979) Landsat Bathymetric Mapping by Multi-temporal Processing, Proceedings of the Thirteenth International Symposium on Remote Sensing of Environment Ann Arbor, Michigan, 23 -27 August 1979, pp. 1269 - 1276.

Polcyn, F.C. and I.J.Satinger (1969) Water Depth Determinations Using Remote Sensing Techniques, Proceedings of the Sixth International Symposium on Remote Sensing of Environment, Ann Arbor, Michigan, 6 - 10 October 1969, pp. 1017 - 1028.

Richards, J.A. (1986) Remotely Sensed Digital Image Analysis: An Introduction, Springer-Verlag, Berlin, Germany, 281 pp.

Richardson, J. (1989) Satellites Serving Australia. Australian Geographic, No. 13, pp. 19 - 27.

Ripley, B.D. (1981) Spatial Statistics, John Wiley and Sons, New York, N.Y., 251 pp.

Schowengerdt, R.A. (1983) Techniques for Image Processing and Classification in Remote Sensing, Academic Press, New York, N.Y., 249 pp.

Simonett, D.S. (1983) The Development and Principles of Remote Sensing, in Manual of Remote Sensing, Vol. 1, R.N.Colwell (ed), American Society of Photogrammetry, Falls Church, Virginia, pp. 1 - 32.

Smith, V.E., R.H.Rogers and L.E.Reed (1975) Thematic Mapping of Coral Reefs Using Landsat Data, Proceedings of the Tenth International Symposium on Remote Sensing of the Environment, Ann Arbor, Michigan, 6 -10 October 1975, pp. 585 - 594.

Spitzer, D. and R.W.J.Dirks (1987) Bottom Influence on the Reflectance of the Sea, International Journal of Remote Sensing, Vol. 8, pp. 279 - 290.

Tanis, F.J. and H.J.Byrnes (1985) Optimisation of Multispectral Sensors for Bathymetry Applications. Proceedings of the Nineteenth International Symposium on Remote Sensing of Environment, Ann Arbor, Michigan, 21 -25 October 1985, pp. 865 - 874.

Tanis, F.J. and W.A.Hallada (1984) Evaluation of Landsat Thematic Mapper Data for Shallow Water Bathymetry, Proceedings of the Eighteenth International Symposium on Remote Sensing of Environment, Paris, France, 1 -5 October 1984, pp. 629 - 643.

van Hengel, W. and D.Spitzer (1991) Multi-temporal Water Depth Mapping by Means of Landsat TM, International Journal of Remote Sensing, Vol. 12, No. 4, pp. 703 - 712.

Wald, L. and J.M. Monget (1983) Sea Surface Winds from Sun Glitter Observations, Journal of Geophysical Research, Vol. 88, No. C4, pp 2547 - 2555.

Warne, D.K. (1978a) Landsat as an Aid in the Preparation of Hydrographic Charts. Photogrammetric Engineering and Remote Sensing, Vol. 44, pp. 1011 - 1016.

Warne, D.K. (1978b) Landsat Image Analysis: Application to Hydrographic Mapping, Technical Report EP-T 22, Dept of Engineering Physics, Australian National University, Canberra, A.C.T., 217 pp.

Weidmark, W.C., S.C.Jain, H.H.Zwick and J.R.Miller (1981). Passive Bathymetric Measurments in the Bruce Peninsula Region of Ontario, Proceedings of the Fifteenth International Symposium on Remote Sensing of Environment, Ann Arbor, Michigan, 11 -15 May 1981, pp. 811 - 821.

# APPENDIX A

## PROPRIETARY SOFTWARE USED

The research described in this thesis made use of a number of proprietary software packages. Whilst some of these, such as LOTUS 1-2-3, are sufficiently prevalent as to be regarded as standard tools, the more specialised software systems are less well known. This appendix contains a brief description of four of the systems used. Only those modules or routines used for major sections of data analysis are described, and the list is by no means exhaustive of all the routines used. The four systems described are :

(a) DISIMP

(b) IDRISI

(c) GRASS

(d) IDL

## DISIMP

The acronym DISIMP stands for Device Independent Software for IMage Processing. The system was initially written by the CSIRO Division of Information Technology but is now handled in a commercial arrangement with Clough Engineering. It is available for a variety of Unix based platforms.

The DISIMP system is a fully featured image processing environment specifically designed for the processing of remotely sensed imagery. It is designed on a modular basis with overall control through an executive program. Routines available are grouped into the following modules.

(a) Image file transfer

(b) Image administration

(c) Statistical analyses

(d) Intensity transformations

(e) Classification

(f) Display control

(g) Three-dimensional image display

(h) Image registration

(i) Hardcopy utilities

(j) Colour transforms

(k) Sensor processing

(l) Graphics

Routines from six of these categories were used in the course of the study. The system is capable of handling data in byte, integer and real form. Initially DISIMP version 4.0, running on a DUAL minicomputer at Curtin University was used. Subsequently the system at the CSIRO Remote sensing Group at Floreat Park, was used. The CSIRO system, running on a SUN SPARCstation has progressed from Version 5 to version 6.3 during the course of this work. Both systems incorporate 24 bit high resolution graphics terminals. A number of custom routines which make use of low level library calls to DISIMP modules are also available in the CSIRO implementation. Brief descriptions of modules used in this study follow.

**INHDD : Image file transfer module**

This module transfers intensity data from a band interleaved by line disk file into an image file that may be read by other DISIMP utilities. Data with one, two or four bytes per pixel can be handled, with up to 100 channels in any one image.

**SUBSET : Display control module**

This routine is used to transfer a subset of an image, or an entire image, to the display device. A large variety of options are available within this utility. Parameters such as aspect ratio, expansion factors and intensity scaling may be set. Subsets are selected by line, pixel and band addresses. A file containing a particular combination of parameters may be stored, enabling the rapid redisplay of the same image at a later date. Once the image is displayed, the user has access, through a mouse driven menu, to tools which allow zooming and roaming, adjustment of lookup tables and the manipulation of graphic overlay display planes. Lookup tables of particular enhancements may be saved for future use. A further utility, LOCATE, which is accessed via SUBSET, allows the user to determine the row/column coordinates of any point in the image. This utility enables control points, such as the intersection of two linear features, to be established to sub pixel accuracy.

**IMPCPY : Image file transfer module**

This is a general purpose image file transfer utility. It enables data to be transferred from disk to disk, disk to tape and disk to display device. In addition, display device image and graphic planes may be used as the input to the transfer process. The utility allows conversion of data between byte, integer and real types as well as scaling of data, either linearly or exponentially. Data subsets may be selected using line, pixel and band addresses.

**MODCON : Image registration module**

MODCON allows modification and editing of the control point files used by image registration procedures such as WARP. The utility may be used either to edit control point files selected from the screen using the utility CONPTS, or , as in this study, to create control point files from scratch using coordinates chosen using other utilities.

**WARP : Image registration module**

This utility takes a control point file and an image file as input. The control point file is used to develop the transformation between the image and the desired output coordinates. This transformation is then, optionally, applied to the whole image. A least squares fit is used to develop the transformation relationship with any power of polynomial being user selectable. Error statistics are reported and the option to try other powers of fit is offered. Once the user is satisfied with a transformation the warp may be carried out using either nearest neighbour, bilinear or cubic convolution resampling. Options for the selection of output pixel size and image extremity coordinates are offered.

**DSPSIG : Statistical Analysis module**

As preparation for input to a multispectral classification, this routine is used to select areas of the image for use as training sites. Areas are drawn on the image using a cursor and may be of any arbitrary shape. Up to 50 polygons may be selected for inclusion in any one training area. A signature file is created by this process. Optional output files include area files, containing the coordinates of the training sites, histogram and statistics files.

**CLMXL : Classification module**

This routine is the DISIMP implementation of a standard maximum likelihood classifier. The *a priori* probabilities of all classes are assumed to be equal and each pixel is assigned to the class which has the maximum likelihood value. Inputs to the process are an image file and a signature file, created by DSPSIG. Output is a classified image file with one byte per pixel.

**MODTRN : Intensity transformation module**

MODTRN computes the modal value, for each channel, of the intensities in a three by three neighbourhood and assigns that value to the pixel lying at the centre of the neighbourhood. This routine may be used to 'clean up' classified images produced by routines such as CLMXL. The procedure may be iterated if desired. The option to scale image data is available.

**DISBSQ : CSIRO WA Remote Sensing Group utility**

The DISIMP image format is a version of the band interleaved by line format, with a header and trailer record containing peripheral image data. This routine allows DISIMP images to be converted to band sequential images without headers for ease of transport to other systems. Options to subset images using line, pixel and band addresses are offered.

## IDRISI

IDRISI is a low cost raster Geographic Information System developed by the Graduate School of Geography at Clark University in Massachusetts. The word IDRISI is not an acronym. The system is named after an early Spanish cartographer who worked at the Sicilian court in the eleventh century.

It is designed to run on IBM compatible personal computers (PCs). The systems used in this research are installed on PC's with Intel 486 processors at Curtin University School of Surveying and Land Information and at the CSIRO Division of Soils at Floreat Park. Both systems are equipped with high resolution eight bit colour displays. Although the software is currently at version 4.0, the work described in this thesis was mainly done using Version 3.0.

Data are stored as single layer raster images in either real, integer of byte format. The data layers have no header of trailer information, making them readily portable to other systems. Header information is stored in associated documentation files. Although primarily a raster system some support for vector data entry, storage, manipulation and display is offered.

The system is modular with individual routines being accessed through a hierarchical menu system. Routines are grouped into the following categories:

(a) System Operation Modules

(b) Data Entry

(c) Data Storage and Management

(d) General Analysis

(e) GIS Modules

(f) Spatial Statistics

(g) Image Processing

(h) Vector / DBMS Modules

The principal individual routines used are described below.

**DIGITIZE : Data Entry Module.**

This is a vector digitising module which supports Summagraphics digitisers, or tablets which emulate them. Point, line and polygon features may be digitised, but not in the same session, as IDRISI stores each feature class in a separate file.

The digitiser is first 'set up' by the entry of four points at the extremes of the data which are used to develop a spatial transformation. The coordinates used may be either those of the map or chart being digitised or an assumed set allowing later transformation of the data. Up to 10,000 points may be digitised from one set up. Control of the software is through a combination of keyboard commands and commands generated via the digitiser puck.

**COLOR85 : Display Module**

This display module is designed for use with high resolution graphics devices capable of displaying 1024 by 768 pixels with 256 colours or grey shades. Real, integer and byte data can be displayed. Automatic scaling is provided for real and integer images and is available as an option for byte images.

The full 256 shades are only used for grey scale display. Colour composite images use 216 levels, whilst other displays of raster GIS layers use 16 colours at a time as the operator scrolls through the data. Overlay of vector line work is supported, as is onscreen digitising to linework files. The image may either be displayed at standard spatial resolution or a scaling factor may be employed. Cursor controlled zooming is available. Direct readout of the coordinates and value of any pixel may be obtained by pointing with the mouse controlled cursor. Interactive editing of colour palettes is offered.

**WINDOW : Data Storage and Management Module**

This routine extracts a rectangular sub-image from an original image. The subarea is referenced by row and column addresses.

**CONVERT : Data Storage and Management**

Data may be converted between the three raster data types, real, integer and byte. Conversions may also be made between data in any one of those representations stored as either ascii, binary or packed binary (run length encoded) and any other combination.

**RECLASS : GIS Module**

Pixels may be reclassified, either by equal intervals or by user defined schemes. Reclassification tables are input via a menu session.

**OVERLAY : GIS Module**

Pixel by pixel operations are performed by this module, which acts on a pair of image data layers at a time. Addition, subtraction, multiplication, division and exponentiation are supported. Also available are maximum, minimum, normalised ratio and 'cover'operations. With the cover operation one image may have pixels replaced by those of another that are non zero. Logical operations on binary images may be executed by using combinations of other operators.

**FILTER : Image Processing Module**

This module enable an image to be convolved in the spatial domain with a three by three pixel neighbourhood filter. Mean, median, modal, edge-enhancement, high and low pass filters are supported, as is the option to define a filter.

## GRASS

GRASS is the United States Army Construction and Engineering Research Laboratory's Geographic Resource Analysis Support System. It is a complex and fully featured raster Geographic Information System, with some support for vector data structures.

It is essentially in the public domain with a number of companies offering supported versions. It requires the Unix operating system but may be run on either PC or workstation platforms. The version used in this study is installed on a SUN SPARCstation of the CSIRO W.A. Remote Sensing Group. The system is primarily command line driven with in excess of 250 different primary commands available. The list of command groupings includes but is not limited to, the following.

(a) Digitising and map development

(b) Image processing

(c) Raster data analysis

(d) Map display and printing

(e) Report generation

(f) Digital terrain modelling

Apart from a number of core graphics display functions, only two analytical commands were used in this work. This description is brief and limited to those analytical commands.

**r.surf.idw**

This command generates a surface from an input raster layer containing a number of cells of known value in a raster whose other values are unknown. Inverse distance squared weighting is used to interpolate the surface. The number of neighbours used in the interpolation of any one pixel, is operator selectable.

**r.mask**

This command is used to generate a geographic mask within which processes may be confined in the spatial domain. The mask is generated in response to data values in a selected raster map layer and is essentially a reclassification of that map layer according to a user defined table.

# INTERACTIVE DATA LANGUAGE (IDL)

IDL is a software system for the analysis of scientific data. It is at once a programming language, a plotting and an image display package. It is the product of Research Systems Inc. of Boulder Colorado, USA. The system is complex and may be operated at a number of levels. Simple functions and procedures may be accessed by command line control or, at an other level of complexity, applications may be built as with any other programming language.

The software offers a comprehensive range of data analysis and plotting tools. Only the regression routines and some basic plotting routines were used in this research. A brief description of the regression routine follows.

The operation of such routines in IDL can be controlled by the use of scripts, somewhat similar to unix shell scripts.

**REGRESSION : Statistics routine**

This IDL routine performs a multivariate or univariate regressions and is called by the following sequence:

Regression, X,Y,W,A0,COEFF,resid,yfit,sigma,ftest,r,rmult,chisqr

Parameters capitalised are required, those in lower case are optional.

Parameters are :

Input

| | |
|---|---|
| X | An array of independent variable data of dimension nterms,npoints |
| Y | Column vector of dependant variable values, dimension npoints |
| W | Vector of weights fro each equation, dimension npoints |

Output

| | |
|---|---|
| AO | Constant term |
| COEFF | Vector of coefficients, dimension nterm |
| resid | Vector of residuals , dimension npoints |
| yfit | Vector of fitted values, dimension npoints |
| sigma | Vector of standard deviations of coefficients |
| ftest | Value of F for test of fit |
| Rmul | Multiple correlation coefficient |
| R | Vector of linear correlation coefficient |
| chisqr | Reduced weighted chi square for fit |

An ANOVA table to test the hypothesis that all coefficients are zero is output to screen or user specified file together with the regression summary.

Optional input includes keywords to denote missing values and variable names.

# APPENDIX B

## LISTING OF CUSTOM WRITTEN SOFTWARE

The research described in this thesis was carried out, where possible, using available software. There were however some tasks for which programs were not available. To perform these tasks software was written in C for use on a SUN SPARCstation 2.

The three programs written are :

| | | |
|---|---|---|
| (a) | dsoffset | To destripe single band images using offset correction only. |
| (b) | sounder | To extract values from three real valued, destriped images, apply log transform. Also extracts values from a classmap and optional residual image. |
| (c) | sit2img | Sets values of pixels in otherwise zero 2 byte image in response to scaled values in input list file. |

Listings of these three programs appear on the following pages.

```
/* Program dsoffset
        This program is designed to destripe over water landsat tm images
        using the offst only method proposed by Gee and Forster (1984)
        The program is capable of handling images that do not comprise a whole number
        of swaths. Provision is made for both leading and trailing partial swaths.


Required input files are :
        A single band byte image for destriping ( max size 1600 rows)
        A file containing offset values for each detector
         for each pattern of destriping.
        A file listing the striping pattern for each whole swath in the
         image

Variables used.

        Name            Type            Description

        inbuff          u char  line array used for data input
        outbuff         float   line array used for data output
        offset          float   10 by 16 array for up to 10 set of 16 detector offsets
        ftemp           float   temporary variable used on input
        i,j,k           int     loop counters
        si1             int     index to offset type before first whole swath
        si2             int     index to offset type after last whole swath
        si              int     array of indices to offset type for up to 100 swaths
        num_types       int     number of types of stripping pattern
        nrow            int     number of rows in the image
        ncol            int     number of collumns in the image
        temp1,temp2     int     temporary variables used on input
        num_groups      int     number of whole striping swaths in image
        first_line      int     line number of start of first whole swath
        trail           int     number of rows in trailing partial swath
        fp1* to fp5*    FILE    pointers to files
        infile          char    name of input file
        outfile         char    name of output file
        logfile         char    name of log file
        ofsfile         char    name of file containing offsets
        stripfile       char    name of file containing strip indices
```

```
Algorithm:

        Step 1: Dialogue with user to get file names and image size
                Open files

        Step 2: Allocate memory for line buffers

        Step 3: Read in offsets files, strip indices, start lines etc

        Step 4: Calculate number of whole swaths, size of trailing swath;
                read in the strip indices

        Step 5: In a get line, calculate, put line loop, apply offsets to leading part swath

        Step 6: In a series of get line, calculate, put line loops, apply offsets to main
                body of image

        Step 7: In a get line, calculate, put line loop, apply offsets to trailing part swath

        Step 8: Free memory, close files


Note
                Program is of simple design with no user defined functions.


*/


#include <stdio.h>
#include <math.h>
#include <malloc.h>

main() {

/*   set up variables */
        unsigned char *inbuff;
        float *outbuff,offset[10][16],ftemp;
        int i,j,k,si1,si2,si[100],num_types;
        int nrow,ncol,temp1,temp2,num_groups,first_line,trail;
        FILE *fp1,*fp2,*fp3,*fp4,*fp5;
        char infile[40],outfile[40],logfile[40],ofsfile[40],stripfile[40];


/*              Step 1: Dialogue with user to get file names and image size
                Open files                                                    */

        Get1:
        printf("\nEnter input image file name  : ");
        gets(infile);
        if((fp1 = fopen(infile,"rb"))==NULL){
                printf("\nUnable to open %s",infile);
                goto Get1;
        }
```

```
        Get2:
        printf("\nEnter output image file name  : ");
        gets(outfile);
        if((fp2 = fopen(outfile,"wb"))==NULL){
                printf("\nUnable to open %s",outfile);
                goto Get2;
        }

        Get3:
        printf("\nEnter log file name  : ");
        gets(logfile);
        if((fp3 = fopen(logfile,"w"))==NULL){
                printf("\nUnable to open %s",logfile);
                goto Get3;
        }

        Get4:
        printf("\nEnter offsets file name  : ");
        gets(ofsfile);
        if((fp4 = fopen(ofsfile,"r"))==NULL){
                printf("\nUnable to open %s",ofsfile);
                goto Get4;
        }


    Get5:
        printf("\nEnter stripes file name  : ");
        gets(stripfile);
        if((fp5 = fopen(stripfile,"r"))==NULL){
                printf("\nUnable to open %s",stripfile);
                goto Get5;
        }

        printf("\nEnter number of rows,columns in the image  :");
        fscanf(stdin,"%d,%d",&nrow,&ncol);

        printf("\nEnter number of types of stripe  :");
        fscanf(stdin,"%d",&num_types);

/*  Step 2:     Allocate memory for line buffers        */


        if ((inbuff = ( unsigned char *) calloc(ncol,sizeof(unsigned char))) == NULL)
                fprintf(stderr," Memory allocation fault for variable inbuff");
        if ((outbuff = ( float *) calloc(ncol,sizeof(float))) == NULL)
                fprintf(stderr," Memory allocation fault for variable outbuff");

/* Step 3:      Read in offsets files,  start lines etc    */

        for (i=0;i<16;i++) {
                for (j=0;j<num_types;j++) {
                        fscanf(fp4,"%f",&ftemp);
                        offset[j][i] = ftemp;
                }
        }
```

```
        printf("\n This routine uses IDRISI numbering conventions  Top left coords are  0,0");
        printf("\nEnter Idrisi line number for start of first whole swath.");
        fscanf(stdin,"%d",&first_line);

        printf("\n Enter strip index for strip prior to first full strip ");
        fscanf(stdin,"%d",&si1);

        printf("\n Enter strip index for strip after last full strip ");
        fscanf(stdin,"%d",&si2);


/*      Step 4: Calculate number of whole swaths, size of trailing swath    */

        printf("\nnrow first_line\n %d   %d\n",nrow,first_line);
        num_groups = (nrow-first_line)/16;
        trail = nrow - first_line - (16 * num_groups) ;

/* read in the strip indices */

        for (i=0;i<num_groups;i++) {

                fscanf(fp5,"%d",&temp1);
                si[i] = temp1;
        }


/*      Step 5: In a get line, calculate, put line loop, apply offsets to leading part swath
*/

        for (i=0;i<first_line;i++) {
                fread(inbuff,sizeof(unsigned char),1000,fp1);
                for (j=0;j<ncol;j++){
                        outbuff[j] = (float)(inbuff[j]) + offset[si1-1][16-first_line+i];
                }
                fwrite(outbuff,sizeof(float),ncol,fp2);

        }


/*      Step 6: In a series of get line, calculate, put line loops, apply offsets to main
                body of image                                                          */

        for (i=0;i<num_groups;i++) {
                for (j=0;j<16;j++) {
                        fread(inbuff,sizeof(unsigned char),1000,fp1);
                        /* report to log file */
                        fprintf(fp3,"\noffset for group %d line %d is %f: index is
                                        %d",i,j,offset[si[i]-1][j],si[i]-1);
                        for (k=0;k<ncol;k++) {
                                outbuff[k] = (float)(inbuff[k]) + offset[si[i]-1][j];
                        }
                        fwrite(outbuff,sizeof(float),ncol,fp2);
                }
```

```
        }

/*      Step 7: In a get line, calculate, put line loop, apply offsets to trailing part swath
*/

        for (i=0;i<trail;i++) {
                fread(inbuff,sizeof(unsigned char),1000,fp1);
                for (j=0;j<ncol;j++) {
                        outbuff[j] =(float)(inbuff[j]) + offset[si2-1][i];
                }
                fwrite(outbuff,sizeof(float),ncol,fp2);
        }

/*Step 8: Free memory, close files   */

        free(inbuff);
        free(outbuff);

        fclose(fp1);
        fclose(fp2);
        fclose(fp3);
        fclose(fp4);
        fclose(fp5);

        return (0);
}
```

```
/* program sounder                10-10-92

     This program is designed to read values from three real valued raster
     images, and optionaly from a classification map in byte form and a
     residual surface map in short integer (2 byte form).
     All image files are presumed to be coregistered.
     Site file is in real image coords with pixel size of 1.
     Values extracted from the real images are offseted and log transformed.


Variables used
     Name        Type            Description

     easting     float    x coordinate of point
     northing    float    y coordinate of point
     xtl,ytl     float    coordinate of extreme top left corner of images
                           in the coord system used by input points
     rightedge   float    right edge of image in same coord system
     bottom      float    bottom of image in same coord system
     nrow,ncol   int      image dimensions
     numpoints   int      number of points in input points file
     notin       int      number of points falling outside image
     notdone     int      number of points with uncalulated output value
     getresid    int      flag for processing of residual file
     i,k         int      counters
     *raster1    float    pointer to array for first raster file
     *raster2    float    pointer to array for second raster file
     *raster3    float    pointer to array for third raster file
      z          float    linear array of values extracted from raster files
      temp1      float    temp variable for i/o
      temp2      float    temp variable for i/o
      temp3      float    temp variable for i/o
      zed1       float    input depth value , echoed to output
      offs       float    array of deepwater offsets
      sig        float    used in calculation of output values
      j          long     address reference into image arrays
      *clasras   u char   pointer to array for classmap raster file
      class      u char   value extracted from classmap
      *residras  short    pointer to array for 2 byte residual file
      resid      short    value extracted from  residual map
      *fp1 to 7  FILE     file handles
      file_name  char     used for input of file names
      ans        char     answer to user question
```

```
Algorithm

     Step 1:  Dialogue with user to check if residual file is to be read and then
              get file names and open files.

     Step 2:  Dialogue with user to get file sizes and offset values

     Step 3:  Allocate memory for image data

     Step 4:  Read image file data into memory

     Step 5:  in a loop, read in site data, extract values from images
              apply offsets and log transform, output results


     Step 6:  Tidy up, close files etc


Note:
     This program is of simple design and uses no user defined functions
     memory useage is high. Program compiles and runs on Sun SPARC2

                                                                        */
#include <stdio.h>
#include <math.h>
#include <malloc.h>

/* global variables*/

       float  easting,northing,xtl,ytl;
       float  rightedge,bottom,cellx,celly;
       int   nrow,ncol,numpoints,notin,i,k,notdone,getresid;
       float*raster1,*raster2,*raster3,z[3],temp1,temp2,temp3,zed1,offs[3],sig[3];
       long j;
       unsigned char *clasras,class;
       short *residras,resid;
       FILE *fp1,*fp2,*fp3,*fp4,*fp5,*fp6,*fp7;
       char file_name[40],ans;


main()  {

       printf("\nTHIS PROGRAM IS DESIGNED TO EXTRACT VALUES FOR BATHYMETRIC PROCESSING");
       printf("\nREQUIRED INPUT FILES ARE :");
       printf("\n                          THREE REAL SINGLE BAND IMAGES");
       printf("\n                          ONE BYTE CLASSIFICATION IMAGE");
       printf("\n                          ONE 2 BYTE RESIDUAL IMAGE (OPTIONAL)");
       printf("\n                          ONE BLANK DELIMITED X Y Z POINTS FILE");
```

```
/*      Step 1:  Dialogue with user to get file names and open files.      */

        Get1:
        printf("\nEnter input site file name  : ");
        gets(file_name);
        if((fp1 = fopen(file_name,"r"))==NULL) {
                printf("\nUnable to open %s",file_name);
                goto Get1;
        }

        Get2:
        printf("\nEnter output list file name  : ");
        gets(file_name);
        if((fp2 = fopen(file_name,"w"))==NULL) {
                printf("\nUnable to open %s",file_name);
                goto Get2;
        }

        Get3:
        printf("\nEnter input raster file name 1 : ");
        gets(file_name);
        if((fp3 = fopen(file_name,"rb"))==NULL) {
                printf("\unnable to open %s",file_name);
                goto Get3;
        }

        Get4:
        printf("\nEnter input raster file name 2 : ");
        gets(file_name);
        if((fp4 = fopen(file_name,"rb"))==NULL) {
                printf("\unnable to open %s",file_name);
                goto Get4;
        }

        Get5:
        printf("\nEnter input raster file name 3 : ");
        gets(file_name);
        if((fp5 = fopen(file_name,"rb"))==NULL) {
                printf("\unnable to open %s",file_name);
                goto Get5;
        }

        Get6:
        printf("\nEnter input classification file name : ");
        gets(file_name);
        if((fp6 = fopen(file_name,"rb"))==NULL) {
                printf("\unnable to open %s",file_name);
                goto Get6;
        }
```

```
/* see about the residual file */

        printf("Do you wish to query a  2 byte residual file (y/n) :");
        ans = getchar();
        if ((ans == 'y') || (ans == 'Y'))   {
                getresid = 1;
                Get7:
                printf("\nEnter residual file name : ");
                gets(file_name);
                if((fp7 = fopen(file_name,"rb"))==NULL) {
                      printf("\unnable to open %s",file_name);
                      goto Get7;
                }
         }

/*      Step 2:  Dialogue with user to get file sizes and offset values      */


        printf("\nEnter easting,northing of top left of image: ");
        fscanf(stdin,"%f,%f",&xtl,&ytl);
        printf("\nEnter number of rows,cols in input images :  ");
        fscanf(stdin,"%d,%d",&nrow,&ncol);

        printf("\nEnter offset for first raster file  : ");
        fscanf(stdin,"%f",&temp1);
        offs[0] = temp1;

        printf("\nEnter offset for second raster file  : ");
        fscanf(stdin,"%f",&temp1);
        offs[1] = temp1;

        printf("\nEnter offset for third raster file  : ");
        fscanf(stdin,"%f",&temp1);
        offs[2] = temp1;

        printf("\nEnter number of points in input site file : ");
        fscanf(stdin,"%d",&numpoints);


/*       Step 3:  Allocate memory for image data       */


        if((raster1=(float *) calloc(nrow*ncol,sizeof(float))) == NULL)
            printf(stderr,"Error allocating memory \n");

        if((raster2=(float *) calloc(nrow*ncol,sizeof(float))) == NULL)
            printf(stderr,"Error allocating memory \n");

        if((raster3=(float *) calloc(nrow*ncol,sizeof(float))) == NULL)
            printf(stderr,"Error allocating memory \n");

        if((clasras=(unsigned char*) calloc(nrow*ncol,sizeof(unsigned char))) == NULL)
            printf(stderr,"Error allocating memory \n");

        if (getresid) {
                  if((residras=(short*) calloc(nrow*ncol,sizeof(short))) == NULL)
```

```
                printf(stderr,"Error allocating memory \n");
        }
/*      Step 4:  Read image file data into memory       */

        fread(raster1,sizeof(float),nrow*ncol,fp3);
        printf("read in raster file 1\n");
        fread(raster2,sizeof(float),nrow*ncol,fp4);
        printf("read in raster file 2\n");
        fread(raster3,sizeof(float),nrow*ncol,fp5);
        printf("read in raster file 3\n");
        fread(clasras,sizeof(unsigned char),nrow*ncol,fp6);
        printf("read in classification file \n");
        if(getresid) {
              fread(residras,sizeof(short),nrow*ncol,fp7);
              printf("read residual file \n");
        }


/* Step 5 : Loop to read and process the site data  */

/* set up some variables */

        notin=0;
        notdone=0;
        rightedge=xtl+(float)(ncol);
        bottom=ytl+(float)(nrow);

/* start loop */
        for (i=0;i<numpoints;i++) {
                    fscanf(fp1,"%f %f %f", &easting,&northing,&zed1);
                    printf("%d %f %f %f\n",i,easting,northing,zed1);
                    if (easting<xtl || easting>rightedge ||northing>bottom || northing < ytl){
                             notin++;
                    }
                    else  {     /* calculate cell to read and get values */
                            cellx= easting-xtl;
                            celly= northing-ytl;
                            j=(long)(celly)*ncol+(long)(cellx);
                            z[0]=raster1[j];
                            z[1]=raster2[j];
                            z[2]=raster3[j];
                            class=clasras[j];
                            if (getresid) resid=residras[j];
                            for(k=0;k<3;k++) {
                                   sig[k] = (z[k]-offs[k]);
                                   if (sig[k] < 0.00000001)  {
                                           /* value cannot be calculated */
                                           z[k]= -999;
                                           notdone++;
                                   }
                                   else {
                                           z[k] = log(sig[k]);
                                   }
                            }
                            temp1=z[0];
                            temp2=z[1];
```

```
                                temp3=z[2];
                                if(getresid) {
                                        fprintf(fp2,"%f   %f   %f   %f   %f   %f   %d   %ld\n",
                                           easting,northing,zed1,temp1,temp2,temp3,class,resid);
                                }
                                else {
                                        fprintf(fp2,"%f %f %f %f %f %f%d\n",
                                           easting,northing,zed1,temp1,temp2,temp3,class);
                                }
                        }

        }
/* Step 6:  Tidy up, close files etc.   */

        printf("\n%d points in input site file",numpoints);
        printf("\n%d points not in image area",notin);
        printf("\n%d points have un-calculated values\n",notdone);

        fclose(fp1);
        fclose(fp2);
        fclose(fp3);
        fclose(fp4);
        fclose(fp5);
        fclose(fp6);
        fclose(fp7);
        return(0);

}
```

```
/* program sit2img     10/10/92

Description
        This program is designed to take xyz triplet files and
        construct a raster image in 2 byte form. Cell values are set to zero
        except where a point is found in a cell. Point values are scaled.
        program is written specificaly to process output residuals from
        bathymetric regression. Coordinate system is assumed to have origin at
        top left, (DISIMP type), and output image has pixel size of 1.

Varaiuble used:
        Name            Type            Description

        xin             float   x coordinate of input point
        yin             float   y coordinate of input point
        xtl             float   x coordinate of top left of image
        ytl             float   y coordinate of top left of image
        zed             float   z coordinat of input point
        rightedge       float   right edge of resulting image
        bottom          float   bottom of resulting image
        nrow            int     number of rows in resultant image
        ncol            int     number of columns in resultant image
        npoints         int     number of points in the input file
        notin           int     count of points falling outside resulting image
        i               int     counter
        *raster         short   pointer to 2 byte array for image data
        z               short   scaled input data
        j               long    address into raster data block
        *fp1 to 3       FILE    file handles
        filename        char    used to get file names


Algorithm

        Step 1: Dialogue with user to get file names, open files.

        Step 2: Dialogue with user to get parameters

        Step 3: Calculate raster size, allocate memory.

        Step 4: Loop to read in site data, scale and allocate to pixel.

        Step 5: Write out image file, tidy up, close files.


Note

        This program is simple in design and comprises only a main. No
        functions are defined. Memory requirement is dependant on size of image
        This program has been sucessfully compiled and run on a SUN SPARC2.    */
```

```
#include <stdio.h>
#include <math.h>

 /* Set up global variables*/

        float  xin,yin,xtl,ytl,zed;
        float  rightedge,bottom,cellx,celly;
        int   nrow,ncol,notin,i,npoints;
        short *raster,z,out;
        long j;
        FILE *fp1,*fp2,*fp3;
        char filename[40];


main()  {

/*      Step1:  Dialogue with user to get file names, open files.  */

        Get1:
        printf("\nEnter input site file name  : ");
        gets(filename);
                if((fp1 = fopen(filename,"r"))==NULL){
                printf("\nUnable to open %s",filename);
                goto Get1;
        }

        Get2:
        printf("\nEnter output list file name  : ");
        gets(filename);
        if((fp2 = fopen(filename,"w"))==NULL){
                printf("\nUnable to open %s",filename);
                goto Get2;
        }

        Get3:
        printf("\nEnter output raster file name  : ");
        gets(filename);
        if((fp3 = fopen(filename,"wb"))==NULL){
                printf("\unnable to open %s",filename);
                goto Get3;
        }

/*      Step 2: Dialogue with user to get parameters    */


        printf("\nEnter top left x,y coordinates : ");
        fscanf(stdin,"%f,%f",&xtl,&ytl);
        printf("\nEnter number of rows,cols : ");
        fscanf(stdin,"%d,%d",&nrow,&ncol);
        printf("\nEnter number of points in input file");
        fscanf(stdin,"%d",&npoints);


/*      Step 3: Calculate raster size, allocate memory.   */

        rightedge=xtl+(float)(ncol);
```

```
        bottom=ytl+(float)(nrow);

        if((raster=(short *) calloc((nrow*ncol),sizeof(short))) == NULL)
           printf(stderr,"Error allocating memory \n");

/*      Step 4: Loop to read in site data, scale and allocate to pixel. */

        notin=0;
        for (i=0;i<npoints;i++) {
               fscanf(fp1,"%f %f %f", &xin,&yin,&zed);
               if (xin<xtl || xin>rightedge ||yin>bottom || yin < ytl) {
                      notin++;
               }
               else  {
                      cellx= xin-xtl;
                      celly= yin-ytl;

                      j=(int)(celly)*ncol+(int)(cellx);
                      /* scale data by 100 */
                      z= (short) (zed*100) ;
                      /* echo to screen and list file/*
                      fprintf(fp2,"%d 1 \n%f %f\n",z,cellx,celly);
                      printf("%d %f %d %d\n",i,zed,z,raster[j]);
                      /* allocate value to pixel */
                      raster[j]=  z;

               }

        }


/*      Step 5:  Write out image file, tidy up, close files. */

        printf("\n%d points not in image area\n",notin);
        fwrite(&raster[0],sizeof(short),(nrow*ncol),fp3);

        fclose(fp1);
        fclose(fp2);
        fclose(fp3);
        return(0);
}
```

# APPENDIX C

## FILES USED IN THE DESTRIPING PROCESS

This appendix contains listings of the files used as input to the destriping process. Also listed are the spreadsheet output files used to determine the offsets. The spreadsheet files are followed by graphs showing the striping patterns.

For each of the four bands destriped, there are two input files. These are the striping index file which lists for each whole swath in the image the set of offsets to be applied. A second file, the offsets file lists the offset for each line in each type of striping.

**Input files for destriping Band 1**

| Index file | Offset file |
|---|---|
| 1 1 1 1 | -0.07 |
| 1 1 1 1 | 0.28 |
| 1 1 1 1 | -0.04 |
| 1 1 1 1 | 0.34 |
| 1 1 1 1 | 0.19 |
| 1 1 1 1 | 0.33 |
| 1 1 1 1 | -0.11 |
| 1 1 1 1 | 0.39 |
| 1 1 1 1 | -0.11 |
| 1 1 1 1 | 0.01 |
| 1 1 1 1 | 0.04 |
| 1 1 1 1 | 0.20 |
| 1 1 1 1 | -0.11 |
| 1 1 1 1 | 0.13 |
| 1 1 1 | 0.05 |
| 1 1 1 | -0.22 |

**Input files for destriping Band 2**

| Index file | Offset files |
|---|---|
| 1 2 1 2 | -0.82 0.48 |
| 1 2 1 2 | -0.58 0.24 |
| 1 1 1 1 | -0.50 0.31 |
| 1 1 1 1 | -0.50 0.35 |
| 1 1 1 2 | -0.49 0.17 |
| 2 1 1 2 | -0.61 0.19 |
| 2 1 1 1 | -0.62 0.06 |
| 2 1 1 2 | -0.33 0.31 |
| 2 1 1 2 | -0.62 0.06 |
| 2 1 1 2 | -0.41 0.36 |
| 2 1 1 1 | -0.61 -0.06 |
| 1 1 1 1 | -0.36 0.35 |
| 1 1 1 1 | 0.01 -0.14 |
| 1 1 2 1 | -0.68 0.18 |
| 1 1 2 | -0.09 -0.19 |
| 1 1 2 | -1.30 -0.69 |

**Input files for destriping Band 3**

| Index file | Offset files |
|---|---|
| 1 4 4 4 | 0.41 -0.10 0.20 0.60 |
| 2 3 2 3 | 0.60 0.05 0.64 1.34 |
| 1 1 1 1 | 0.49 -0.01 0.42 0.65 |
| 2 2 2 2 | 0.57 -0.13 0.36 0.96 |
| 1 1 1 4 | 0.41 -0.10 0.25 0.77 |
| 3 2 2 3 | 0.28 -0.43 0.22 0.92 |
| 4 1 1 1 | 0.48 0.38 0.48 0.65 |
| 3 2 2 3 | 0.40 -0.41 0.14 0.88 |
| 4 1 1 4 | 0.48 0.38 0.48 0.65 |
| 3 2 2 3 | 0.42 -0.28 0.01 0.85 |
| 4 1 1 1 | 0.24 -0.45 0.50 0.78 |
| 2 2 2 2 | 0.29 -0.20 0.26 0.83 |
| 1 1 1 1 | 0.26 -0.37 0.20 0.69 |
| 2 2 3 2 | 0.10 -0.67 0.18 0.66 |
| 1 1 4 | 0.38 -0.16 0.12 0.46 |
| 2 3 3 | -0.37 -1.17 -0.42 0.24 |

**Input files for destriping Band 4**

| Index file | Offset files |
|---|---|
| 1 1 1 1 | 0.34 -0.22 |
| 2 2 2 2 | 0.16 -0.11 |
| 1 1 1 1 | 0.06 -0.21 |
| 2 2 2 2 | 0.02 -0.24 |
| 1 1 1 1 | 0.09 -0.11 |
| 2 2 2 2 | 0.13 -0.20 |
| 1 1 1 1 | 0.00 -0.23 |
| 2 2 2 2 | 0.03 -0.20 |
| 1 1 1 1 | 0.00 -0.23 |
| 2 2 2 2 | 0.01 0.12 |
| 1 1 1 1 | 0.08 -0.19 |
| 2 2 2 2 | 0.06 0.32 |
| 1 1 1 1 | 0.04 -0.47 |
| 2 2 2 2 | 0.07 -0.26 |
| 1 1 1 | 0.02 -0.33 |
| 2 2 2 | 0.35 -1.00 |

**Spreadsheet output file Band 1 Pattern 1**

| | | | Means | |
|---|---|---|---|---|
| Line | Raw | Rounded | Half int. | Offset |
| 1 | 62.07 | 62 | 62 | -0.07 |
| 2 | 61.72 | 62 | 61.5 | 0.28 |
| 3 | 62.04 | 62 | 62 | -0.04 |
| 4 | 61.66 | 62 | 61.5 | 0.34 |
| 5 | 61.81 | 62 | 62 | 0.19 |
| 6 | 61.67 | 62 | 61.5 | 0.33 |
| 7 | 62.11 | 62 | 62 | -0.11 |
| 8 | 61.61 | 62 | 61.5 | 0.39 |
| 9 | 62.11 | 62 | 62 | -0.11 |
| 10 | 61.99 | 62 | 62 | 0.01 |
| 11 | 61.96 | 62 | 62 | 0.04 |
| 12 | 61.8 | 62 | 62 | 0.20 |
| 13 | 62.11 | 62 | 62 | -0.11 |
| 14 | 61.87 | 62 | 62 | 0.13 |
| 15 | 61.95 | 62 | 62 | 0.05 |
| 16 | 62.22 | 62 | 62 | -0.22 |
| | | | | |
| | mean all 61.89375 | 62 | | |
| | Desired mean | 62 | | |

**Spreadsheet output file Band 2 Pattern 1**

| | | | Means | |
|---|---|---|---|---|
| Line | Raw | Rounded | Half int. | Offset |
| 1 | 16.82 | 17 | 17 | -0.82 |
| 2 | 16.58 | 17 | 16.5 | -0.58 |
| 3 | 16.5 | 17 | 16.5 | -0.50 |
| 4 | 16.5 | 17 | 16.5 | -0.50 |
| 5 | 16.49 | 16 | 16.5 | -0.49 |
| 6 | 16.61 | 17 | 16.5 | -0.61 |
| 7 | 16.62 | 17 | 16.5 | -0.62 |
| 8 | 16.33 | 16 | 16.5 | -0.33 |
| 9 | 16.62 | 17 | 16.5 | -0.62 |
| 10 | 16.41 | 16 | 16.5 | -0.41 |
| 11 | 16.61 | 17 | 16.5 | -0.61 |
| 12 | 16.36 | 16 | 16.5 | -0.36 |
| 13 | 15.99 | 16 | 16 | -0.01 |
| 14 | 16.68 | 17 | 16.5 | -0.68 |
| 15 | 16.09 | 16 | 16 | -0.09 |
| 16 | 17.3 | 17 | 17.5 | -1.30 |
| | | | | |
| | mean all 16.51375 | 17 | | |
| | Desired mean | 16 | | |

**Spreadsheet output file Band 2 Pattern 2**

| | | | Means | |
|---|---|---|---|---|
| Line | Raw | Rounded | Half int. | Offset |
| 1 | 15.52 | 16 | 15.5 | 0.48 |
| 2 | 15.76 | 16 | 16 | 0.24 |
| 3 | 15.69 | 16 | 15.5 | 0.31 |
| 4 | 15.65 | 16 | 15.5 | 0.35 |
| 5 | 15.83 | 16 | 16 | 0.17 |
| 6 | 15.81 | 16 | 16 | 0.19 |
| 7 | 15.94 | 16 | 16 | 0.06 |
| 8 | 15.69 | 16 | 15.5 | 0.31 |
| 9 | 15.94 | 16 | 16 | 0.06 |
| 10 | 15.64 | 16 | 15.5 | 0.36 |
| 11 | 16.06 | 16 | 16 | -0.06 |
| 12 | 15.65 | 16 | 15.5 | 0.35 |
| 13 | 16.14 | 16 | 16 | 0.86 |
| 14 | 15.82 | 16 | 16 | 0.18 |
| 15 | 16.19 | 16 | 16 | -0.19 |
| 16 | 16.69 | 17 | 16.5 | -0.69 |
| | | | | |
| | mean all 15.87813 | 16 | | |
| | Desired mean | 16 | | |

**Spreadsheet output file Band 3 Pattern 1**

| | | | Means | |
|---|---|---|---|---|
| Line | Raw | Rounded | Half int. | Offset |
| 1 | 11.59 | 12 | 11.5 | 0.41 |
| 2 | 11.4 | 11 | 11.5 | 0.60 |
| 3 | 11.51 | 12 | 11.5 | 0.49 |
| 4 | 11.43 | 11 | 11.5 | 0.57 |
| 5 | 11.59 | 12 | 11.5 | 0.41 |
| 6 | 11.72 | 12 | 11.5 | 0.28 |
| 7 | 11.52 | 12 | 11.5 | 0.48 |
| 8 | 11.6 | 12 | 11.5 | 0.40 |
| 9 | 11.52 | 12 | 11.5 | 0.48 |
| 10 | 11.58 | 12 | 11.5 | 0.42 |
| 11 | 11.76 | 12 | 12 | 0.24 |
| 12 | 11.71 | 12 | 11.5 | 0.29 |
| 13 | 11.74 | 12 | 11.5 | 0.26 |
| 14 | 11.9 | 12 | 12 | 0.10 |
| 15 | 11.62 | 12 | 11.5 | 0.38 |
| 16 | 12.37 | 12 | 12.5 | -0.37 |
| | | | | |
| | mean all 11.6575 | 12 | | |
| | Desired mean | 12 | | |

**Spreadsheet output file Band 3 Pattern 2**

| | | | Means | |
|---|---|---|---|---|
| Line | Raw | Rounded | Half int. | Offset |
| 1 | 12.1 | 12 | 12 | -0.10 |
| 2 | 11.95 | 12 | 12 | 0.05 |
| 3 | 12.01 | 12 | 12 | -0.01 |
| 4 | 12.13 | 12 | 12 | -0.13 |
| 5 | 12.1 | 12 | 12 | -0.10 |
| 6 | 12.43 | 12 | 12.5 | -0.43 |
| 7 | 11.62 | 12 | 11.5 | 0.38 |
| 8 | 12.41 | 12 | 12.5 | -0.41 |
| 9 | 11.62 | 12 | 11.5 | 0.38 |
| 10 | 12.28 | 12 | 12.5 | -0.28 |
| 11 | 12.45 | 12 | 12.5 | -0.45 |
| 12 | 12.2 | 12 | 12 | -0.20 |
| 13 | 12.37 | 12 | 12.5 | -0.37 |
| 14 | 12.67 | 13 | 12.5 | -0.67 |
| 15 | 12.16 | 12 | 12 | -0.16 |
| 16 | 13.17 | 13 | 13 | 1.17 |
| | | | | |
| | mean all 12.25563 | 12 | | |
| | Desired mean | 12 | | |

**Spreadsheet output file Band 3 Pattern 3**

| | | | Means | |
|---|---|---|---|---|
| Line | Raw | Rounded | Half int. | Offset |
| 1 | 11.8 | 12 | 12 | 0.20 |
| 2 | 11.36 | 11 | 11.5 | 0.64 |
| 3 | 11.58 | 12 | 11.5 | 0.42 |
| 4 | 11.64 | 12 | 11.5 | 0.36 |
| 5 | 11.75 | 12 | 12 | 0.25 |
| 6 | 11.78 | 12 | 12 | 0.22 |
| 7 | 11.52 | 12 | 11.5 | 0.48 |
| 8 | 11.86 | 12 | 12 | 0.14 |
| 9 | 11.52 | 12 | 11.5 | 0.48 |
| 10 | 11.99 | 12 | 12 | 0.01 |
| 11 | 11.5 | 12 | 11.5 | 0.50 |
| 12 | 11.74 | 12 | 11.5 | 0.26 |
| 13 | 11.8 | 12 | 12 | 0.20 |
| 14 | 11.82 | 12 | 12 | 0.18 |
| 15 | 11.88 | 12 | 12 | 0.12 |
| 16 | 12.42 | 12 | 12.5 | -0.42 |
| | | | | |
| | mean all 11.74625 | 12 | | |
| | Desired mean | 12 | | |

**Spreadsheet output file Band 3 Pattern 4**

| Line | Raw | Rounded | Means Half int. | Offset |
|---|---|---|---|---|
| 1 | 11.4 | 11 | 11.5 | 0.60 |
| 2 | 10.66 | 11 | 10.5 | 1.34 |
| 3 | 11.35 | 11 | 11.5 | 0.65 |
| 4 | 11.04 | 11 | 11 | 0.96 |
| 5 | 11.23 | 11 | 11 | 0.77 |
| 6 | 11.08 | 11 | 11 | 0.92 |
| 7 | 11.35 | 11 | 11.5 | 0.65 |
| 8 | 11.12 | 11 | 11 | 0.88 |
| 9 | 11.35 | 11 | 11.5 | 0.65 |
| 10 | 11.15 | 11 | 11 | 0.85 |
| 11 | 11.22 | 11 | 11 | 0.78 |
| 12 | 11.17 | 11 | 11 | 0.83 |
| 13 | 11.31 | 11 | 11.5 | 0.69 |
| 14 | 11.34 | 11 | 11.5 | 0.66 |
| 15 | 11.54 | 12 | 11.5 | 0.46 |
| 16 | 11.76 | 12 | 12 | 0.24 |
| | mean all 11.24313 | 11 | | |
| | Desired mean | 12 | | |

**Spreadsheet output file Band 4 Pattern 1**

| Line | Raw | Rounded | Means Half int. | Offset |
|---|---|---|---|---|
| 1 | 5.66 | 6 | 5.5 | 0.34 |
| 2 | 5.84 | 6 | 6 | 0.16 |
| 3 | 5.94 | 6 | 6 | 0.06 |
| 4 | 5.98 | 6 | 6 | 0.02 |
| 5 | 5.91 | 6 | 6 | 0.09 |
| 6 | 5.87 | 6 | 6 | 0.13 |
| 7 | 6 | 6 | 6 | 0.00 |
| 8 | 5.97 | 6 | 6 | 0.03 |
| 9 | 6 | 6 | 6 | 0.00 |
| 10 | 5.99 | 6 | 6 | 0.01 |
| 11 | 5.92 | 6 | 6 | 0.08 |
| 12 | 5.94 | 6 | 6 | 0.06 |
| 13 | 5.96 | 6 | 6 | 0.04 |
| 14 | 5.93 | 6 | 6 | 0.07 |
| 15 | 5.98 | 6 | 6 | 0.02 |
| 16 | 5.65 | 6 | 5.5 | 0.35 |
| | mean all 5.895625 | 6 | | |
| | Desired mean | 6 | | |

**Spreadsheet output file Band 4 Pattern 2**

| Line | Raw | Rounded | Means Half int. | Offset |
|---|---|---|---|---|
| 1 | 6.22 | 6 | 6 | -0.22 |
| 2 | 6.11 | 6 | 6 | -0.11 |
| 3 | 6.21 | 6 | 6 | -0.21 |
| 4 | 6.24 | 6 | 6 | -0.24 |
| 5 | 6.11 | 6 | 6 | -0.11 |
| 6 | 6.2 | 6 | 6 | -0.20 |
| 7 | 6.23 | 6 | 6 | -0.23 |
| 8 | 6.2 | 6 | 6 | -0.20 |
| 9 | 6.23 | 6 | 6 | -0.23 |
| 10 | 5.88 | 6 | 6 | 0.12 |
| 11 | 6.19 | 6 | 6 | -0.19 |
| 12 | 5.68 | 6 | 5.5 | 0.32 |
| 13 | 6.47 | 6 | 6.5 | -0.47 |
| 14 | 6.26 | 6 | 6.5 | -0.26 |
| 15 | 6.33 | 6 | 6.5 | -0.33 |
| 16 | 7 | 7 | 7 | -1.00 |
| | | | | |
| | mean all 6.203125 | 6 | | |
| | Desired mean | 6 | | |

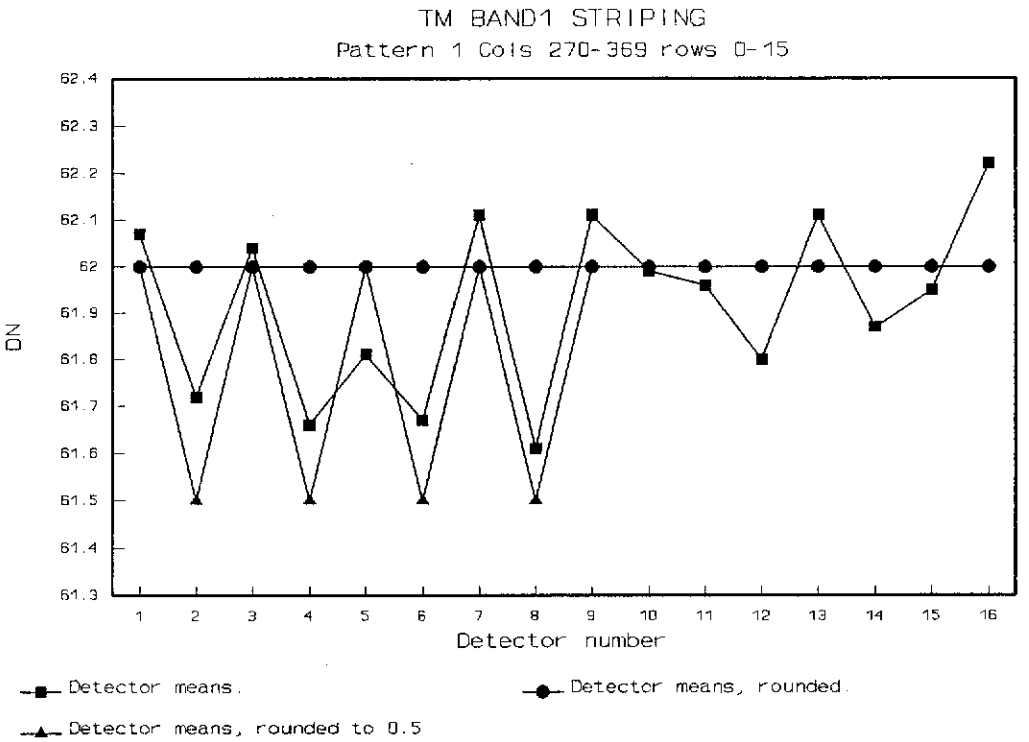
TM BAND1 STRIPING
Pattern 1 Cols 270-369 rows 0-15
DN
62.4
62.3
62.2
62.1
62
61.9
61.8
61.7
61.6
61.5
61.4
61.3
1 2 3 4 5 6 7 8 9 10 11 12 13 14 15 16
Detector number
Detector means.
Detector means, rounded.
Detector means, rounded to 0.5

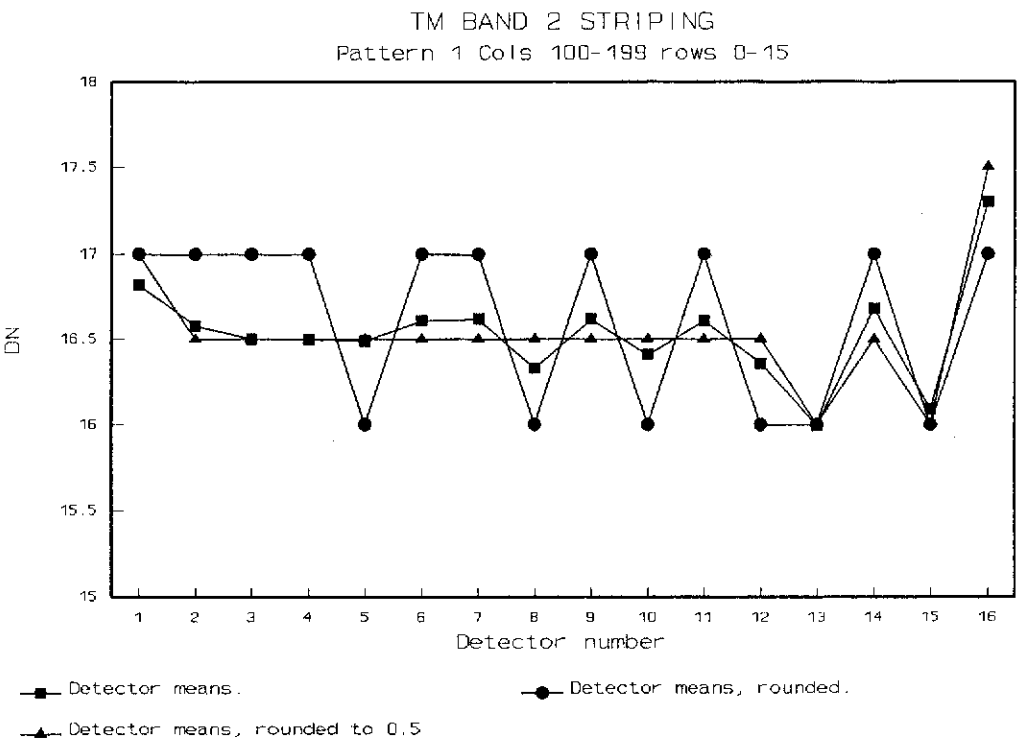
TM BAND 2 STRIPING
Pattern 1 Cols 100-199 rows 0-15
DN
18
17.5
17
16.5
16
15.5
15
1 2 3 4 5 6 7 8 9 10 11 12 13 14 15 16
Detector number
Detector means.
Detector means, rounded.
Detector means, rounded to 0.5

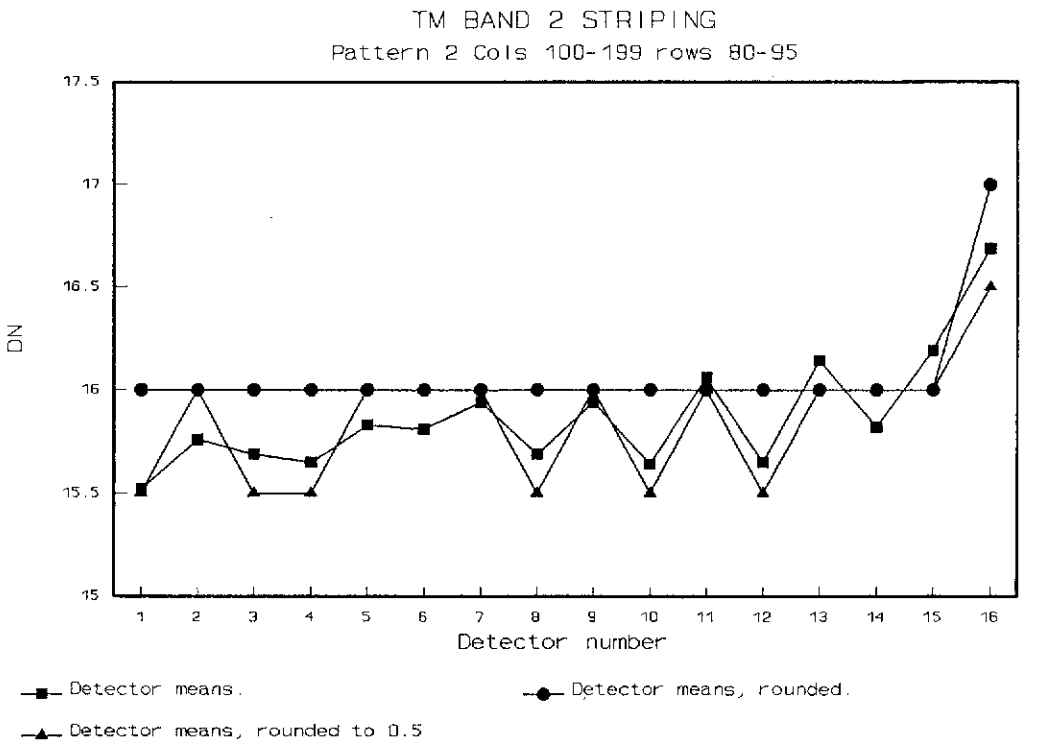
TM BAND 2 STRIPING
Pattern 2 Cols 100-199 rows 80-95
17.5
17
16.5
16
15.5
15
DN
1 2 3 4 5 6 7 8 9 10 11 12 13 14 15 16
Detector number
Detector means.
Detector means, rounded.
Detector means, rounded to 0.5

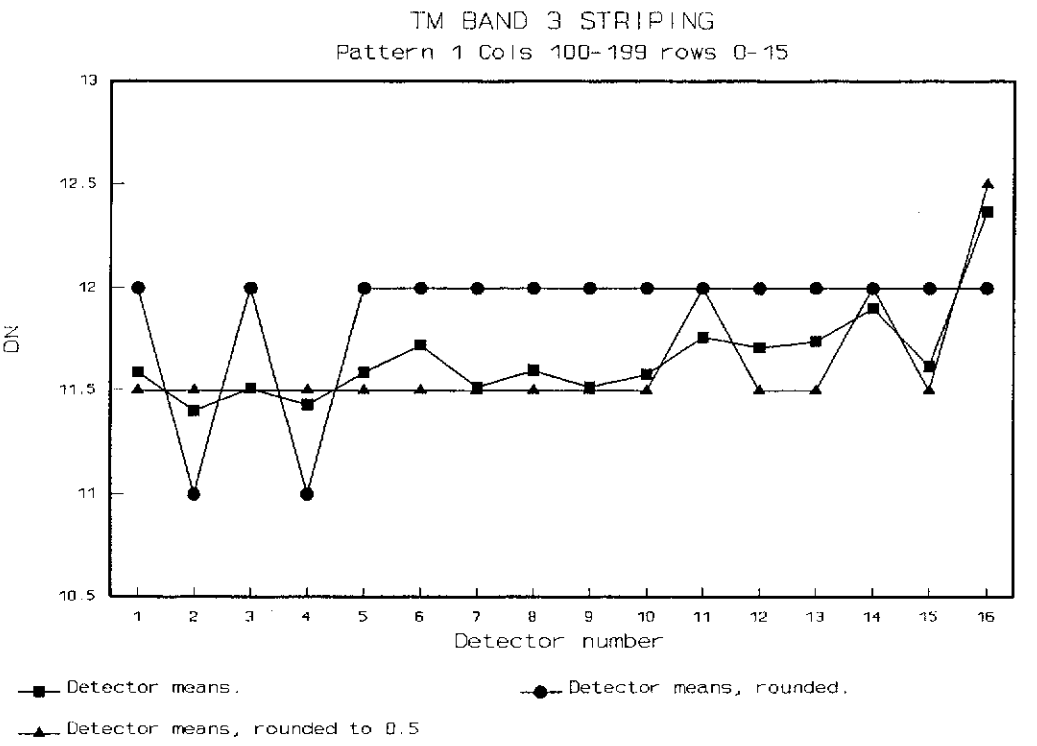
TM BAND 3 STRIPING
Pattern 1 Cols 100-199 rows 0-15
13
12.5
12
11.5
11
10.5
DN
1 2 3 4 5 6 7 8 9 10 11 12 13 14 15 16
Detector number
Detector means.
Detector means, rounded.
Detector means, rounded to 0.5

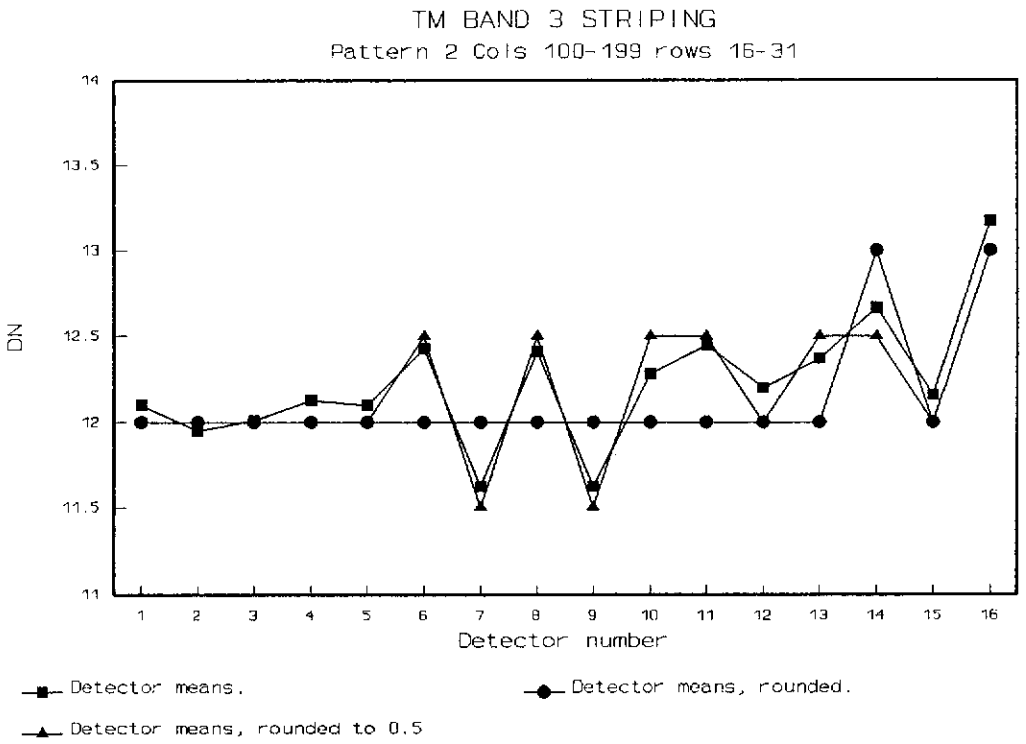
TM BAND 3 STRIPING
Pattern 2 Cols 100-199 rows 16-31
DN
Detector number
Detector means.
Detector means, rounded.
Detector means, rounded to 0.5

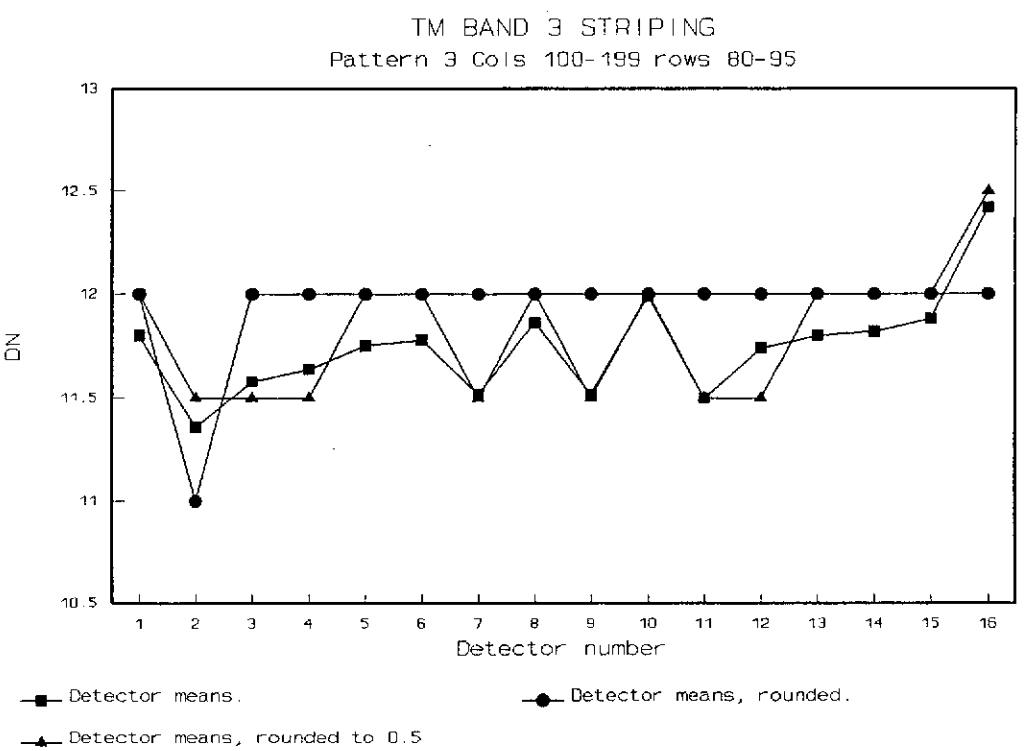
TM BAND 3 STRIPING
Pattern 3 Cols 100-199 rows 80-95
DN
Detector number
Detector means.
Detector means, rounded.
Detector means, rounded to 0.5

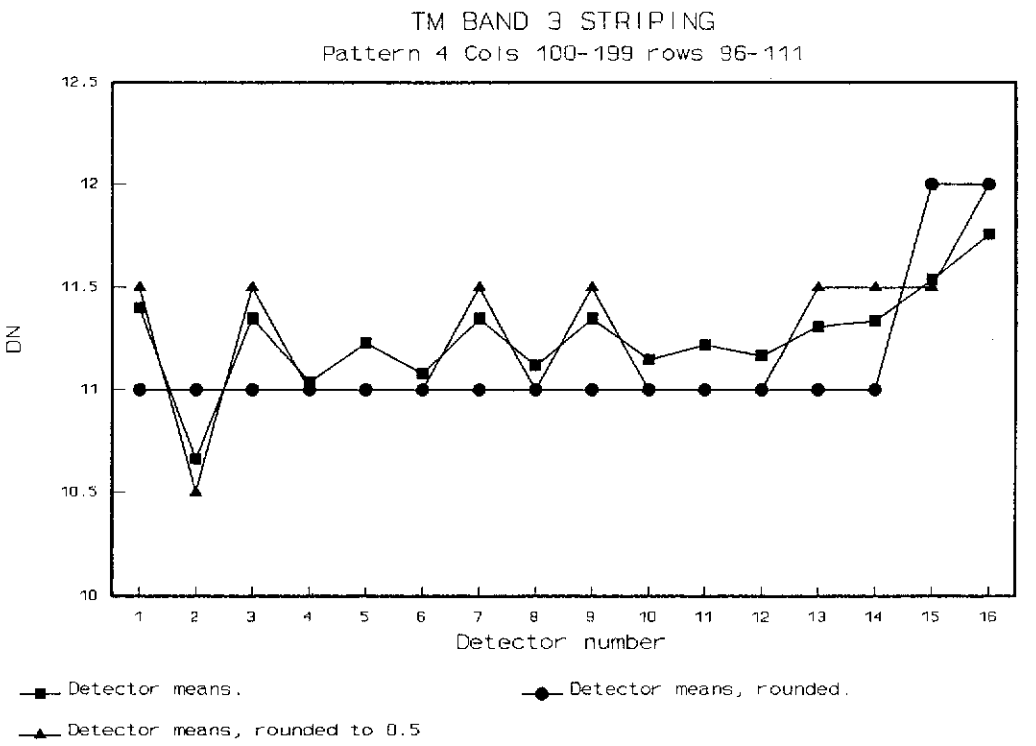
TM BAND 3 STRIPING
Pattern 4 Cols 100-199 rows 96-111
DN
12.5
12
11.5
11
10.5
10
1 2 3 4 5 6 7 8 9 10 11 12 13 14 15 16
Detector number
Detector means.
Detector means, rounded.
Detector means, rounded to 0.5

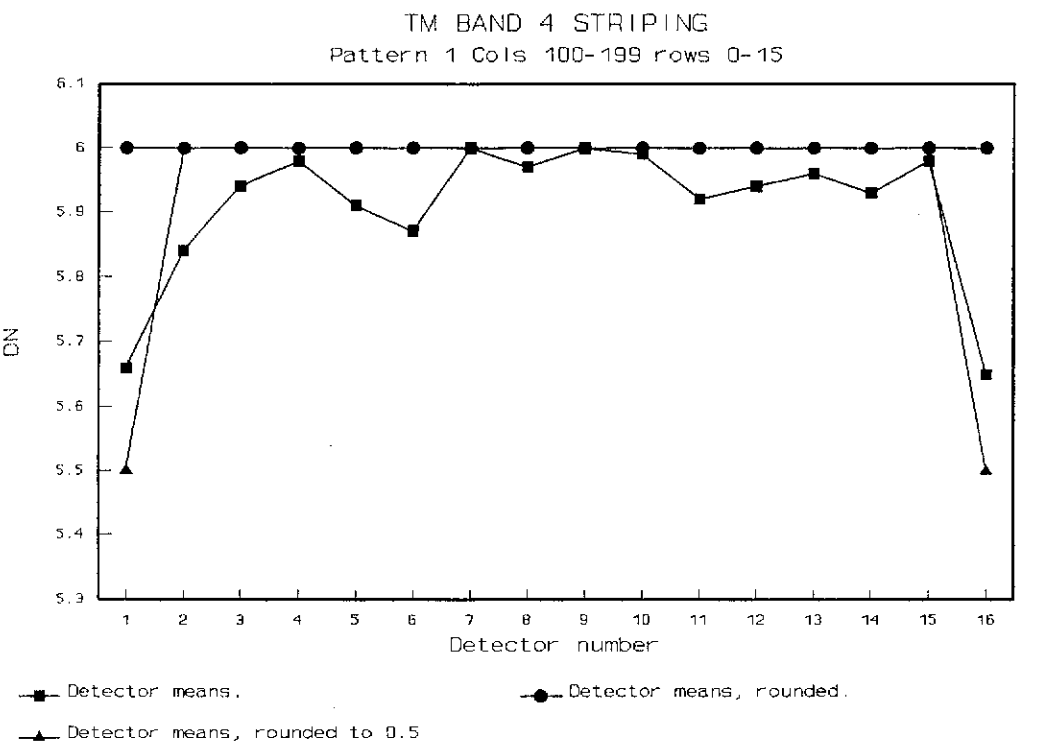
TM BAND 4 STRIPING
Pattern 1 Cols 100-199 rows 0-15
DN
6.1
6
5.9
5.8
5.7
5.6
5.5
5.4
5.3
1 2 3 4 5 6 7 8 9 10 11 12 13 14 15 16
Detector number
Detector means.
Detector means, rounded.
Detector means, rounded to 0.5

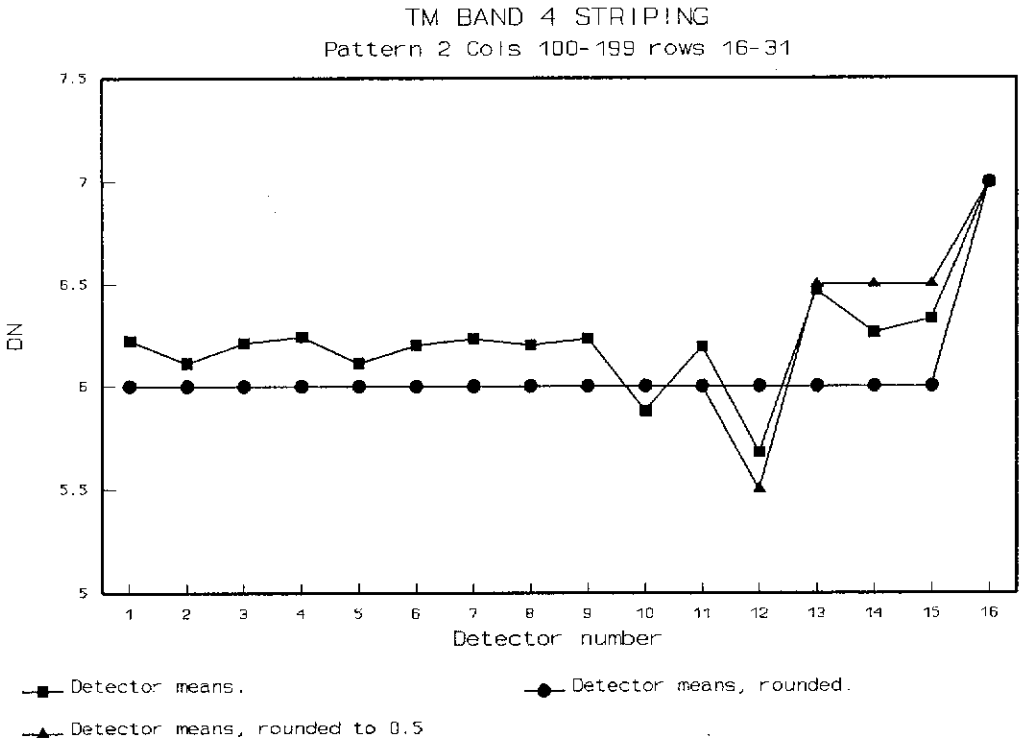
TM BAND 4 STRIPING
Pattern 2 Cols 100-199 rows 16-31
DN
7.5
7
6.5
6
5.5
5
1
2
3
4
5
6
7
8
9
10
11
12
13
14
15
16
Detector number
Detector means.
Detector means, rounded.
Detector means, rounded to 0.5